**Dewberry**®

Dewberry Engineers Inc.  |  856.802.0843
1015 Briggs Road, Suite 210  |  856.802.0846 fax
Mount Laurel, NJ 08054  |  www.dewberry.com

November 26, 2018

Ms. Wanda Parrish, AICP, Director
County of Spotsylvania
Department of Planning
9019 Old Battlefield Boulevard, Suite 320
Spotsylvania, VA  22553

RE:     **Application:     sPower cases SUP18-0001, 0002 and 003**
        **Applicant:        sPower**
        **Dewberry File No.:  50107769**
        **Engineering Review #1**

Dear Director and Board Members:

In accordance with your authorization, Dewberry has reviewed the following plans and documents for the above referenced project:

- "Generalized Development Plan Narratives for Center A, B and C", prepared by sPower, undated.
- "Generalized Development Plan, Spotsylvania Solar Energy Center A, Special Use Permit – SUP 18-0001", prepared by Kimley Horn and Associates, Inc., dated 10/26/2018.
- "Generalized Development Plan, Spotsylvania Solar Energy Center B, Special Use Permit – SUP 18-0002", prepared by Kimley Horn and Associates, Inc., dated 10/26/2018.
- "Generalized Development Plan, Spotsylvania Solar Energy Center C, Special Use Permit – SUP 18-0003", prepared by Kimley Horn and Associates, Inc., dated 10/26/2018.
- "Spotsylvania Solar Energy Center Decommissioning and Restoration Plan", prepared by sPower, dated June 2018.
- "sPower Group Conceptual Cost Estimate for Decommission Highlander a 647,735.1kW (STC) PV System", signed and sealed by Sean Millot, VA PE Lic. No. 0402052322, dated 5/15/2018.
- "Cadmium Telluride Panel Integrity and Safety Executive Summary", undated.
- "Limited Soil Sampling, Sierra Solar Greenworks, West Avenue I and 120th Street, Lancaster, Los Angeles, CA", dated June 15, 2018, prepared by Terracon Consultants, Inc.
- "Heat Island Effect Literature Review and Executive Summary, prepared by sPower", undated.
- "Noise Study – Memorandum", prepared by Kimley Horn and Associates, Inc., dated 9/20/2018.

Based on our review of the submitted information we offer the following comments:

**PROJECT OVERVIEW**

The subject property is located in Spotsylvania County, Virginia and consists of three sites (Sites A, B & C). Site A consists of approximately 5,200 acres, Site B consists of approximately 245 acres and Site C consists of approximately 905 acres.  The land is currently made up of mostly vacant land, which is rural cleared forested areas as well as wooded areas and some silvicultural areas.  The site also contains a large amount of wetlands areas, some gravel roadways and power lines.  The surrounding areas are mostly silvicultural areas with some agricultural areas and some rural residential areas.

The applicant is seeking Special Use Permits to construct a Solar Energy Facility on the three sites that will

disturb approximately 3,500 acres. The project proposes that a total amount of 500 MWac (Megawatts AC) of power will be generated by the facility. Site A will generate 400 MWac, Site B will generate 30 MWac and Site C will generate 70 MWac. There will be several access points to the site, with the main access points being from Orange Plank Road, West Catharpin Road and Post Oak Road.

**DECOMMISSIONG AND RESTORATION PLAN REVIEW**

Dewberry conducted a review of the "Spotsylvania Solar Energy Center Decommission and Restoration Plan" dated June 2018 and the "sPower Group Conceptual Cost Estimate for Decommission Highlander a 647,735.1kW (STC) PV System", dated 5/15/2018. Dewberry also reviewed Section 23-4.5.7(d) of the Spotsylvania County Zoning Ordinance and we offer the following recommendations:

1) The report shall be updated to include the contact information for the applicant/party responsible during the decommissioning.

2) More information regarding normal work hours shall be provided, typical days and hours shall be included.

3) A phasing plan for the decommissioning and restoration of the project shall be provided. This plan shall include phasing, locations of staging of materials and a truck route/access map and plan.

4) The applicant shall provide additional information regarding recycling and disposal activities. Specifically, the following questions shall be answered in the report:

   a. What type of equipment will be used to transport the different materials off site?
   b. How long will materials remain on site after they are broken down?
   c. Where will they be stored prior to being hauled off?
   d. Will the materials be protected from being damaged prior to being hauled off?

5) The report shall be updated to address noise standards and how they will compare with noise levels that are created during typical construction that were included in the provided noise study.

6) The project proposes several wetlands crossings with access roads, Dewberry recommends removal of the access roads and restoration of the wetlands to the existing condition. Details shall be provided on how this will be achieved. The applicant shall provide documentation from the Virginia Department of Environmental Quality.

7) The Decommissioning Plan does not address restoration of compacted soils, resulting from construction traffic and activities during decommissioning of the site. Dewberry recommends the applicant address the following at a minimum:

   • Method of identifying and delineating the soils that have been compacted.
   • VSPZ (Vegetation and Soil Protection Zones) shall be delineated in the field. This would include all areas that are not to be disturbed. Methods of delineation (i.e., protective fencing) shall be addressed, mitigation methods if these areas are disturbed and penalties for contractor is they are disturbed.

**Dewberry**

- Plan of restoration proposed including; equipment, soil types, and criteria.
- Soil testing shall be done prior to construction to determine types of soils, infiltration rates, chemical makeup of soils, biological functions of soils, etc. to compare to post-decommissioning conditions.
- Soil Testing shall also be done post-decommissioning to determine what needs to be done to return the soils back to the natural state.

8) Clarification shall be provided regarding the restoration of the proposed gravel access roads and stormwater management facilities. There are conflicting statements regarding if they will be restored or not. Section 1.6 states that the gravel roads will be restored and Section 2.2.1 states that roads may be restored or left in place and sPower's responses to Round 3 comments, dated September 24 state that roads and stormwater improvements will remain in place. Also, the provided cost estimate assumptions state that they are removing and salvaging the gravel access roads.

9) Additional information/detail shall be provided on the restoration of the ground after the existing underground conduits and lines are removed.

10) The applicant shall address if the proposed landscaped buffers will remain in place after the life of the project.

11) Additional language shall be included that will verify how the panels will be recycled and/or disposed of and the process explained on how the metals will be contained and not allowed into the environment.

12) Provisions shall be added to the report stating that documentation will be provided from the recycling and disposal sites which shall include descriptions and quantities of materials.

13) Dewberry recommends that the County require bonding the actual cost of the decommissioning before the recycling amounts are figured in.

**CADMIUM TELLURIDE REVIEW**

Dewberry conducted a review of the "Cadmium Telluride Panel Integrity and Safety Executive Summary", undated as well as conducted research and found the following documents, which have been included for your review:

1) "Cadmium Telluride – The Good and the Bad." Cadmium Telluride: Advantages &amp; Disadvantages, Alchemie Limited Inc., 2010-2013, www.solar-facts-and-advice.com/cadmium-telluride.html.

2) "Cadmium Telluride – Photovoltaics (PV), Solar Cells, Msds, Toxicity." Chemistry Learner, 2 Mar. 2012, www.chemistrylearner.com/cadmium-telluride.html.

3) Fthenakis, Vasilis, "Environmental Life Cycle Assessment of Cadmium Telluride Solar Cells: Cd Emissions".

4) Martin, Terry, and Sanja Jelic. "The Health Risks of Cadmium in Cigarette Smoke." Verywell Mind, Dotdash, 18 June 2018, www.verywellmind.com/cadmium-in-cigarette-smoke-2824729.

**Dewberry**

Based upon our review of the above referenced documents, we offer the following:

Overview of Cadmium Telluride (CdTe)
Cadmium Telluride (CdTe) is a compound that contains cadmium and tellurium.  It is a black crystalline powder that is odorless, not water soluble and non-flammable.  It has a melting point of above 1000 °C and the boiling point is above 1100 °C.  Cadmium by itself is a highly toxic material, however, based on research cadmium telluride is much less toxic than pure cadmium.  CdTe can be toxic if it is ingested, inhaled or comes in direct contact with skin.

Advantages of using Panels containing CdTe
- Cost – Manufacturing costs are less, the manufacturing process is much simpler for these panels, which keeps the cost lower than silicon based panels.

- The absorption rate for sunlight is ideal for solar use, it captures energy at shorter wavelengths than silicon panels.

- Cadmium is a material that is very abundant in supply as it is a byproduct of other manufacturing processes.

Disadvantages of using Panels containing CdTe
- Fear of toxicity from the cadmium contained.  There have been studies showing that there are little to no impacts on the environment.  However, there still are some risks as stated before, with ingestion, inhalation and skin contact.  These risks are more isolated to the people that produce the CdTe from the raw materials.

- The efficiency of the panels is very low compared to the efficiency of the silicon based panels, meaning that more of the panels are required to create the same amount of energy.  The footprint of the system could be reduced if silicon panels are used.

- The supply of tellurium is not abundant like the supply of Cadmium.  Tellurium is considered a rare element, which limits how many panels are produced.

Findings
Based upon our review of the above referenced documents, there is little evidence to suggest that CdTe based solar panels present risk to the population or environment.  If they are handled properly during all phases of construction and disposal, they will not emit any toxicity into the environment.

According to "Environmental Life Cycle Assessment of Cadmium Telluride Solar Cells: Cd Emissions", emissions of Cd can only happen during an accidental fire.  Experiments have been conducted with fire and almost none of the Cd (0.04%) was actually released into the environment.

Below are some risks associated with everyday life, where risks are prevalent.

Some common uses of Cd that pose a risk include:

- Ni-Cd batteries – these batteries use Cd, which is less stable than CdTe.
- Coal & Petroleum – Coal and petroleum both contain Cd and it is emitting during burning.
- Plastic – Cd is used as a stabilizer and for pigments in plastics.

**Dewberry**

According to "The Health Risks of Cadmium in Cigarette Smoke":

- Cadmium is present in water and foods because it is naturally occurring in water and soils.
- Per the EPA, a safe level of Cadmium in drinking water is 5 ppb (parts per billion).
- Cadmium occurs naturally in food: it is highest in vegetables, potatoes, meats, shellfish
- Most foods in US contain 2 to 40 ppb.
- Single cigarettes contain 1-2 mcg (micrograms) of Cadmium and produce 1,000 – 3,000 ppb in the smoke that is emitted. For each pack of cigarettes, the body will absorb approximately 1-3 mcg of cadmium.
- It is estimated that the average person also ingested 30 mcg of Cadmium per day. The body only retains about 1-3 mcg of what it ingests.

Recommendations

It is Dewberry's recommendation that the applicant be required to perform soil screenings for cadmium and other heavy metals prior to construction as a baseline in accordance with Virginia Department of Environmental Quality's (VDEQ) requirements. Consideration of a testing program during the lifetime of the solar facility should be implemented in the event that panels are broken with potential for Cadmium release into the soil. Periodic screening of soils should be considered for levels to insure that the levels are in accordance with VDEQ standards. The standards shall include testing procedures, inspection protocol and reporting procedures to the County and VDEQ. Provisions shall also be included for notification to the County and VDEQ for witnessing, if warranted.

**HEAT ISLAND EFFECT REVIEW**

Dewberry conducted a review of the "Heat Island Executive Summary" provided by s-Power. The following research information was provided and is included for your review:
[1] "Solar panels reduce both global warming and urban heat island"; Frontiers in Environmental Science, June 4th, 2014
[2] "The Photovoltaic Heat Island Effect: Larger solar power plants increase local temperatures"
[3] "Analysis of the Potential for a Heat island Effect in Large Solar Farms",
[4] "Impacts of land use land cover on temperature trends over the continental United States: Assessment using the North American Regional Reanalysis", Souleymane Fall, et al., International journal of climatology, 2009.
[5] "Ecological Climatology", Gordon Bonan, 2nd ed., New York: Cambridge University Press. 550 pp. ch. 13 on surface energy fluxes, 2008. (not included)
[6] "Washington Solar Project Local Heating", Dr. Clinton J. Andrews, Rutgers University, 09/09/2012

A "heat island" effect refers to an increase in the ambient temperature due to a change in land use. This is common in urban environments, but the same effect will occur within solar farms. This is referred to as the Photovoltaic Heat Island (PVHI) effect. Temperature increase is mainly attributed to:
- **Removal of Vegetation**
  a. **Shading is decreased**. Direct sunlight heats up soils and surroundings
  b. **Evapotranspiration is decreased**. Plants and trees are removed, which use heat to evaporate water.

- **Albedo Decrease**
    a. Albedo, the proportion of light reflected to light absorbed, increases. For example, asphalt paving, building materials, dark covered roofs, solar panels, etc. All have very low albedo (highly absorptive). There is more available energy to be re-radiated as heat, which attributes an increase in overall temperature.
- **Thermal Mass Increases**
    a. Urban building materials such as asphalt paving, bricks, and roofs retain heat well, which in turn releases thermal energy slowly.

Questions have been raised by Spotsylvania County regarding any significant adverse impact on neighboring properties.

The effect of the heat island can be described by considering an energy balance at the Earth's surface [5]. When land use is altered in any of the manners described above, the energy balance of the area changes. This can cause an increase in sensible heat in the area. The net radiation from the sun at the Earth's surface is equal to the sensible, latent, and conductive heat fluxes.

Net radiation (power absorbed) is uncontrollable and is strongly influenced by albedo. Albedo values for solar panels are comparable to the pre-existing conditions on the Spotsylvania site. Values for panels range from 0.16-0.27, where trees and grass range from 0.15 – 0.26, respectively [4]. This results in a similar amount of net radiation at the Earth's surface. This is different than asphalt for example, in which albedo can be as low as 0.04 (more absorption).

Conductive heat flux describes heat conducted to the ground. Shading is very important in preventing the ground from heating up which in turn increases conductive heat flux. For example, fallow agricultural land will have greater conductive heat flux from the ground than a solar farm because it is under direct sunlight. For a solar farm, shading provided by panels lowers this term which will result in more sensible heat. However, this increase is not 1:1 because not all radiation hits the ground.

In the case of Spotsylvania, the spacing of the panels from each other (rather than a solid mass of panels) encourages conductive heat flux in open areas which in turn will lower overall sensible heat. Also, trees provide significant shading of the ground currently. Thus, there will be little if no change in the conductive heat flux in the overall area.

Latent heat flux describes heat used by plants and trees for evapotranspiration. Dense vegetation that absorb soil moisture and increase the amount of latent heat flux by the means of evapotranspiration. The heat island effect in Spotsylvania will benefit greatly from grasses growing underneath panels that provide latent cooling. Encouraging latent heat flux in the area as much as possible proves very useful as a mitigation strategy.

Thermal mass of the panels should also be noted. Panels have low thermal mass as compared to soils, meaning that they do not retain heat very well. They will lose heat quickly, so a prolonged sense of heat will not be carried out into the evening and night time. This will not create a consistent increase in temperature of the area which would suggest a micro-climate.

Temperature increases have been observed within solar farms, but increased temperatures dissipate as distance from the panel's increases. Heat will dissipate in a manner similar to that of light or sound. In an idealized situation where there is no interference with surroundings, the strength of a power source

will decreases exponentially as distance increases. Exact quantification can be complex due to wind, spatial orientation, and surroundings. However, this describes the way heat will dissipate into the air. Buffers should be placed at the point where the rate of temperature decrease minimizes.

Dewberry has reviewed s-Power's heat island executive summary and supporting information. The following PVHI effects were observed:

- Temperatures within and around the solar farm were consistently higher than the surroundings. Temperatures within the solar farms could be as much as 4 degrees higher.
- Reference [3] quantifies heat dissipation. Temperatures decrease to within a degree within the first 330 ft. of horizontal distance. Temperatures return to ambient at a height of 60 ft. above the panels.
- Module temperatures can rise to 36 °F above ambient during the day, and cool to ambient temperatures by sunset.

Dewberry previously conducted a study on the impact of a solar farm on local heating on a previous project in Washington, NJ. This provided insight into the results provided in s-Power's executive summary. It is attached to the appendix for review. The following was observed:

- Temperatures were several degrees higher directly above the panels within the solar farm
- Temperatures decreased to ambient at the perimeter of the solar farm.

Based on our understanding, the results of the data provided by s-Power makes good criteria to follow for the design for the following reasons:

- Desert areas have little to no vegetative coverage, resulting in a lower amount of latent heat flux in the area.
- Conductive heat flux in the desert will be lower, due to the shading provided by panels.
- Desert areas receive higher solar irradiance (power per area) which increases the overall energy input/output of the balance.

Mitigation Strategies & Recommendations
Typical mitigation strategies against the effect of a PVHI involve minimizing change to the energy balance. This is encouraged by providing dense vegetation of the area around and underneath the panels to maximize latent heat flux contribution to the area to lower sensible heat. Increased setbacks and planted buffers help control any impact on residential properties.

s-Power has proposed the following mitigation strategies within their summary:

- A minimum setback of 250 ft. from the residential properties of Fawn Lake
- s-Power will maintain and/or install vegetative buffers and berms that will reduce heat emanating from the arrays through absorption.

Dewberry offers the following recommendations based on the independent research and s-Power's executive summary:

- The setbacks from the properties of Fawn Lake be increased to 350 ft., matching the results found in reference [3].
- The vegetative buffers and berms must be installed with shade trees as well as shrubs and to create a dense screen and maximize absorption of any radiative heat.
  - Buffers must be maintained and a maintenance plan should state procedures for removal and replacement.

**Dewberry**

- • Vegetative coverage in the area must be maximized. Dense grasses that grow well in shade should be used throughout the site. This will help mitigate evapotranspiration and heat absorbed by soils. A comprehensive landscaping coverage plan should be required.

Dewberry reserves the right to present additional comments following public hearing testimony and/or receipt of revised plans. If you have any questions regarding the contents of this letter, or require additional information, please contact the undersigned.

Very truly yours,

**Dewberry Engineers Inc.**

EVAN D. HILL, P.E., C.M.E.*
*Associate/Department Manager, Site/Civil Services*
*\*Licensed in NJ, PA & DE*

cc:   Board Members
       Applicant's Engineer
       Applicant's Attorney
       Applicant

# Cadmium Telluride – The Good and the Bad

**Cadmium telluride (CdTe)** is a photovoltaic (PV) technology based on the use of a thin film of CdTe to absorb and convert sunlight into electricity. CdTe is growing rapidly in acceptance and now represents the second most utilized solar cell material in the world. The first is still silicon.
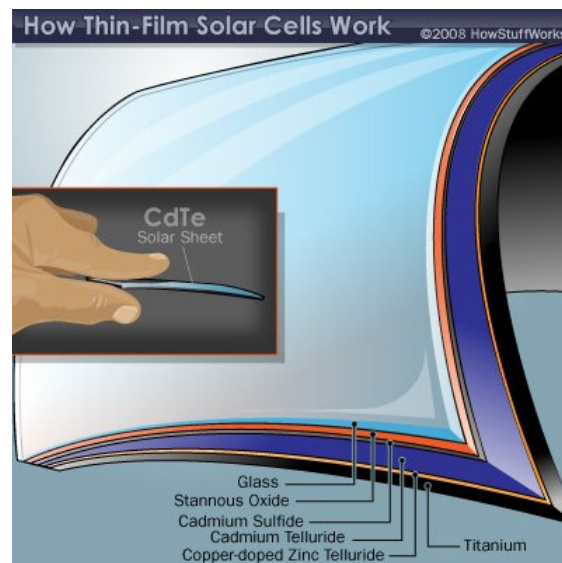


Solar panels based on CdTe are the first and only thin film photovoltaic technology to surpass crystalline silicon PV in cheapness for a significant portion of the PV market, namely in multi-kilowatt systems.

## History

Research in Cadmium telluride dates back to the 1950's because it is almost perfectly matched to the distribution of photons in the solar spectrum in terms of optimal conversion to electricity. Early leaders in CdS/CdTe cell efficiencies were General Electric in the 1960s, and then Kodak, Monosolar, Matsushita, and AMETEK.

Professor Ting L. Chu of Southern Methodist University and subsequently of University of South Florida, Tampa, made significant contributions to moving the efficiency of CdTe cells to above 15% in 1992, a critical level of success in terms of potential commercial competitiveness. This was the first thin film to reach this level, as verified at the National Renewable Energy Laboratory (NREL).

Matsushita claimed an 11% module efficiency using CSS and then dropped out of the technology, perhaps due to internal corporate pressures over cadmium which is highly toxic. A similar efficiency and fate eventually occurred at BP Solar, which dropped the technology in the early 2000s.

## Cell efficiency

Best cell efficiency has plateaued at 16.5% since 2001 (a record held by NREL). The opportunity to increase current has been almost fully exploited, but more difficult challenges associated with junction quality, with properties of CdTe and with contacting have not been as successful.

Improved doping of CdTe and increased understanding of key processing steps (e.g., cadmium chloride recrystallization and contacting) are key to

improving cell efficiency. Since CdTe has the optimal band gap for single-junction devices, it may be expected that efficiencies close to exceeding 20% (such as already shown in CIS alloys) should be achievable in mass produced CdTe cells.

In 2009, EMPA, the Swiss Federal Laboratories for Materials Testing and Research, demonstrated a 12.4% efficient solar cell on flexible plastic substrate.

## Low Cost Manufacturing

The major advantage of this technology is that the panels can manufactured at lower costs than silicon based solar panels. First Solar was the first manufacturer of Cadmium telluride panels to produced solar cells for less than $1.00 per watt.

Some experts believe it will be possible to get the solar cell costs down to around $0.5 per watt. With commodity-like margins and combined with balance-of-system (BOS) costs, installed systems near $1.5/W seem achievable. With sufficient levels of sunlight – this would allow such systems to produce electricity in the $0.06 to $0.08 / kWh range – or for less than fuel based electricity costs.

## Advantages of Cadmium Telluride Solar Panels

CdTe panels have several advantages over traditional silicon technology. These include:

1. Ease of manufacturing: The necessary electric field, which makes turning solar energy into electricity possible, stems from properties of two types of cadmium molecules, cadmium sulfide and cadmium telluride. This means a simple mixture of molecules achieves the required properties, simplifying manufacturing compared to the multi-step process of joining two different types of doped silicon in a silicon solar panel.

2. Good match with sunlight: Cadmium telluride absorbs sunlight at close to the ideal wavelength, capturing energy at shorter wavelengths than is possible with silicon panels

3. Cadmium is abundant: Cadmium is abundant, produced as a by-product of other important industrial metals such as zinc, consequently it has not had the wider price swings that have happened in the past two years with silicon prices.

## Cadmium telluride drawbacks

While price is a major advantage, there are some drawbacks to this type of solar panels, namely:

1. Lower efficiency levels: Cadmium telluride solar panels currently achieve an efficiency of 10.6%, which is significantly lower than the typical efficiencies of silicon solar cells.

2. Tellurium supply: While Cadmium is relatively abundant, Tellurium is not. Tellurium (Te) is an extremely rare element (1-5 parts per billion in the Earth's crust. According to USGS, global tellurium production in 2007 was 135 metric tons. Most of it comes as a by-product of copper, with smaller byproduct amounts from lead and gold. One gigawatt (GW) of CdTe PV modules would require about 93 metric tons (at current efficiencies and thicknesses), so the availability of tellurium will eventually limited how many panels can be produced with this material.

Since CdTe is now regarded as an important technology in terms of PV's future impact on global energy and environment, the issue of tellurium availability is significant. Recently, researchers have added an unusual twist – astrophysicists identify tellurium as the most abundant element in the universe with an atomic number over 40. This surpasses, e.g., heavier materials like tin, bismuth, and lead, which are common. Researchers have shown that well-known undersea ridges (which are now being evaluated for their economic recoverability) are rich in tellurium and by themselves could supply more tellurium than we could ever use for all of our global energy. It is not yet known whether this undersea tellurium is recoverable, nor whether there is much more tellurium elsewhere that can be recovered.

However, as I was doing research for this article I found more than one article (in mining publications) that suggested that the capacity for manufacturing thin-film photovoltaic solar cells from cadmium telluride is very close to the maximum supply of tellurium available, or that may become available and that the ability of companies like First Solar to

continue to expand at the rates they have been growing at over the past several years will become increasingly difficult to maintain because of lack of available tellurium (even with recovery from recyclying).

3. <u>Toxicity of Cadmium</u>

Cadmium is one of the top 6 deadliest and toxic materials known. However, CdTe appears to be less toxic than elemental cadmium, at least in terms of acute exposure.

This is not to say it is harmless. Cadmium telluride is toxic if ingested, if its dust is inhaled, or if it is handled improperly (i.e. without appropriate gloves and other safety precautions). The toxicity is not solely due to the cadmium content. One study found that the highly reactive surface of cadmium telluride quantum dots triggers extensive reactive oxygen damage to the cell membrane, mitochondria, and cell nucleus. In addition, the cadmium telluride films are typically recrystallized in a toxic compound of cadmium chloride.

The disposal and long term safety of cadmium telluride is a known issue in the large-scale commercialization of cadmium telluride solar panels. Serious efforts have been made to understand and overcome these issues. Researchers from the U.S. Department of Energy's Brookhaven National Laboratory have found that large-scale use of CdTe PV modules does not present any risks to health and the environment, and recycling the modules at the end of their useful life resolves any environmental concerns. During their operation, these modules do not produce any pollutants, and furthermore, by displacing fossil fuels, they offer great environmental benefits. CdTe PV modules appear to be more environmentally friendly than all other current uses of Cd.

The approach to CdTe safety in the European Union and China is however, much more cautious: cadmium and cadmium compounds are considered as toxic carcinogens in EU whereas China regulations allow Cd products for export only. The issue about regulating the use of Cadmium Telluride is currently being discussed in Europe.

At the present time – the most common opinion is that the use of Cadmium Terlluride in residential / industrial rooftop installations does not pose a major environmental problem.

However, some groups have expressed concern about large utility sized projects in the desert and the possibility of release of cadium gases or water table contamination. <u>Click here to read more about this subject.</u>

## Ongoing Research

Research on CdTe research focuses on several of today's challenges:

1. Boosting efficiencies by, among other things, exploring innovative transparent conducting oxides that allow more light into the cell to be absorbed and that collect more efficiently the electrical current generated by the cell.

2. Studying mechanisms such as grain boundaries that can limit the voltage of the cell.

3. Understanding the degradation that some CdTe devices exhibit at contacts and then redesigning devices to minimize this phenomenon.

4. Designing module packages that minimize any outdoor exposure to moisture.

5. Engaging aggressively in both indoor and outdoor cell and module stress testing. For example, we propose to test thin-film modules in hot and humid climates.

Click on the appropriate link to return to the top of this page about <u>Cadmium Telluride technology</u> or to return to the previous section about <u>Thin Film Technologies.</u>

**Share this page:**
<u>What's this?</u>

Facebook    Twitter    Google
Pinterest    Tumblr    Reddit

<u>Enjoy this page? Please pay it forward. Here's how...</u>

# Chemistry Learner

**It's all about Chemistry**

Home
Inorganic chemistry
Materials chemistry
Organic chemistry
Periodic Table

**Home / Inorganic chemistry** / Cadmium Telluride

# Cadmium Telluride

**Cadmium** Telluride is a cadmium-**tellurium** compound. This crystalline compound is mainly used as a solar-cell material and an infrared optical window. It is highly suitable for solar energy conversion. Cadmium Telluride is highly toxic as it contains cadmium.

**TABLE OF CONTENTS**

## Cadmium Telluride Identification

**CAS number:** 1306-25-8

**ChemSpider:** 82622

**TRENDING TOPICS**

**Markovnikov's Rule**

Table Of ContentsWhat Is the Markovnikov's RuleWhat Is the Markovnikov's Rule The...

**Radium-223**

Table Of ContentsWhat is Radium-223What is Radium-223 Radium-223 is a radioactive...

**Aluminum**

Table Of ContentsWhat is AluminumWhat is Aluminum Aluminum (pronounced as ah-LOO-men-em)...

**Rutherfordium**

Table Of ContentsWhat is RutherfordiumWhat is Rutherfordium Rutherfordium (pronunciation...

**Silver**

Table Of ContentsWhat is SilverWhat is Silver Silver (pronounced as SIL-ver) is a...

**Hydrogen**

Table Of ContentsWhat is HydrogenWhat is Hydrogen Hydrogen (pronounced as Hi-dreh-jen)...

**Sodium**

Table Of ContentsWhat is SodiumWhat is Sodium Sodium (pronunciation SO-dee-em [2]),...

**Palladium**

Table Of ContentsWhat is PalladiumWhat is Palladium Palladium (pronunciation peh-LAY-dee-em...

**Titanium**

Table Of ContentsWhat is TitaniumWhat is Titanium Titanium (pronunciation: ti-TAY-nee-em)...

**Lithium**

Table Of ContentsWhat is LithiumWhat is Lithium Lithium (pronounced as LITH-ee-em)...

## Cadmium Telluride Preparation

Purified cadmium and tellurium is combined in stoichiometric proportions in order to produce Cadmium Telluride. The reaction is done in an evacuated Vycor tube. Thin films of this compound accumulate between Aquadag electrodes in the Dewar-type tubes.

**Picture 1 –** Cadmium Telluride

## Cadmium Telluride Chemical Formula

The formula for this crystalline compound is CdTe.

## Cadmium Telluride Properties

Here are some of the physical, chemical and thermal properties of this material:

**Appearance:** it is a black crystalline powder.

**Odor:** It is odorless.

**Solubility:** This is an insoluble material.

**Molar Mass:** The molar mass of this substance is 240.01 g/mol.

**Melting Point:** It has a melting point of 1092 °C.

**Boiling Point:** Its boiling point is 1130 °C.

**Density:** The density of this compound is 6.2 g/cm$^3$.

**Vapor Pressure:** Its vapor pressure is 0.4 mmHg at 760 °C.

**Crystal Structure:** It has a zincblende crystal structure.

**Band Gap:** The band gap of this compound is 1.44 eV (at 300 K, direct).

**Thermal Conductivity:** Its thermal conductivity is 6.2 W/m·K at 293 K.

**Specific Heat Capacity:** The specific heat capacity of this crystalline compound is 210 J/kg·K at 293 K temperature.

**Thermal Expansion Coefficient:** 5.9×10−6/K at 293 K.

**Lattice Constant:** 0.648 nm at 300K

**Young's Modulus:** 52 GPa

**Poisson Ratio:** 0.41

**Refractive Index:** 2.67 (at 10 μm)

## Cadmium Telluride Uses

This material is used for various industrial purposes despite its toxicity. Different uses of Cadmium Telluride include:

**Solar Cells:** It is used for making highly efficient and low cost thin film solar cells. Its physical characteristics are ideal for this purpose. These cells usually use the n-i-p structure. Around 6% of the total solar cells installed in 2010 use this compound. The band gap of this compound can be easily perfected using various low cost methods. In 2010, this material was used for producing around 1.5 GW$_P$ solar cells. Increasing use of Cadmium Telluride in solar cells can result in a dearth of Tellurium which is one of the rarest elements found on earth.

**Infrared Detector:** It is alloyed with **mercury** for making infrared detector materials. Cadmium Telluride-zinc alloy is excellent for solid state gamma ray and X ray detector. Small amounts of zinc are used for making Cadmium zinc telluride alloy.

**Optical Windows and Lenses:** It is sometimes used as optical materials for infrared optical windows and lenses. However, this application is limited due to the toxicity of this compound. Earlier, this compound was marketed under the trademarked name "Irtran-6" which now obsolete.

**Electro-Optic Modulators:** Its electro-optic coefficient of linear electro-optic effect is the greatest among all II-VI compound crystals. This makes it useful in electro-optic modulators.

**Radiation Detectors:** Cadmium Telluride is doped with **chlorine** for the purpose of using it as a radiation detector for Alpha and beta particles, X rays and gamma rays. It has various applications in the field of nuclear spectroscopy as it can function at room temperatures. The large band gap, high atomic number and high electron mobility makes it suitable for making high performance X ray and gamma ray detectors.

## Cadmium Telluride Advantages and Disadvantages

There are some advantages and disadvantages of using this crystalline compound. The advantages make it highly useful in different industries while the disadvantages limit its uses in many ways.

### Advantages

- The manufacturing process is simpler than that of many other similar materials.

- It can absorb sunlight at an almost ideal wavelength. It captures energy at a shorter wave length than **silicon** panels.

- The abundance of cadmium is another advantage of this compound. Cadmium is easily produced as a by-product of other important metals like zinc.

### Disadvantages

- The Cadmium Telluride solar panels attain low efficiency levels of only around 10.6%. It is considerably lower than that of silicon solar cells.

- The extreme rarity of tellurium is another obstacle in the applications of this cadmium- tellurium compound. Tellurium is counted among the rarest material found in earth's crust. This fact limits the number of panels made each year using this material.

- The high toxicity level of Cadmium Telluride is another disadvantage of applying it many purposes.

## Cadmium Telluride MSDS

This compound can cause serious health problems in case of inhalation and ingestion. Direct skin contact may also be harmful for humans. It is important to take necessary precautions while handling this toxic material.

### Toxicology

Cadmium is considered to be one of the six most toxic materials know to humans. It is the main cause for the toxicity of Cadmium Telluride. However, this compound is much less toxic than cadmium metal. There is another reason behind the toxic properties of this cadmium- tellurium compound. According to one study, the high reactivity of this substance triggers **oxygen** damage to living cell membrane, nucleus and mitochondria. The Cadmium Telluride films typically re-crystallize into toxic cadmium chloride solution.

### First Aid Measures

**Eye Contact:** It can cause severe eye irritation in case of direct eye contact. One should remove any contact lenses and flush the eyes with plenty of lukewarm water at least for 15 minutes. It is important to get immediate medical assistance.

**Skin Contact:** Victim should immediately wash the contaminated area with a disinfectant soap and plenty of water. The infected clothes and shoes should be removed and washed properly before re-use. Prolonged or repeated exposure can even cause dermatitis. One should obtain medical attention immediately.

**Inhalation:** Accidental Inhalation can cause chest pain, cough, irritation of the respiratory system and weakness. The victim should be removed to fresh air. Tight clothing such as collar, belt and tie should be loosened. Oxygen or artificial respiration should be provided if the victim is experiencing breathing difficulty. Performing mouth-to-mouth resuscitation can be hazardous for the person providing the aid. The tellurium content can cause garlic-like odor in the breath and perspiration in case of acute exposure. It can also cause dry mouth, loss of appetite, sleepiness and nausea. Severe inhalation may even result in pulmonary edema and death. Immediate medical attention is required.

**Ingestion:** Accidental ingestion of this toxic material can cause vomiting, diarrhea, abdominal cramps and nausea. Acute ingestion may also cause garlic-like odor in the breath and perspiration. It is not advisable to induce vomiting without proper medical guidance. The victim should drink 1 to 2 glasses of water to dilute the toxic compound. One should never give anything by mouth if the victim is unconscious. It is important to obtain medical aid as soon as possible.

## Personal Safety Measures

NIOSH approved lab coat, dust respirator, protective gloves and safety goggles should be used for proper personal protection.

## Fire Fighting Measures

It is a non-flammable substance. However, it decomposes and emits toxic fumes when heated. Firefighters should use proper fire fighting gear and protective clothing and full faced self-contained breathing apparatus while extinguishing a fire around it.

## Storage Instruction

It should be stored in tightly sealed containers in cool, dry and well ventilated areas.

## Accidental Release Measure

The spilled material should be covered with dry sand to prevent it from spreading in a wider area. The spillage should be transferred to a labeled and tightly sealed metal container. The spillage area should be washed properly with soap and water.

## Waste Disposal

One should consult the local, state and federal laws in order to dispose of this toxic compound.

# Cadmium Telluride Availability

Cadmium and tellurium are much more affordable compared to the solar cells and other Cadmium Telluride devices. However, tellurium is not as easily available as cadmium.

Cadmium Telluride is among the most useful compounds used in various industries. The advantages offered by this crystalline compound make it useful for many applications. Despite the disadvantages, it is widely used for various purposes.

**References**:

http://en.wikipedia.org/wiki/Cadmium_telluride

http://www.solar-facts-and-advice.com/cadmium-telluride.html

http://www.wolframalpha.com/input/?i=Cadmium+Telluride

http://www.cadmiumtelluride.net/

http://www.testbourne.com/im/pdf/material-safety-data-sheets/Cadmium-Telluride-CdTe.pdf

**You Might Also Like**                                                                 ?

# ENVIRONMENTAL LIFE CYCLE ASSESSMENT OF CADMIUM TELLURIDE SOLAR CELLS: Cd EMISSSIONS

**Article** · January 2004

**1 author:**

Vasilis Fthenakis
Brookhaven National Laboratory
**197** PUBLICATIONS **4,578** CITATIONS

SEE PROFILE

# ENVIRONMENTAL LIFE CYCLE ASSESSMENT OF CADMIUM TELLURIDE SOLAR CELLS: Cd EMISSSIONS

Vasilis M. Fthenakis

[1] National Photovoltaic Environmental Research Center, Department of Environmental Sciences,
Brookhaven National Laboratory, Upton, NY 11973
*email: vmf@bnl.gov; tel. (631)344-2830; fax (631)344-4486

ABSTRACT: This analysis focuses on cadmium flows and atmospheric emissions in the life cycle of cadmium telluride solar cells. New data in the mining/smelting and utilization phases were used. Published estimates were cross-referenced with current environmental impact reports from metal smelting facilities, and experimental investigations were conducted to quantify emissions during fires. It was estimated that the total of atmospheric emissions of cadmium during all the phases of the modules' life is about 0.02 g of Cd per GWh of electricity produced. These life-cycle emissions are two orders of magnitude lower than the controlled routine Cd emissions during the operation of modern coal-fired power plants.

   Keywords: CdTe, Environmental Effect, Manufacturing and Processing

## 1   INTRODUCTION

This assessment focuses on cadmium flows and emissions in the "cradle to grave" life cycle of cadmium telluride solar cells. It examines only the photovoltaic compounds (i.e. CdTe and CdS); other materials in the PV module (e.g., glass, EVA, metal contacts) are generic to all technologies and are not included. The prime focus is on cadmium flows and cadmium emissions in the environment. The life-stages of the cadmium compounds involve:1) production of raw materials (Cd and Te), 2) purification of Cd and Te, 4) production of CdTe, 5) manufacture of CdTe PV modules, 6) use of CdTe PV modules, and 7) disposal of spent modules. A detailed description of these phases can be found in a recent review article [1].

## 2. CADMIUM PRODUCTION

### 2.1 Mining

CdTe is manufactured from pure Cd and Te, both of which are byproducts of smelting prime metals (e.g., Zn, Cu, Pb, and Au). Cadmium minerals are not found alone in commercial deposits. The major cadmium-bearing mineral is sphalerite (ZnS), present in both zinc and lead ores. Cadmium is generated as a byproduct of smelting zinc ores (~80%), lead ores (~20%), and, to a lesser degree, of copper ores.
Zinc ores contain 3% to 11% zinc, along with cadmium, copper, lead, silver and iron, and small amounts of gold, germanium, indium, and thallium. The mean Cd concentration in the zinc ores is about 220 ppm. The concentration of zinc in the recovered ore (called beneficiating) is done by crushing, grinding, and flotation processes (Figure 1). These activities, if not adequately controlled could generate significant levels of dust. However, ASARCO and Cominco, two major metal producers, report that implement controls which minimize dust emisons. All of the mining, crushing, and grinding takes place underground and wet scrubbers and dry cyclones are utilized to collect the dust. Cominco uses a wet grinding proces resulting in a slurry from which,

reportedly, there are essentially no dust emisions [2]. Based on these reports and the range of emissions reported

in the literature, we determined that controlled emissions during mining are about 30g of dust per ton ore.
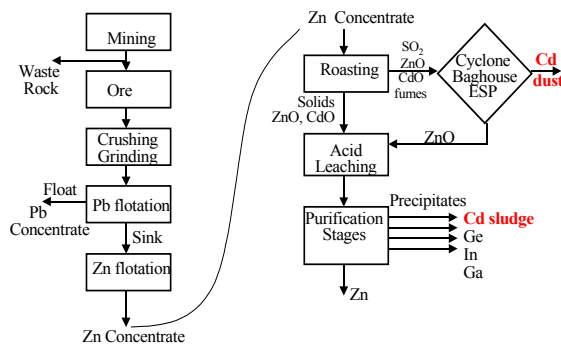


Fig. 1. Cd Flows in Zn mining and smelting

### 2.2 Smelting/Refining

The zinc and lead concentrates are transferred to smelters/refiners to produce the primary metals; sulfuric acid and other metals are frequent byproducts from most smelters. In addition to Zn, the mines in the United States also produce 100% of the Cd, Ge, In, and Th, 10% of Ga, 6 % of Pb, 4% of Ag and 3% of Au used in the country [3]. Since economic growth has steadily increased the demand for zinc for decades, impure cadmium is produced, regardless of its use. Before cadmium production started in the United States in 1907, about 85% of the Cd content of the zinc concentrates was lost in roasting the concentrate, and in the fractional distillation of Zn metal [4]. Zinc can be refined by either pyrometallurgical or hydrometallurgical treatment of its concentrates. The four primary zinc-smelting operations of the United States use electrolytic technology [5]. Older roast/retort smelters are no longer employed in North America and Northern Europe. Berdowski et al. [6] reported on the emissions from zinc-smelting operations in several countries. Cd emissions vary widely depending on the ore used and the abatement measures applied. The

shift from pyrometallurgical to electrolytic processing has drastically reduced cadmium emissions (Table 1). The most recent data show 0.2 g Cd per ton of Zn product for North American and European Union countries [6, 7]. This numbers agrees with the emisssions reported for 2002 in one of the largest smelters of the world, the Trail, Canada Teck Cominco facility [8]. The air emissions of Cd in this facility have reportedly decreased by 84% between 1999 and 2002. The electrolytic zinc process consists of five main operations, roasting, leaching, purification, electrodeposition and melting/casting. Details of these operations can be found elsewhere [1].

Table 1. Cadmium Emissions from Old and New Zinc-Production Processes

| Process | Cadmium Emissions | |
|---|---|---|
| | g Cd /ton Zn | (% Cd Loss) |
| Roast/leach/ electrowinning | 0.2 | (0.008 %) |
| Roast/blast furnace smelting (replaced in Canada & Europe) | 50 | (2 %) |
| Roast/blast furnace smelting (not in use any more) | 100 | (4 %) |

The feed material for producing cadmium consists of residues from the electrolytic production of zinc, and of fume and dust, collected in baghouses from emissions during roasting [5]. Wastewater produced from leaching, purification and electrowinning usually is treated and re-used, with a small fraction of it discharged. Solid wastes include slurries from the sulfuric-acid plant, sludge from the electrolytic cells and copper cakes, and the byproducts of zinc production from the purification cells which contain cadmium, germanium, indium, and other metals. Purification byproducts and other solid wastes are recycled or stockpiled until they can be economically used.

Thus, Cd is a byproduct of zinc and lead and is collected from the emissions and waste streams of these major metals. Emissions in joint production of metals are allocated according to the International Standard Organization procedure ISO 14041, in proportion to the mass output or to the economic output of Zn, Cd, Ge and In from the smelters. The allocation to Cd ranged was 0.50% and 0.58% depending on the criterion employed [1]. These percentages are applied to emissions from mining and smelting, whereas, in the subsequent steps, 100% of the emissions are allocated to cadmium.

2.3 Cadmium Production from Zinc Electrolyte Purification Residue

The cadmium sponge, a purification product from precipitating zinc sulfate solution with zinc dust at the zinc smelter, is 99.5% pure cadmium. This sponge is

transferred to a cadmium recovery facility where it is oxidized in steam. Cadmium oxide, the product, is leached with spent cadmium electrolyte and sulfuric acid to produce a new recharged electrolyte. Impurities are precipitated with a strong oxidizing agent. The cathodes are removed once a day and are rinsed and stripped. The stripped cadmium is melted under flux or resin and cast into shapes. In a slightly different route, purification residues from the oxide and the sulfide-leaching processes are further leached with sulfuric acid and filtered through three stages to remove zinc, copper, and thallium before recovering the dissolved cadmium. Cadmium can be further purified with vacuum distillation to 99.9999% purity [8].

2.4. Purification of Cadmium and Production of CdTe

Metallurgical grade (i.e., 99.99% pure) metal is used in all current applications except for semiconductor materials that require higher purity. Purification residues from leaching plants undergo additional leaching with sulfuric acid and are filtered though three stages to remove zinc, copper, and thallium. The final step is vacuum-distillation [8]. High purity Cd and Te powders from other manufacturers are produced by electrolytic purification and subsequent melting and atomization (Figure 2), or by vacuum distillation.
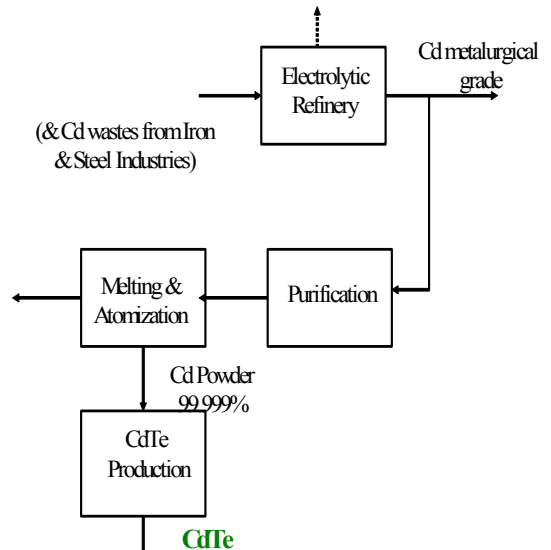


Fig. 2. Cd Flows from Cd Concentrates to CdTe

Both methods are proprietary and information about emissions is not published. Electrolytic purification does not produce any gaseous emissions. The melting and atomization steps needed to form the powder produce about 2% emissions that are captured by HEPA filters.

The efficiency of HEPA filters in collecting particulates of mean diameter of 0.3 μm is 99.97%.

## 3. MANUFACTURING OF CdTe PHOTOVOLTAICS

Currently, the leading methods of making CdTe/CdS thin films is high-rate vapor transport, in which CdTe and CdS are deposited from the compounds in powder form after vaporization in a close-spaced reactor. The current material utilization rates range from 35% to 70%, but higher utilization rates are expected in optimized scaled-up production. Most of the unused vapors condense on the reactor's walls or rollers from where they are removed periodically; recycling of the residuals is both feasible and economic. Approximately 1% of the vapors are carried in the exhaust stream; these are collected at 99.97% efficiencies[1] using HEPA filters. The controlled Cd emissions correspond to 6 g per ton of Cd used in CdTe feedstock.

## 4. OPERATION OF CdTe PV MODULES

Thin-film α-Si, CdTe, and CIGS solar cells are durable and do not produce any emissions during extreme conditions of accelerated aging in thermal cycles from +80 °C to -80 °C [9]. Every PV generation, regardless of technology, is a zero-emissions process. Emissions could only be produced accidentally, if the metals are emitted during a fire. The fire effect on glass-to-glass encapsulated CdTe modules was recently investigated with emissions analysis and synchrotron x-ray fluorescence microprobe analysis of the molten glass and the results are presented by Fthenakis et al. in paper 5BV.1.32 of this conference. In these experiments CdTe was captured in the molten glass and almost none (~0.04%) was released.

## 5. END-OF-LIFE DISPOSAL OR RECYCLING

PV modules are expected to last 25 to 30 years. Should the modules at the end of their useful life end up in municipal landfills or incinerators, heavy metals could be released into the environment. CdTe PV modules that pass leaching criteria for non-hazardous waste could be disposed of in landfills, according to current laws. The leachability of metals in landfills currently is characterized by elution tests such as the US-EPA Toxicity Characterization Leachate Profile (TCLP), and the German DEV S4 (Deutsches Einheitsverfahren). Previous studies showed that PV recycling is technologically and economically feasible, although complete separation of Cd from the other metals of the module has not been accomplished yet [10,11]. Metals from used solar- panels in large centralized applications can be reclaimed in metal-smelting facilities, which use glass as a fluxing agent and recover most of the metals by incorporating them into their product streams. For dispersed operations and small-scale recycling, hydrometallurgical separations are economical [12]. A valid assumption is that CdTe PV modules will be either recycled or properly disposed off at the end of their

useful life; therefore atmospheric emissions during/after decommissioning will be zero. Even if pieces of modules inadvertently make it to a municipal waste incinerator, cadmium will likely dissolve in the molten glass and would become part of the solid waste.

## 6. DISCUSSION

Our most likely estimates of atmospheric cadmium emissions during all the phases of the life of CdTe PV modules are shown in Table 2.

Our reference estimate of total air emissions is 0.02 g Cd/GWh of electricity produced, which is 25 times lower than the estimate (i.e., 0.5 g Cd/GWh] reported in an early study [13]. The main contributor to Cd air emission in the later assessment was PV utilization, under the assumption of Cd loss during fires. However, recent experimental tests proved that Cd is not emitted during fires. Also, our assessment uses more up-to-date assumptions and detailed calculations for determining emissions during mining, smelting/refining, and decommissioning of end-of-life products. It is interesting to compare Cd flows in CdTe PV with those in Ni-Cd batteries and coal-burning power plants. These comparisons are given in [1] and are summarized below:

Cadmium in Ni-Cd batteries is in the form of Cd and Cd $(OH)_2$, materials which are less stable and more soluble than CdTe. Based on data from the NiCd battery industry, a battery would produce an average of 0.046 kWh per g of its weight, which corresponds to 0.306 kWh per g of Cd contained in the battery. This is a 2500 times lower efficiency in using Cd than in a CdTe PV module.

Coal and oil-burning power plants, routinely produce Cd emissions (since Cd exists in both coal and petroleum), whereas CdTe PV does not emit anything during operation. According to data from the U.S. Electric Power Research Institute (EPRI), under the best/optimized operational and maintenance conditions, burning coal for electricity releases into the air generates a minimum of 2 g to 7.2 g of Cd per GWh (assuming well-maintained electrostatic precipitators or baghouses operating at 98.6% efficiency, and median concentration of Cd in US coal of 0.5 ppm (median) and 1.8 ppm (average) [14]. It is noted, that although very high effectiveness is expected for ESPs operating in North American Western European and Japanese power plants, ESPs are much less effective, if they are installed at all, in developing, coal-burning countries. In addition, 140 g/GWh of Cd inevitably collects as fine dust in boilers, baghouses, and ESPs, thereby posing occupational health- and environmental-hazards. Furthermore, a typical US coal-power plant emits per GWh about 1000 tons of $CO_2$, 8 tons of $SO_2$, 3 tons of NOx, and 0.4 tons particulates.

A last point is that cadmium is produced anyway as a byproduct of zinc production, and it can either be put to *beneficial* uses or *discharged* into the environment. When the market does not absorb the Cd generated by metal

---

[1] For particles of 0.3 μm or larger

smelters/refiners, it is cemented and buried, stored for future use, or disposed of to landfills as hazardous waste. Arguably, encapsulating cadmium as CdTe in PV modules is much more environmentally-friendly than all its current uses and disposal.

Table 2. Atmospheric Cd Emissions from the Life-Cycle of CdTe PV Modules

| Process | Total Emissions (g Cd/ton Cd*) | Allocated Air Emissions (g Cd/ton Cd) | (mg Cd/m2) | (mg Cd/GWh) |
|---|---|---|---|---|
| 1. Mining of Zn ores | 2.7 | 0.0157 | 0.0001 | 0.02 |
| 2. Zn Smelting/Refining | 40 | 0.2320 | 0.0016 | 0.30 |
| 3. Cd purification | 6 | 6 | 0.042 | 7.79 |
| 4. CdTe Production | 6 | 6 | 0.042 | 7.79 |
| 5. CdTe PV Manufacturing | 3 | 3 | 0.021 | 3.90 |
| 6. CdTe PV Operation | 0 | 0 | 0.0003 | 0.06 |
| 7. CdTe PV Disposal/Recycling | 0 | 0 | 0 | 0.00 |
| TOTAL EMISSIONS | | 15.25 | 0.11 | 20.40 |

*ton of Cd used in manufacturing
Assumptions:
1. Mining of zinc ores produces 3 g of dust per ton of ore
2. Smelting/refining of Zn produces 0.2 g of Cd per ton of Zn production
3. The ratio of Zn to Cd content of Zn ores is 200
4. The mean concentration of Cd in Zn ores is 220 ppm
5. Emissions allocation to Cd in mining/smelting is 0.58% [1]
6. HEPA filters have a 99.97% effectiveness in collecting submicron size particulates in PV manufacturing exhaust streams
7. Emissions per module area and energy output are based on:
7 g Cd/m$^2$ module; 10 % Electric conversion PV efficiency; Average US insolation (1800 kWh/m2/yr); 30 yrs PV module life expectancy, thus; 1 kg Cd produces 0.77 GWh over its life-time in PV.

7. REFERENCES

[1] Fthenakis V.M., Life Cycle Impact analysis of Cadmium in CdTe PV production Renewable and Sustainable Energy Reviews, 8(4), 303-334, 2004.
[2] US EPA. Compilation of air pollutant emission factors. AP-42, Section 12.18; Lead-Bearing Ore Crushing and Grinding, 1995.
[3] Andersson B. Materials availability for large-scale thin-film photovoltaics. Progress in Photovoltaics 2000; 8:61-76.
[4] Liewellyn T. Cadmium (material flow). Bureau of Mines Information Circular 1994, US Department of the Interior.
[5] US EPA. Compilation of air pollutant emission factors. AP-42, 5th Edition, Volume I: Stationary Point and Area Sources, Chapter 12: Metallurgical Industry 1995. http://www.epa.gov/ttn/chief/ap42/
[6] Berdowski J, van der Most P, Veldt C, Bloos J. Emissions Inventory Guidebook, Activity 030305, Primary Zinc Production, February 2003, Inspectorate for the Environment, Dept. for Monitoring and Information Management, Den Haag, The Netherlands.
[7] Pacyna J. Survey on heavy metal sources and their emission factors for the ECE countries. ECE Convention on Long-range Transboundary Air Pollution Working Group on Technology. Prague, 15-17 October 1991, 1990. p. 27-55.
[8] Description of Cominco Trail Operations/Emissions, April 2001. http://www.teck.com/environment/articles.htm
[9]. Fairbanks e., Gates M. Adaptation of thin film technology for use in space. 26th IEEE PV Specialist Conference, Anaheim, CA 1997.
[10] Fthenakis V, Eberspacher C, Moskowitz P. Recycling strategies to enhance the commercial viability of photovoltaics. Progress in Photovoltaics 1996; 4:447-456.
[11] Fthenakis V. End of life management and recycling of PV modules. Energy Policy Journal 2000; 28:1051-1058.
[12] Bohland J, Dapkus T, Kamm K, Smigielski K. Photovoltaics as hazardous materials: The recycling solution. Proceedings of the 2nd IEEE World Photovoltaic Specialists Conference, 1998. p. 716-719.
[13] Alsema E. Environmental aspects of solar cell modules. Summary Report. Modules. Department of Science, Technology and Society. Utrecht University, The Netherlands. Report 96074, ISBN 90-73958-17-2. 1996.
[14] Electric Power Research Institute (EPRI). PISCES data base for US power plants and US coal, Copyright EPRI 2002.

**verywell** mind

# The Health Risks of Cadmium in Cigarette Smoke

By Terry Martin ⓘ | Reviewed by Sanja Jelic, MD

Updated June 18, 2018

Cadmium is a toxic heavy metal that occurs in nature. Cadmium is also produced as a by-product of the process of smelting (heating and melting ores to extract metals). Cadmium is present in low levels in food, and in high levels in cigarette smoke.

## How Cadmium Is Used

Cadmium does not corrode easily, so it works well in batteries; its primary use. Cadmium is also used in metal plating, plastics, and textile manufacturing.

The most common form of cadmium exposure for the general population is through food and cigarette smoke.

## Cadmium in Food

Cadmium occurs naturally in many foods because it is present in the soil and water. Cadmium levels in most U.S. foods are between 2 and 40 parts per billion (2-40ppb). Fruits and beverages contain the least amount of cadmium, while leafy vegetables and raw potatoes contain the most. Shellfish, liver, and kidney meats are also high in cadmium.

It's estimated that of the 30 micrograms (mcg — millionths of a gram) of cadmium the average person ingests daily, 1-3 mcg is retained by the body.

## Cadmium in Cigarette Smoke

A single cigarette typically contains 1-2 mcg of cadmium. When burned, cadmium is present at a level of 1,000-3,000 ppb in the smoke. Approximately 40 to 60 percent of

the cadmium inhaled from cigarette smoke is able to pass through the lungs and into the body. This means that for each pack of cigarettes smoked, a person can absorb an additional 1-3 mcg of cadmium over what is taken in from other sources in their daily life. Smokers typically have twice as much cadmium in their bodies as non-smokers.

## Other Sources of Exposure

People who work in certain high-risk occupations may face an increased risk of cadmium exposure. This would include people who work with:

- Soldering

- Welding

- Battery, plastics and textile manufacturing

## The Safe Level of Exposure

The U.S. Environmental Protection Agency (EPA) suggests that a safe level of cadmium in drinking water is 5 ppb or less. The EPA believes that this level of exposure to cadmium will not produce any of the health problems associated with cadmium.

## Associated Health Risks

Acute exposure to ingested cadmium can produce the following symptoms:

- nausea, vomiting

- diarrhea

- muscle cramps

- salivation

- sensory disturbances

- liver injury

- convulsions

- shock

- renal failure

Acute exposure to inhaled cadmium can cause lung problems including pneumonitis and pulmonary edema.

Chronic, long-term exposure to cadmium at levels above what is considered safe by the EPA may cause lung, kidney, liver, bone or blood damage.

## Cadmium and Cancer

While definitive conclusions have yet to be drawn, the International Agency for Research on Cancer and U.S. Environmental Protection Agency have determined that cadmium probably causes cancer.

## The Bottom Line

Cadmium is a toxic heavy metal and is present in large quantities in inhaled cigarette smoke. It damages lung tissue and can build up over time to cause kidney, liver, bone and blood damage. Cadmium is just one of the hundreds of toxins present in cigarette smoke. Waste no time kicking your smoking habit to the curb. It offers you nothing more than disease and ultimately — death.

Sources:

*Consumer Factsheet on Cadmium.* 28 November, 2006. U.S. Environmental Protection Agency.

*Cadmium Factsheet.* April, 2010. Centers for Disease Control.

*Public Health Statement for Cadmium.* July 1999. Agency for Toxic Substances and Disease Registry.

# Solar panels reduce both global warming and urban heat island

**Valéry Masson[1]\*, Marion Bonhomme[2], Jean-Luc Salagnac[3], Xavier Briottet[4] and Aude Lemonsu[1]**

[1] Météo-France/CNRS, Centre National de Recherches Météorologiques/Groupe d'étude de l'atmosphère Météorologique, Toulouse, France

[2] Laboratoire de Recherche en Architecture, Toulouse, France

[3] Centre Scientifique et Technique du Bâtiment, Marne-La-Vallée, France

[4] French Center for Aerospatial Research, Toulouse, France

The production of solar energy in cities is clearly a way to diminish our dependency to fossil fuels, and is a good way to mitigate global warming by lowering the emission of greenhouse gases. However, what are the impacts of solar panels locally? To evaluate their influence on urban weather, it is necessary to parameterize their effects within the surface schemes that are coupled to atmospheric models. The present paper presents a way to implement solar panels in the Town Energy Balance scheme, taking account of the energy production (for thermal and photovoltaic panels), the impact on the building below and feedback toward the urban micro-climate through radiative and convective fluxes. A scenario of large but realistic deployment of solar panels on the Paris metropolitan area is then simulated. It is shown that solar panels, by shading the roofs, slightly increases the need for domestic heating (3%). In summer, however, the solar panels reduce the energy needed for air-conditioning (by 12%) and also the Urban Heat Island (UHI): 0.2 K by day and up to 0.3 K at night. These impacts are larger than those found in previous works, because of the use of thermal panels (that are more efficient than photovoltaic panels) and the geographical position of Paris, which is relatively far from the sea. This means that it is not influenced by sea breezes, and hence that its UHI is stronger than for a coastal city of the same size. But this also means that local adaptation strategies aiming to decrease the UHI will have more potent effects. In summary, the deployment of solar panels is good both globally, to produce renewable energy (and hence to limit the warming of the climate) and locally, to decrease the UHI, especially in summer, when it can constitute a health threat.

**Keywords: urban heat island, solar energy, solar panels, cities, adaptation to climate change**

## 1. INTRODUCTION

Renewable energy is seen as a necessary step toward sustainable energy development, diminution of the use of fossil fuels and mitigation of climate change, as stated for example by Elliott (2000): "With concerns about Climate Change growing, the rapid development of renewable energy technologies looks increasingly important." However, the recent analysis of Nugent and Sovacool (2014) showed that, when their complete life-cycle is considered, renewable energies are not $CO_2$ sinks yet. Nevertheless their greenhouses gas emission rate per unit of energy produced is much less than for energy sources based on fossil fuels and slightly less than for nuclear power. They also "uncover best practices in wind and solar design and deployment that can better inform climate change mitigation efforts in the electricity sector." Elliott (2000) underlines that renewable energy deployment requires a new paradigm, of decentralized energy production and small production systems. The implementation of renewable energy will need social and institutional changes, even if technology for these systems already exists (Gross et al., 2003, while still needing improvements and further research Jader-Waldau, 2007). Funding, incentive policies and statutory obligations on electricity suppliers may be needed to develop renewable energy faster. Lund (2007) demonstrates that, in Denmark, a transition toward

100% of renewable energy production is possible. Sovacool and Ratan (2012) conclude that nine factors linked to policy, social and market aspects favor or limit the development of wind turbines and solar energy, and explain why renewable energy is growing fast in Denmark and Germany compared to India and the USA.

Sims et al. (2003) show that most renewable energies can, in certain circumstances, reduce cost as well as $CO_2$ emissions, except for solar power, which remains expensive. However, Hernandez et al. (2014) review the environmental impacts of utility-scale solar energy installations (solar farms), which are typically implemented in rural areas, and show that they have low environmental impacts relative to other energy systems, including other renewables. Furthermore, solar power is also one of the few renewable energy sources that can be implemented on a large scale within cities themselves. Arnette (2013) shows that, compared to solar farms, individual rooftop solar panels are a very cost-effective means of increasing renewable energy generation and decreasing greenhouse gas emissions. So they conclude that solar panel implementation on roofs should be part of a balanced approach to energy production. Here, we aim to evaluate the environmental impacts on the local climate, of implementing such a strategy at city scale.

The main impact of cities on the local weather is the Urban Heat Island (UHI). Cities are warmer than the surrounding countryside, and this can lead to a health crisis during heat waves, as was the case in Paris in 2003 with 15,000 premature deaths (Fouillet et al., 2006) or in Moscow with 11,000 premature deaths in 2010 (Porfiriev, 2014). It also has to be considered that, due to climate warming, the UHI impacts will become even larger than they are now (Lemonsu et al., 2013). Therefore, several strategies are being studied to reduce the UHI in summer. Gago et al. (2013) have reviewed several research works analyzing strategies to mitigate the UHI, including changes in green spaces, trees, albedo, pavement surfaces, vegetation, and building types and materials. Santamouris et al. (2011) have reviewed of several advanced cool materials systems usable to reduce the UHI. Such materials could be implemented on roofs in order to reflect more energy to the sky (high albedo, high emissivity) or to delay the heat transfer toward the inside the building (phase change materials). Masson et al. (2013) showed that changes in agricultural practices in the vicinity of Paris and the use of cool materials for roofs and pavement would decrease the UHI by 2 K and 1 K, respectively. However, the question of the ability of solar panels to contribute to the same goal is not addressed in these papers, and extremely few studies focus on, or even take into account, the effect of solar panels on the UHI.

It is thus necessary to analyze whether the two objectives of mitigating the global climate warming by increasing renewable energy production in cities, especially through solar panels, and of attenuating the UHI are compatible. Solar panels modify the nature of the rooftop and may thus influence the energy transfers to the atmosphere and the resulting UHI. The aim of this paper is then to evaluate the impact of solar panels, known to be good for global warming mitigation, on the local climate, especially the UHI.

## 2. SOLAR PANELS INTO THE URBAN CANOPY MODEL TEB

The objective of this section is to present how solar panels can be included in the Town Energy Balance (TEB, Masson, 2000) scheme, in terms of both energy production and interactions with the roofs below (shading, modification of the roof energy balance, etc.). The solar panels themselves can be either photovoltaic panels or thermal panels that heat water.

### 2.1. MODELING STRATEGY

The solar panel exchanges energy with the other components of the system. Very few parameterizations taking these exchanges into account exist in the literature. The level of detail depends strongly on the objectives of the authors. On the one hand, when looking at the building scale, it is possible to consider some implementation characteristics of the panels, as in Scherba et al. (2011), who modified the Energy+ software (software dedicated to building energetics) to improve its previous solar panel model (which only computed the energy production). Their solar panel model considers the tilting of the panels and associated sky-view factors. They then perform an analysis of the impact of several types of roofs on sensible heat fluxes toward the atmosphere, but are unable to link these fluxes to the UHI, which needs to take all the buildings of the entire city into account. On the other

hand, Taha (2013) studies the impact of solar panels on the whole urban area of Los Angeles. To do this, he uses the very simplified approach of effective albedo, which accounts for both the albedo and the solar conversion efficiency (linked to the energy produced). This approach estimates the impact on the UHI, but does not take account of the interactions with the urban canopy below (solar panel shadowing may lead to less cooling energy being used in buildings for example, leading to less waste heat outside).

In order to study the impact of solar panels implementations on the urban atmosphere and on the population and buildings, we need an approach that looks at both spatial scales: buildings and city. The TEB scheme is able to simulate the energy, water and momentum exchanges between cities and the atmosphere at a resolution as high as the urban block (say down to 100 m by 100 m). The energetics of buildings have also been included in TEB by Bueno et al. (2012) and Pigeon et al. (2014), to simulate the energy behavior of a typical building representative of the block. The focus is to keep the maximum of key processes, while making some approximations in the geometry that are pertinent at block scale (building shapes are averaged into road canyons, only one thermal zone is kept in the buildings, individual windows are averaged into a glazing fraction, etc.). Gardens and greenroofs modules have also been implemented (Lemonsu et al., 2012; DeMunck et al., 2013a). The modeling strategy chosen here for the implementation of solar panels is similar: key processes are kept while some geometrical assumptions are made to avoid unnecessary details of individual buildings.

In TEB, it is necessary to take account not only of the production of energy by the panels but also the influence of the panels on the underlying roofs. We must therefore calculate the complete energy balance of the panel to determine what is exchanged with the roof or the atmosphere. The TEB model will then be able to estimate the impact of solar panel implementation on the UHI at city scale, as well as the production of energy.

### 2.2. ENERGY BALANCE OF THE SOLAR PANEL

Geometrically, the solar panels are assumed to be horizontal when calculating the radiative heat exchange with the other elements: exchanges between the roof, the solar panels and the sky above are considered to be purely vertical (**Figure 1**). Note that we take the inclination of the panel into account to calculate the irradiance for power production.
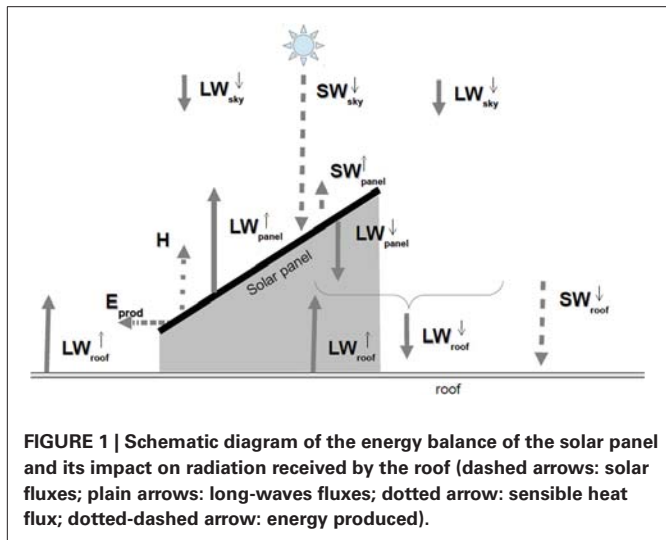
The energy balance equation of the solar panel is written:

$$SW_{sky}^{\downarrow} + LW_{sky}^{\downarrow} + LW_{roof}^{\uparrow} = SW_{panel}^{\uparrow} + LW_{panel}^{\uparrow} + LW_{panel}^{\downarrow}$$
$$+ H + E_{prod} \qquad (1)$$

The terms on the left hand side are incoming energy to the solar panel:

$SW_{sky}^{\downarrow}$    is the incoming Short-Wave radiation from the sun. It can be diffuse or direct, and is considered as forcing data for TEB.

$LW_{sky}^{\downarrow}$    is the incoming Long-Wave radiation from the atmosphere. It is diffuse and is also used as forcing data for TEB.

**FIGURE 1 | Schematic diagram of the energy balance of the solar panel and its impact on radiation received by the roof (dashed arrows: solar fluxes; plain arrows: long-waves fluxes; dotted arrow: sensible heat flux; dotted-dashed arrow: energy produced).**

$LW^{\uparrow}_{roof}$ is the Long-Wave radiation coming up from the roof and being intercepted by the solar panel. It is computed by TEB from the roof emissivity and surface temperature and the long-wave radiation received by the roof:

$$LW^{\uparrow}_{roof} = \epsilon_{roof}\sigma T^4_{roof} + (1 - \epsilon_{roof})LW^{\downarrow}_{roof} \quad (2)$$

The terms on the right hand side of Equation (1) are outgoing energy from the panel:

$SW^{\uparrow}_{panel}$ is the solar radiation reflected by the solar panel. It is classically parameterized using the albedo of the solar panel ($\alpha_{panel}$): $SW^{\uparrow}_{panel} = \alpha_{panel}SW^{\downarrow}_{panel}$. It is also assumed to go back to the sky (we neglect the effect of the inclination of the solar panel on the direction of the reflected light). According to Taha (2013), the value of the albedo of the solar panel ranges from 0.06 to 0.1. We performed measurements of the albedo for a sample of solar panel (under several inclinations) by integrating the hemispheric directional reflectance measured with a goniometer (see section 2.4 for details). From our measurements, the value of 0.11 is used for $\alpha_{panel}$ in the present paper.

$LW^{\uparrow}_{panel}$ is the long-wave radiation emitted (and reflected) by the solar panel to the sky. It depends on the surface temperature of the solar panel, which is estimated following the ISPRA center method:

$$T_{panel} = T_{air} + k_T Irr \quad (3)$$

where $T_{air}$ is the air temperature, $Irr$ is the irradiance received by the solar panel (cf section 2.5) and $k_T$ is a constant coefficient equal to $0.05\,\mathrm{K/(Wm^{-2})}$. In this formulation, the nocturnal dependency of the panel surface temperature on the sky temperature proposed by Scherba et al. (2011) is not used. It would be an improvement to be considered in the future. Also using

the emissivity of the solar panel $\epsilon_{panel}$, equal to 0.93 in our measurements (cf section 2.4), the upward long-wave radiation from the solar panel can be written:

$$LW^{\uparrow}_{panel} = \epsilon_{panel}\sigma T^4_{panel} + (1 - \epsilon_{panel})LW^{\downarrow}_{sky} \quad (4)$$

$LW^{\downarrow}_{panel}$ is the long-wave radiation emitted by the solar panel to the roof (downwards). It is computed under the hypothesis that the temperature of the downward face of the solar panel is always approximately equal to the air temperature. This is probably a limitation of our model during daytime. However, even if the temperature of the downwards face of the solar panel is underestimated (due to the warming of the solar panel and the heat diffusion inside it), this temperature will still be higher than the sky temperature. So, from the point of view of the roof below the solar panel, the incoming radiation will be higher. This captures at least the first order of an effect of the solar panel on the roof. Given the uncertainties, we also neglect the dependency in emissivity for this face of the panel. This gives:

$$LW^{\downarrow}_{panel} = \sigma T^4_{air} \quad (5)$$

$E_{prod}$ is the energy produced by the panel. It depends of the nature (thermal or photovoltaic) and characteristics of the panel, the irradiance on the panel, the inclination of the panel (not taken into account in the other terms), and the air temperature. Details are given in sections 2.5, 2.6 for PV and thermal panels, respectively.

H is the sensible heat flux from the solar panel to the atmosphere. We assume that the solar panel is thin, has no significant thermal mass and hence is in quasi-equilibrium. This means that the sensible heat flux, the only term that is not parameterized, is taken to be equal to the residue of the solar panel energy budget. Besides the fact that it is difficult to have a parameterization of this term, this ensures conservation of energy balance.

### 2.3. MODIFICATION OF THE ENERGY BALANCE OF THE ROOF

For the energy balance of the roof, the most important key parameter will, of course, be the proportion of roof area occupied by the solar panels. As mentioned above, we only consider the projection of the panels onto the horizontal surface (it would be absurd to make accurate calculations taking the inclination of the panels into account—except as noted above for production—when it is already assumed in TEB that all roofs are flat). The fraction of the roof covered by solar panels is noted $f_{panel}$.

The following simplifying assumptions are made:

- An average temperature is still calculated for the roof, without distinguishing between the parts of the roof under or beside the panel. This is reasonable, in particular for flat roofs with inclined panels, because the shadows cast by the panels can modify the radiative contribution to the roof beside as well as below the panels.

- The coefficient for heat transfer from the roof to the sensible heat flux is not changed (it is already in a heterogeneous environment with a roughness length of 5 cm).
- The effect of humidity on panels is neglected: the water interception reservoir treating rainwater and evaporation concerns the whole surface of the roof.
- The effect of solar panels on snow is neglected. The snow mantel, if any, accumulates uniformly on the roof. Note that snow might change the energy produced by the solar panel (but this is not taken into account yet).

These assumptions allow us to change only the radiative contributions to the energy balance of the roof. Assuming that the surface area of the shadows is equal to the surface area of the solar panels, the incoming solar radiation on the roof is:

$$SW^{\downarrow}_{roof} = (1 - f_{panel})SW^{\downarrow}_{sky} \qquad (6)$$

The long-wave incoming radiation on the roof is modified by the long-wave radiation emitted downwards by the solar panels:

$$LW^{\downarrow}_{roof} = (1 - f_{panel})LW^{\downarrow}_{sky} + f_{panel}LW^{\downarrow}_{panel} \qquad (7)$$

This way of implementing the interactions between solar panels and the roof below allows the considerations of the way the roof is built to be separated from the question of whether there are solar panels on it or not. For example, although it is not the case in this paper, it is possible to have greenroofs with or without solar panels. If there are solar panels, the vegetation of the greenroof will simply be more in the shade and receive slightly more infrared radiation.

## 2.4. RADIATIVE CHARACTERISTICS OF SOLAR PANELS

To establish the energy balance of the equivalent urban canyon, the TEB model needs the albedo (integrated between 0.4 and 2.5 μm) and the emissivity in the thermal infrared (integrated between 5 and 12 μm) for the following main areas: road, roofs, facades, glazing. The French Center for Aerospace Research (ONERA) laboratory maintains a current database of optical properties of urban materials. Specific measurements were made for emerging materials: rough white paints, photovoltaic solar panels, metal cladding, and glass (including low emissivity). The measurements for large samples of materials, e.g., for solar panels, were made using a goniometer (**Figure 2**, left).

The measurement process is fully automated in the 0.4–2.5 μm spectral domain. The position measurements acquired by the detector are regular in azimuth (0–180° range) and zenith (0–60° range) with an angular accuracy of 1°, except for the region of specular reflection, which is meshed more precisely.

The reflectance is measured with reference to a reflectance reference (Spectralon). Thereafter, the reflectance of the solar panel placed in the center of the goniometer is acquired for all recorded positions of the detector and the light source. The reference measurement is repeated at the end of the process.

The albedo of the solar panels is then computed by integrating the radiance in all directions over the entire spectral range.



**FIGURE 2 | Left:** Goniometer used for albedo measurements. **Right:** Instrument used for emissivity measurements.

It typically varies from 11 to 16% depending on the position of the sun and the sensor inclination. When the panel is favorably oriented relative to the sun (and hence when the incoming radiation per square meter of panel is the largest), as is usually implemented, the albedo is in the low range, and equal to about 11%.

The emissivity was measured using a SOC 400T apparatus (**Figure 2**, right). It measures the directional hemispheric reflectance for wavelengths between 2.5 and 20 μm. The resulting emissivity was 0.93 for solar panels.

## 2.5. ENERGY PRODUCED BY PHOTOVOLTAIC PANELS

In TEB, two different types of solar panels: thermal and photovoltaic (PV) are considered. The aim of thermal solar panels is to warm the water necessary for the occupants of the building. They are much more efficient (in terms of energy produced) than photovolatic panels, but only produce heat, not electricity.

For PV panels, the energy produced is usually parameterized as:

$$E_{PV\,prod} = Eff_{PV} \times Irr \times R(T_{panel}) \quad (W/m^2 \text{ of solar panel}) \qquad (8)$$

where $Eff_{PV}$ is the conversion efficiency of the PV panel and $R(T_{panel})$ a coefficient to reproduce the fact that solar panels are most efficient at 25°C and present a decrease in efficiency for warmer panel temperatures. The efficiency coefficient varies from 5% to 19% (Taha, 2013), with values as high as 30% possible in the far future (Nemet, 2009). In France, most PV panels use the usual crystalline silicon (xSi) technology (Leloux et al., 2012), for which the efficiency is approximately $Eff_{PV} = 14\%$. To relate the irradiance received by the panel (possibly tilted) to the incident radiation on a horizontal surface ($SW^{\downarrow}_{sky}$), it is possible either to perform geometric calculations on the relative position of the sun and panels or to apply *a priori* correction factors. This second, simpler approach is chosen here, and the coefficient of the French thermal Regulations of 2005 is used:

$$Irr = FT \times SW^{\downarrow}_{sky} \qquad (W/m^2 \text{ of solar panel}) \quad (9)$$

The correction factor FT is typically 1.11 on annual average for a South facing panel in Paris. Assuming that solar panels are placed fairly optimally, i.e., with an approximately 30° tilt and oriented between South-East and South-West (as is usually the case in

France, Leloux et al., 2012), we can estimate that the coefficient $FT$ is equal to $FT = 1.10$ in France. The temperature dependent coefficient can be written as:

$$R(T_{panel}) = \min \left\{ 1; 1 - 0.005 \times (T_{panel} - 298.15) \right\} \quad (10)$$

Finally, the production of the PV panels is parameterized, also using the relationship between panel temperature and irradiance, as:

$$E_{PV\ prod} = Eff_{PV} \times FT \times SW_{sky}^{\downarrow} \times$$

$$\min \left\{ 1; 1 - 0.005 \times (T_{air} + k_T FT \times SW_{sky}^{\downarrow} - 298.15) \right\}$$

$$(W/m^2 \text{ of solar panel}) \quad (11)$$

### 2.6. ENERGY PRODUCED BY THERMAL SOLAR PANELS

The amount of energy produced by solar thermal panels is usually defined on an annual basis (Philibert, 2006). This can partly be justified by the fact that the limitation of energy production is not linked solely to the available sunlight but also to the objective in terms of quantity of water heated (there is no point in heating water beyond the set-point, typically 60°C for hot water, nor for more people than those actually occupying the building, 32$l$ per person). From French regulations, for one person, the annual production with thermal solar panels is:

$$\int_{year} E_{ther\ prod} = \frac{1}{2} \times 1.16 \times 32 \Delta T \quad (\text{kWh/year/person}) \quad (12)$$

where $\Delta T$ is the temperature difference between cold and hot water (typically 45 K in France). The factor $\frac{1}{2}$ comes from an adjustment to account for the fact that only a part of the need for warm water can be covered by solar energy. This factor can vary depending on location, climate (frequency of presence of clouds), seasonality (less sun radiation in winter) and technical features of the installation (ADEME, 2002). A typical value of $\frac{1}{2}$ is taken here. Furthermore, it is considered that this per capita energy requirement can be satisfied by 1 m$^2$ of thermal panel. So, the power averaged over the year would be:

$$< E_{ther\ prod} > = \frac{1}{2} \times 1.16 \times 32 \Delta T \times 1000/24/365$$

$$(W/m^2 \text{ of solar panel}) \quad (13)$$

Here, in order to better take the variability in production due to solar irradiation into account, instead of an annual mean computation, instantaneous production is considered in connection with the daily need for warm water. This mimics the fact that the water is heated during the day and stored until it is used during the next 24 h. So, using the regulation information above, the target energy production for 1 day can be defined as:

$$E_{ther\ target} = 1.16 \times 32 \Delta T \times 1000/365 \times 3600$$

$$(J/m^2 \text{ of solar panel}) \quad (14)$$

The $\frac{1}{2}$ factor has disappeared here because we consider ideal heating (i.e., sunny) conditions for the definition of the target. The production of the thermal panel is then computed in three steps:

1. The instantaneous production is defined as $E_{ther\ prod} = Eff_{ther} \times Irr$ ($W/m^2$ of solar panel) where $Eff_{ther}$ is the efficiency coefficient of the thermal panel and $Irr$ the irradiance received by the panel. The efficiency of new thermal solar panels typically ranges between 0.70 and 0.80. However, in real conditions of use, especially in cities, dirt and dust on the panel reduce its energy production. Elminir et al. (2006) found a decrease of between 6% and 20% in the output power due to dust (17.4% for a 45° tilt angle of the solar panel). A similar effect of dirt had already been found by Garg (1974), with attenuation of 10–20% for tilt angles between 45° and 30°. Therefore, in the present study $Eff_{ther}$ was set to 0.60.
2. The total amount of energy produced is summed from midnight the previous night to the current time $t$: $\int_{midnight}^{t} E_{ther\ prod} dt$ ($J/m^2$ of panel).
3. If the quantity of energy produced since midnight reaches the target $E_{ther\ target}$, then any additional production during the same day is wasted and further energy production is set to zero.

To summarize, for solar thermal panels, the production is parameterized as:

$$\begin{cases} \text{if } \int_{midnight}^{t} E_{ther\ prod} dt < E_{ther\ target} \\ \qquad\qquad\qquad \text{then} \quad E_{ther\ prod} = Eff_{ther} \times Irr \\[2ex] \text{if } \int_{midnight}^{t} E_{ther\ prod} dt = E_{ther\ target} \\ \qquad\qquad\qquad \text{then} \quad E_{ther\ prod} = 0 \end{cases}$$

$$(15)$$

### 2.7. HYPOTHESES ON TYPES OF SOLAR PANELS

As the model is able to consider both thermal and PV solar panels, it is now necessary to define some hypotheses on the use of each type of panel. This is, of course, a scenario-dependent element, in the sense that it can be modified for each study. For example, Taha (2013) only studied the implementation of PV panels in the Los Angeles metropolitan area. The interest of also considering the deployment of thermal solar panels in this paper is that this energy production technology is less greenhouse gas emissive per unit of energy produced (considering its whole lifecycle) than PV (Nugent and Sovacool, 2014). Here, it will thus be supposed that both types of panels are possible. The main hypotheses are:

- On residential buildings and houses, the priority is given to thermal solar panels, which are more efficient. The thermal production is of course limited by the area of panels on the roof but it is also limited by the population in the building: it is not necessary to heat more water than required by the number of people who are going to use it. Therefore, once the necessary area of thermal solar panels is reached, the remaining space

allocated for solar panels on the roof will be devoted to PV panels.
- On other types of buildings (offices, commercial, industrial, etc...) only PV panels will be installed.

The total fraction of the building's roof where solar panels (any type) can be installed is noted $f_{panel}$ (this quantity is also scenario dependent). It is then necessary to define what proportion of the roof area is required for thermal panels, and how much area remains available for PV panels. In France, in residential buildings, the density is typically 1 occupant per $30\,m^2$ of floor area[1]. Furthermore, as mentioned above, $1\,m^2$ of thermal panel is needed per capita. This means $1\,m^2$ of panel per $30\,m^2$ of floor area. For single story accommodation, 1/30 of the roof is then equipped with thermal panels, and $(f_{panel} - 1/30)$ by PV panels. If the building has two stories, thermal panels will occupy 2/30 of the roof area, and so on.

So if $N_{floor}$ is the number of floors of the building (variable calculated in TEB), the proportions of thermal panels ($f_{ther\ panel}$) and PV panels ($f_{phot\ panel}$) are calculated as:

$$f_{ther\ panel} = \min(N_{floor}/30; f_{panel}) \tag{16}$$

$$f_{PV\ panel} = \max(f_{panel} - f_{ther\ panel}; 0) \tag{17}$$

The total production of the solar panels on the roofs can then be written:

$$E_{prod} = (f_{ther\ panel} E_{ther\ prod} + f_{phot\ panel} E_{phot\ prod})/f_{panel}$$
$$(W/m^2 \text{ of solar panel}) \tag{18}$$

This is this quantity that is involved in the energy balance of the panel (section 2.2).

## 3. IMPACT OF SOLAR PANELS ON PARIS URBAN HEAT ISLAND

### 3.1. SIMULATION CONFIGURATION AND SCENARIOS

We are now able to simulate the impact of the implantation of solar panels in a city on the UHI. The simulations are performed on the Paris metropolitan area, with TEB, coupled with the vegetation scheme ISBA (Noilhan and Planton, 1989) for rural areas, within the SURFEX modeling software (Masson et al., 2013b). The simulation domain is $100\,km$ by $100\,km$, with a resolution of $1\,km$. At such a resolution, only the main characteristics of the buildings within the blocks in the grid mesh are kept. Geometric parameters are averaged in order to conserve the surface areas (for walls, roofs, gardens, roads, water, rural areas), while a majority rule applies for the architectural characteristics of buildings (age, materials, equipment) and the use to which they are put (residential, offices, commercial or industrial). These urban data are provided by a database at $250\,m$ resolution (Figure 3 of Masson et al., 2014), which contains block types as well as 60 urban indicators. Some parameters needed by TEB, such as albedos, thermal characteristics or equipment within

buildings, are deduced for each 1-km-by-1-km grid mesh from urban block types and from the use and age of the majority of buildings. Countryside parameters, such as land use and vegetation characteristics are deduced from the ecoclimap database at 1 km resolution (Masson et al., 2003). The methodology presented in Masson et al. (2014), based on a simplified Urban Boundary Layer generator (Bueno et al., 2013; Le Bras, 2014) is chosen, in order to be able to perform a simulation over an entire year. The chosen year of study is 2003, because it demonstrates the impact the solar panels would have during a heat wave.

Some hypotheses have to be made on the proportions of roofs equipped with solar panels. Hypotheses similar to those presented as "reasonably high deployment" in Taha (2013) are taken. On sloping roofs, typically on domestic houses but also old Hausmannian buildings in the historical core of Paris, $\frac{3}{4}$ of the part of the roof oriented between South-East and South-West (after Leloux et al., 2012) is assumed to be covered by solar panels (thermal or PV, or a mix of the two). This corresponds to approximately 19% of the roof being covered. On flat roofs, however, more space is available, and solar panels are taken to be installed on 50% of each roof.

Current albedos of roofing prior to the implementation of solar panels are estimated for each type of building from an architectural analysis. Historical Hausmannian buildings in the very center of Paris are roofed with zinc on top of wood, so their albedo is very high, set to 0.6. In this regard, the solar panels, even maybe thermal ones, would decrease the albedo of the city there, and might tend to increase the UHI. However, only a small proportion of this type of buildings is eligible for solar panels (19% of roofs in our hypothesis), and the spatial coverage of this type of old city blocks is limited (see Figure 3 of Masson et al., 2014). Except for the most recent industrial buildings (built after 1975), for which roof albedo is 0.5 and which, again do not cover a significant part of the metropolitan area, roof albedo for most buildings is estimated as 0.2 (e.g., tiles for houses and old industrial buildings or gray concrete roofs for collective buildings). Therefore, the impact of solar panels on historical or industrial buildings is probably counterbalanced by the other parts of the urban area, where solar panels will probably reduce the amount of solar radiation absorbed by the buildings (due to the reflection and conversion into energy by the solar panels).

Two simulations are run: one is the reference simulation corresponding to Paris in its actual state (without many solar panels) and the second is the one with the reasonably high deployment of solar panels. A comparison of the two simulations will assess the effect of the solar panels on the urban area.

### 3.2. RESULTS FOR ENERGY PRODUCTION AND CONSUMPTION

The impacts of solar panels are discussed in terms of energy production, of course, but also impact on energy consumption and, in the next section, on the UHI and thermal comfort. At the city scale, the production by thermal solar panels is larger than by PV. This comes both from the fact that their deployment is favored for domestic buildings and from their much higher efficiency (the former being linked to the latter). It should nevertheless be noted that, from April to August, production by thermal solar

---
[1]http://www.insee.fr/fr/themes/document.asp?ref_id=ip1396

panels saturates (enough hot water is produced), so their real efficiency decreases. Over the entire year, on average for the whole city, the thermal solar panels would produce approximately 265 MJ/year/m$^2$ of building and the PV panels 113 MJ/year/m$^2$ of building. This would cover an equivalent of 28% of the energy consumption for domestic heating and air-conditioning.

The solar panels also slightly modify the energy consumption of the buildings. During winter, the solar panels could induce a decrease of the energy consumption due to more infra-red energy reaching the roof, or increase it by reducing the amount of solar radiation received or by their effect on the UHI. Overall, the domestic heating demand increases by 3% per year in our scenario. During summer the need for air-conditioning will probably decrease, thanks to the shading of the roofs and the cooling induced in the urban climate (see below). The comparison between the two simulations indicates that the air-conditioning energy demand decreases by 12%. Because the energy consumption for air-conditioning is low compared to that for domestic heating, the balance between the loss in energy in winter and the gain in summer induces an increase of total energy consumption by buildings of 1%. However, in the future, when climate warming induces milder winters and hotter summers, insulation will (hopefully) be better and air-conditioning equipment, currently not widely installed in France, will (probably) take on greater importance so this balance may change. Then, massive installation of solar panels may even be beneficial for energy consumption.

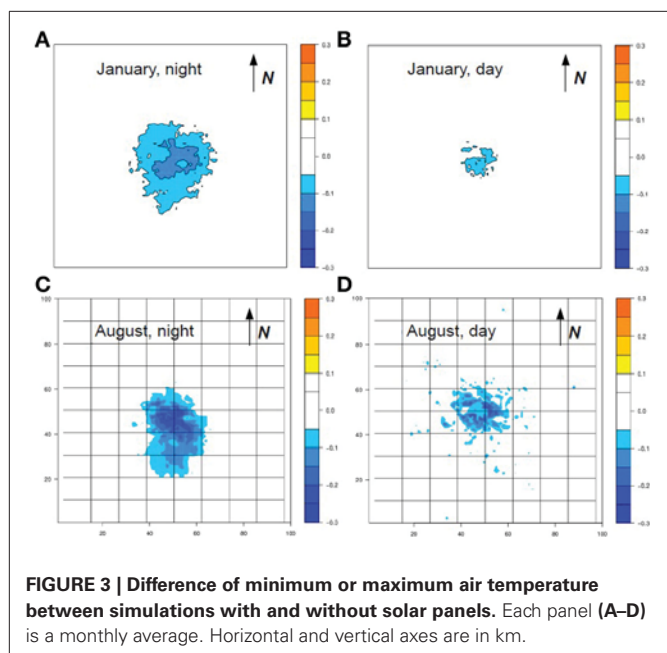### 3.3. RESULTS ON URBAN HEAT ISLAND

The deployment of solar panels in the Paris metropolitan area would not be neutral in terms of urban climate. **Figure 3** presents the difference in the daily minimum and maximum air temperature between the two simulations (for two contrasting months: January and August). In wintertime, when the sun is low, the



**FIGURE 3 | Difference of minimum or maximum air temperature between simulations with and without solar panels.** Each panel **(A–D)** is a monthly average. Horizontal and vertical axes are in km.
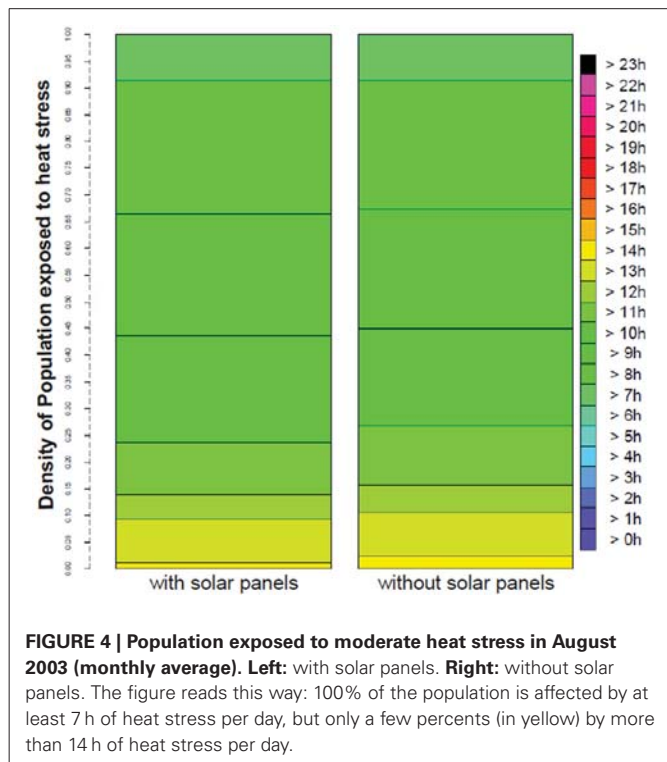
impact of the solar panels on the air temperature is relatively small. Their implementation reduces the maximum air temperature by approximately 0.05 K in the city center and the UHI by more than 0.1 K in Paris and its dense suburbs, and by 0.05 K on the whole metropolitan area. However, we have seen that this is large enough to have a noticeable (if limited) influence on energy consumption for domestic heating.

During the month of August, in the first half of which the famous 2003 heat wave occurred, the impacts of solar panels on air temperature would be larger. In daytime, the presence of solar panels would decrease the air temperature by more than 0.2 K, especially in the dense suburbs, where the density of solar panels is the highest, due to both the high density of building and the fact that unlike the Haussmanian buildings of the city center, the suburban apartment and commercial buildings are flat roofed. This cooling value is consistent with, even though larger than, the value of 0.05 K found for the July 2005 heat wave episode in the Los Angeles area reported by Taha (2013) for present PV panels. When the efficiency of PV panels is improved (up to 30%), Taha (2013) predicts that the cooling will reach 0.15 K. There are two possible explanations for the fact that more intense cooling is simulated for Paris. First, the presence of the sea breeze in Los Angeles could limit local cooling due to solar panels in the city while extending the area of cooling by advection of the (slightly) cooler air. This can explain why a large portion of the metropolitan area of Los Angeles is impacted by the solar panels in these simulations. Second, only PV panels were simulated by Taha (2013). The efficiency of these panels was assumed to be relatively high (20%), larger than the value used in the present study, but much smaller than the efficiency of thermal solar panels (60%). As we investigate a scenario with deployment of both types of solar panels here, the absorption of energy is larger than for PV alone.

At night, the impact of the solar panels is quite strong, even larger than during daytime, with cooling reaching 0.3 K. To the authors' knowledge, this effect is not investigated in the literature. This increased cooling at night is due to a combination of several urban micro-climate processes. First, the heat storage within the buildings is reduced in presence of solar panels, especially thermal ones, because they intercept the solar radiation. The implementation of solar panels as a separate element of the urban surface energy balance system, as done here, allows a fine description of their impact on the underlying building energetics. Second, at night, the urban boundary layer is much thinner than during the day (typically 200 m high instead of 1500 m high in summer). So any modification of the surface energy balance will have up to 10 times more influence on the air temperature at night. Such a counter-intuitive phenomenon was found by DeMunck et al. (2013b) for air-conditioning, which was shown to have more impact at night than in the day (although the heat release itself was, of course, larger in daytime). Here too, while the solar panels primarily modify the daytime processes (by absorption and transformation of the solar radiation into thermal or electrical energy), the influence on air temperature is larger at night, due to the urban fabric and the boundary layer structure.

This cooling effect, though relatively small, can improve the thermal comfort of the inhabitants. For example, it reduces the number of people exposed to any given intensity (e.g., 2 K) of the

**FIGURE 4 | Population exposed to moderate heat stress in August 2003 (monthly average). Left:** with solar panels. **Right:** without solar panels. The figure reads this way: 100% of the population is affected by at least 7 h of heat stress per day, but only a few percents (in yellow) by more than 14 h of heat stress per day.

UHI by 4% ($\pm$0.5%) of the total population of the metropolitan area. The thermal comfort can also be evaluated by considering more environmental parameters, such as the wind, radiation and humidity, that all have an influence on human physiology. The Universal Thermal Climate Index, UTCI (www.utci.org/), is such an indicator. **Figure 4** shows the proportion of the population of the urban area that is under moderate heat stress when outside (in shade). It displays the number of hours per day that a person spends in this or any stronger level of stress. Solar panels, probably by their effect of temperature, decrease the level on thermal stress of the population. For example, while 17% of the total population is affected by heat stress for more than half a day (12 h) in the present city, the implementation of solar panels would reduce this number to 13%. While this difference seems small, it still represents a large number of people. On average, approximately 15 min of comfort is gained for outdoor conditions. This slight improvement in exposure to heat stress, although unplanned (solar panels are primarily implemented for energy production), can add to larger ones, specifically aimed at urban climate cooling, such as greening of the city.

## 4. DISCUSSION

Solar panels absorb solar energy to produce energy usable in buildings, either directly in the form of heat (typically to warm water) or as electricity. However, in doing so, they modify the energy balance of the urban surface in contact with the atmosphere, and so possibly influence the urban micro-climate. They also change the radiation received by the roof, and hence the building energy balance. The present paper presents a way to include solar panels in the TEB scheme. This parameterization simulates their production in a relatively precise way, as it depends

on the evolving meteorological conditions, rather than simply using a rule of thumb annual production as is often done in building design. The panels also influence the building energetics and the heat fluxes (radiative and convective) to the atmosphere. Thus, it is possible to evaluate the influence of solar panels implementation strategies on the UHI.

A scenario of large but realistic deployment of solar panels in the Paris metropolitan area has been simulated. A comparison with the reference, present-day city without (many) solar panels, enables the impact of this scenario to be estimated. Unlike work previously reported in the literature, the present study implemented both thermal and PV solar panels in the model. This allowed realistic scenarios to be simulated, where thermal panels are introduced first. It is shown that solar panels, by shading of the roof, slightly increase the need for domestic heating (3%). With future improvements in insulation, this impact will probably be less significant. In summer, however, the solar panels reduce the energy needed for air-conditioning (by 12%), thanks to the shading of the roof. They also lead to a reduction of the UHI.

During summer, when sunlight is strong, the deployment of solar panels can reduce the temperature by 0.2 K. At night, a simplistic analysis would suggest that the solar panels have no effect (as there is no sunlight). However, the physical simulation performed here shows that the presence of solar panels leads to a mitigation of up to 0.3 K of the UHI at night (so more than during the day). This counter-intuitive result is due to the interaction between the urban surface energy balance (the evolution of which has been modified by solar panels) and the night-time structure of the atmospheric layer above the city. These impacts are larger than those found in previous works, because of the use of thermal panels (that are more efficient than PV panels) and due to the geographical position of Paris, which is relatively far from the sea. This means that it is not influenced by sea breezes, and hence that its UHI is stronger than for a coastal city of the same size. But it also means that local adaptation strategies aiming at decreasing the UHI will have more potent effects.

In addition to these theoretical results, some practical issues have to be taken into consideration in order to better inform decision makers. Installing PV panels or thermal solar collectors on roofs of existing buildings will change the visual appearance of the urban areas concerned. This change may be a difficult issue in towns like Paris, where the tourist industry is important, and installation will probably not be accepted on all potential surfaces. Moreover, the outdoor urban environment is highly polluted and dirt deposits on panel and collector surfaces will inevitably decrease the effectiveness of solar equipment. Regular cleaning could be a way to limit this impact but the consequences of this maintenance activity need to be evaluated (e.g., access paths, security equipment, manpower). Fire risk may also be an issue for PV panels: a series of cases were recorded for newly equipped buildings in Europe in 2013. The products implicated were withdrawn from the market but this situation calls for a rigorous selection of products and contractors as well as for a maintenance plan of the installations. The above mentioned issues require further investigation in the perspective of an economic evaluation taking both positive and negative externalities into account.

To sum up, the deployment of solar panels is good both for producing energy (and hence contributing to a decrease of greenhouse gas emissions) and for decreasing the UHI, especially in summer, when it can be a threat to health. In future climate conditions, solar panels would also help to decrease the demand of air-conditioning. Future work will focus on studying urban adaptation strategies in the long term (as far as the end of the twenty-first century) taking a large panel of possible planning options into consideration, such as city greening, improved insulation, changes in occupants' behavior, different forms of urban expansion and the deployment of renewable energy systems.

## REFERENCES

ADEME. (2002). "Eau chaude solaire - manuel pour la conception, le dimensionnement et la réalisation des installations collectives," in *Technical Report, Agence de l'Environnement et de la Maîtrise de l'Energie in French*, 110.

Arnette, A. N. (2013). Integrating rooftop solar into a multi-source energy planning optimization model. *Appl. Energ.* 111, 456–467. doi: 10.1016/j.apenergy.2013.05.003

Bueno, B., Hidalgo, J., Pigeon, G., Norford, L., and Masson, V. (2013). Calculation of air temperatures above the urban canopy layer from measurements at a rural operational weather station. *J. Appl. Meteorol. Climatol.* 52, 472–483. doi: 10.1175/JAMC-D-12-083.1

Bueno, B., Pigeon, G., Norford, L. K., Zibouche, K., and Marchadier, C. (2012). Development and evaluation of a building energy model integrated in the TEB scheme. *Geosci. Model Dev.* 5, 433–448. doi: 10.5194/gmd-5-433-2012

DeMunck, C. S., Lemonsu, A., Bouzouidja, R., Masson, V., and Claverie, R. (2013a). The greenroof module (v7.3) for modelling green roof hydrological and energetic performances within TEB. *Geosci. Model Dev.* 6, 1941–1960. doi: 10.5194/gmd-6-1941-2013

DeMunck, C. S., Pigeon, G., Masson, V., Meunier, F., Bousquet, P., Tréméac, B., et al. (2013b). How much air conditioning can increase air temperatures for a city like Paris (France)? *Int. J. Climatol.* 33, 210–227. doi: 10.1002/joc.3415

Elliott, D. (2000). Renewable energy and sustainable futures. *Futures* 32, 261–2747. doi: 10.1016/S0016-3287(99)00096-8

Elminir, H. K., Ghitas, A. E., Hamid, R. H., El-Hussainy, F., Beheary, M. M., and Abdel-Moneim, K. M. (2006). Effect of dust on the transparent cover of solar collectors. *Energ. Conver. Manag.* 47, 3192–3203. doi: 10.1016/j.enconman.2006.02.014

Fouillet, A., Rey, G., Laurent, F., Pavillon, G., Bellec, S., Guillenneuc-Jouyaux, C., et al. (2006). Excess mortality related to the August 2003 heat wave in France. *Int. Arch. Occup. Environ. Health* 80, 16–24. doi: 10.1007/s00420-006-0089-4

Gago, E. J., Roldan, J., Pacheco-Torres, R., and Ordonez, J. (2013). The city and urban heat islands: a review of strategies to mitigate adverse effects. *Renew. Sust. Energ. Rev.* 25, 749–758. doi: 10.1016/j.rser.2013.05.057

Garg, H. P. (1974). Effect of dirt on transparent covers in flat-plate solar energy collectors. *Solar Energ.* 15, 299–302. doi: 10.1016/0038-092X(74)90019-X

Gross, R., Leach, M., and Bauen, A. (2003). Progress in renewable energy. *Environ. Int.* 29, 105–122. doi: 10.1016/S0160-4120(02)00130-7

Hernandez, R. R., Easter, S. B., Murphy-Mariscal, M. L., Maestre, F. T., Tavassoli, M., Allen, E. B., et al. (2014). Environmental impacts of utility-scale solar energy. *Renew. Sust. Energ. Rev.* 29, 766–779. doi: 10.1016/j.rser.2013.08.041

Jader-Waldau, A. (2007). Photovoltaics and renewable energies in Europe. *Renew. Sust. Energ. Rev.* 11, 1414–1437. doi: 10.1016/j.rser.2005.11.001

Le Bras, J. (2014). "Fast urban heat island model for thermal comfort studies," in *11th Symposium on the Urban Environment* (Atlanta, CA: American Meteorological Society).

Leloux, J., Narvarte, L., and Trebosc, D. (2012). Review of the performance of residential PV systems in France. *Renew. Sust. Energy. Rev.* 16, 1369–1376. doi: 10.1016/j.rser.2011.07.145

Lemonsu, A., Kounkou-Arnaud, R., Desplat, J., Salagnac, J.-L., and Masson, V. (2013). Evolution of the Parisian urban climate under a global changing climate. *Clim. Change* 116, 679–692. doi: 10.1007/s10584-012-0521-6

Lemonsu, A., Masson, V., Shashua-Bar, L., Erell, E., and Pearlmutter, D. (2012). Inclusion of vegetation in the town energy balance model for modeling urban green areas. *Geosci. Model Dev.* 5, 1377–1393. doi: 10.5194/gmdd-5-1295-2012

Lund, H. (2007). Renewable energy strategies for sustainable development. *Energy* 32, 912–919. doi: 10.1016/j.energy.2006.10.017

Masson, V. (2000). A physically-based scheme for the urban energy budget in atmospheric models. *Bound. Layer Meteorol.* 94, 357–397. doi: 10.1023/A:1002463829265

Masson, V., Champeaux, J.-L., Chauvin, F., Meriguet, C., and Lacaze, R. (2003). A global database of land surface parameters at 1-km resolution in meteorological and climate models. *J. Clim.* 16, 1261–1282. doi: 10.1175/1520-0442-16.9.1261

Masson, V., LeMoigne, P., Martin, E., Faroux, S., Alias, A., Alkama, R., et al. (2013b). The SURFEXv7.2 land and ocean surface platform for coupled or offline simulation of earth surface variables and fluxes. *Geosci. Model Dev.* 6, 929–960. doi: 10.5194/gmd-6-929-2013

Masson, V., Lion, Y., Peter, A., Pigeon, G., Buyck, J., and Brun, E. (2013). Grand Paris: regional landscape change to adapt city to climate warming. *Clim. Change* 117, 769–782. doi: 10.1007/s10584-012-0579-1

Masson, V., Marchadier, C., Adolphe, L., Aguejdad, R., Avner, P., Bonhomme, M., et al. (2014). Adapting cities to climate change: a systemic modelling approach. *Urban Climate*. doi: 10.1016/j.uclim.2014.03.004

Nemet, G. F. (2009). Net radiative forcing from widespread deployment of photovoltaics. *Environ. Sci. Technol.* 43, 2173–2178. doi: 10.1021/es801747c

Noilhan, J., and Planton, S. (1989). A simple parameterization of land surface processes for meteorological models. *Mon. Wea. Rev.* 117, 536–549. doi: 10.1175/1520-0493(1989)117<0536:ASPOLS>2.0.CO;2

Nugent, D., and Sovacool, B. K. (2014). Assessing the lifecycle greenhouse gas emissions from solar PV and wind energy: a critical meta- survey. *Energ. Pol.* 65, 229–244. doi: 10.1016/j.enpol.2013.10.048

Philibert, C. (2006). "Barriers to technology diffusion: the case of solar thermal technologies," in *Technical report, International Energy Agency, Organisation for Economic Cooperation and Development*. Available online at: http://www.iea.org/publications/freepublications/publication/Solar_Thermal.pdf

Pigeon, G., Zibouche, K., Bueno, B., Le Bras, J., and Masson, V. (2014). Evaluation of building energy simulations with the TEB model against energyplus for a set of representative buildings in Paris. *Build. Environ.* 76, 1–14. doi: 10.1016/j.enbuild.2013.10.038

Porfiriev, B. (2014). Evaluation of human losses from disasters: the case of the 2010 heat waves and forest fires in Russia. *Int. J. Disast. Risk Reduct.* 7, 91–99. doi: 10.1016/j.ijdrr.2013.12.007

Santamouris, M., Synnefa, A., and Karlessi, T. (2011). Using advanced cool materials in the urban built environment to mitigate heat islands and improve thermal comfort conditions. *Solar Energ.* 85, 3085–3102. doi: 10.1016/j.solener.2010.12.023

Scherba, A., Sailor, D. J., Rosenstiel, T. N., and Wamser, C. C. (2011). Modeling impacts of roof reflectivity, integrated photovoltaic panels and green roof systems on sensible heat flux into the urban environment. *Build. Environ.* 46, 2542–2551. doi: 10.1016/j.buildenv.2011.06.012

Sims, R. E. H., Rogner, H.-H., and Gregory, K. (2003). Carbon emission and mitigation cost comparisons between fossil fuel, nuclear and renewable energy resources for electricity generation. *Energ. Pol.* 31, 1315–1326. doi: 10.1016/S0301-4215(02)00192-1

Sovacool, B. K., and Ratan, P. L. (2012). Conceptualizing the acceptance of wind and solar electricity. *Renew. Sust. Energ. Rev.* 16, 5268–5279. doi: 10.1016/j.rser.2012.04.048

Taha, H. (2013). The potential for air-temperature impact from large-scale deployment of solar photovoltaic arrays in urban areas. *Solar Energ.* 91, 358–367. doi: 10.1016/j.solener.2012.09.014

Traisnel, J. P., Maizia, M., and Roditi, D. (2004). Habitat et développement durable: Les perspectives offertes par le solaire thermique. *Les cahiers du club d'ingénérie prospective énérgie et environnement* 16, 3–46 (in French).

**Conflict of Interest Statement:** The authors declare that the research was conducted in the absence of any commercial or financial relationships that could be construed as a potential conflict of interest.

# The Photovoltaic Heat Island Effect: Larger solar power plants increase local temperatures (Open access: http://www.nature.com/articles/srep35070)

**5 authors**, including:

Greg Barron-Gafford
The University of Arizona
**122** PUBLICATIONS **2,517** CITATIONS

SEE PROFILE

Rebecca Larkin Minor
The University of Arizona
**10** PUBLICATIONS **13** CITATIONS

SEE PROFILE

Mitchell Pavao-Zuckerman
University of Maryland, College Park
**50** PUBLICATIONS **828** CITATIONS

SEE PROFILE

**Some of the authors of this publication are also working on these related projects:**

Echohydrology View project

Stormwater runoff reduction and nutrient retention of urban forests View project

# SCIENTIFIC REPORTS

# The Photovoltaic Heat Island Effect: Larger solar power plants increase local temperatures

Greg A. Barron-Gafford[1,2], Rebecca L. Minor[1,2], Nathan A. Allen[3], Alex D. Cronin[4], Adria E. Brooks[5] & Mitchell A. Pavao-Zuckerman[6]

While photovoltaic (PV) renewable energy production has surged, concerns remain about whether or not PV power plants induce a "heat island" (PVHI) effect, much like the increase in ambient temperatures relative to wildlands generates an Urban Heat Island effect in cities. Transitions to PV plants alter the way that incoming energy is reflected back to the atmosphere or absorbed, stored, and reradiated because PV plants change the albedo, vegetation, and structure of the terrain. Prior work on the PVHI has been mostly theoretical or based upon simulated models. Furthermore, past empirical work has been limited in scope to a single biome. Because there are still large uncertainties surrounding the potential for a PHVI effect, we examined the PVHI empirically with experiments that spanned three biomes. We found temperatures over a PV plant were regularly 3–4 °C warmer than wildlands at night, which is in direct contrast to other studies based on models that suggested that PV systems should decrease ambient temperatures. Deducing the underlying cause and scale of the PVHI effect and identifying mitigation strategies are key in supporting decision-making regarding PV development, particularly in semiarid landscapes, which are among the most likely for large-scale PV installations.

Electricity production from large-scale photovoltaic (PV) installations has increased exponentially in recent decades[1–3]. This proliferation in renewable energy portfolios and PV powerplants demonstrate an increase in the acceptance and cost-effectiveness of this technology[4,5]. Corresponding with this upsurge in installation has been an increase in the assessment of the impacts of utility-scale PV[4,6–8], including those on the efficacy of PV to offset energy needs[9,10]. A growing concern that remains understudied is whether or not PV installations cause a "heat island" (PVHI) effect that warms surrounding areas, thereby potentially influencing wildlife habitat, ecosystem function in wildlands, and human health and even home values in residential areas[11]. As with the Urban Heat Island (UHI) effect, large PV power plants induce a landscape change that reduces albedo so that the modified landscape is darker and, therefore, less reflective. Lowering the terrestrial albedo from ~20% in natural deserts[12] to ~5% over PV panels[13] alters the energy balance of absorption, storage, and release of short- and longwave radiation[14,15]. However, several differences between the UHI and potential PVHI effects confound a simple comparison and produce competing hypotheses about whether or not large-scale PV installations will create a heat island effect. These include: (*i*) PV installations shade a portion of the ground and therefore could reduce heat absorption in surface soils[16], (*ii*) PV panels are thin and have little heat capacity per unit area but PV modules emit thermal radiation both up and down, and this is particularly significant during the day when PV modules are often 20 °C warmer than ambient temperatures, (*iii*) vegetation is usually removed from PV power plants, reducing the amount of cooling due to transpiration[14], (*iv*) electric power removes energy from PV power plants, and (*v*) PV panels reflect and absorb upwelling longwave radiation, and thus can prevent the soil from cooling as much as it might under a dark sky at night.

Public concerns over a PVHI effect have, in some cases, led to resistance to large-scale solar development. By some estimates, nearly half of recently proposed energy projects have been delayed or abandoned due to local opposition[11]. Yet, there is a remarkable lack of data as to whether or not the PVHI effect is real or simply an issue

[1]School of Geography & Development, University of Arizona, Tucson, AZ, USA. [2]Office of Research & Development; College of Science, Biosphere 2, University of Arizona, Tucson, AZ, USA. [3]Nevada Center of Excellence, Desert Research Institute, Las Vegas, NV, USA. [4]Department of Physics, University of Arizona, Tucson, AZ, USA. [5]Department of Electrical and Computer Engineering, University of Wisconsin-Madison, Madison, WI, USA. [6]Department of Environmental Science & Technology, University of Maryland, College Park, MD, USA. Correspondence and requests for materials should be addressed to G.A.B.-G. (email: gregbg@email.arizona.edu)
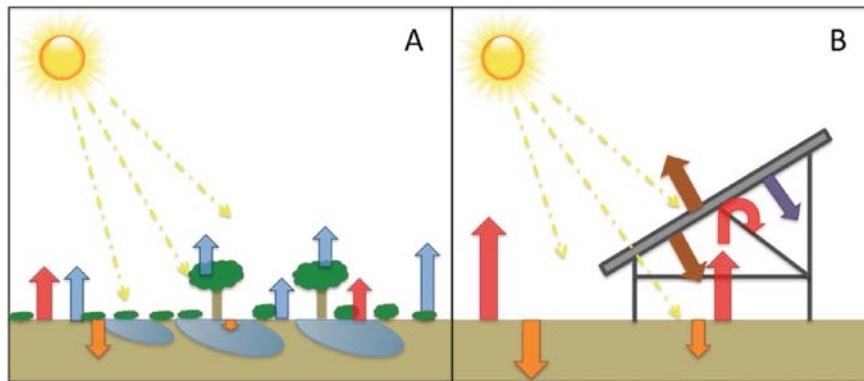
**Figure 1. Illustration of midday energy exchange.** Assuming equal rates of incoming energy from the sun, a transition from (**A**) a vegetated ecosystem to (**B**) a photovoltaic (PV) power plant installation will significantly alter the energy flux dynamics of the area. Within natural ecosystems, vegetation reduces heat capture and storage in soils (orange arrows), and infiltrated water and vegetation release heat-dissipating latent energy fluxes in the transition of water-to-water vapor to the atmosphere through evapotranspiration (blue arrows). These latent heat fluxes are dramatically reduced in typical PV installations, leading to greater sensible heat fluxes (red arrows). Energy re-radiation from PV panels (brown arrow) and energy transferred to electricity (purple arrow) are also shown.

associated with perceptions of environmental change caused by the installations that lead to "not in my back-yard" (NIMBY) thinking. Some models have suggested that PV systems can actually cause a cooling effect on the local environment, depending on the efficiency and placement of the PV panels[17,18]. But these studies are limited in their applicability when evaluating large-scale PV installations because they consider changes in albedo and energy exchange within an urban environment (rather than a natural ecosystem) or in European locations that are not representative of semiarid energy dynamics where large-scale PV installations are concentrated[10,19]. Most previous research, then, is based on untested theory and numerical modeling. Therefore, the potential for a PHVI effect must be examined with empirical data obtained through rigorous experimental terms.

The significance of a PVHI effect depends on energy balance. Incoming solar energy typically is either reflected back to the atmosphere or absorbed, stored, and later re-radiated in the form of latent or sensible heat (Fig. 1)[20,21]. Within natural ecosystems, vegetation reduces heat gain and storage in soils by creating surface shading, though the degree of shading varies among plant types[22]. Energy absorbed by vegetation and surface soils can be released as latent heat in the transition of liquid water to water vapor to the atmosphere through evapotranspiration – the combined water loss from soils (evaporation) and vegetation (transpiration). This heat-dissipating latent energy exchange is dramatically reduced in a typical PV installation (Fig. 1 transition from A-to-B), potentially leading to greater heat absorption by soils in PV installations. This increased absorption, in turn, could increase soil temperatures and lead to greater sensible heat efflux from the soil in the form of radiation and convection. Additionally, PV panel surfaces absorb more solar insolation due to a decreased albedo[13,23,24]. PV panels will re-radiate most of this energy as longwave sensible heat and convert a lesser amount (~20%) of this energy into usable electricity. PV panels also allow some light energy to pass, which, again, in unvegetated soils will lead to greater heat absorption. This increased absorption could lead to greater sensible heat efflux from the soil that may be trapped under the PV panels. A PVHI effect would be the result of a detectable increase in sensible heat flux (atmospheric warming) resulting from an alteration in the balance of incoming and outgoing energy fluxes due to landscape transformation. Developing a full thermal model is challenging[17,18,25], and there are large uncertainties surrounding multiple terms including variations in albedo, cloud cover, seasonality in advection, and panel efficiency, which itself is dynamic and impacted by the local environment. These uncertainties are compounded by the lack of empirical data.

We addressed the paucity of direct quantification of a PVHI effect by simultaneously monitoring three sites that represent a natural desert ecosystem, the traditional built environment (parking lot surrounded by commercial buildings), and a PV power plant. We define a PVHI effect as the difference in ambient air temperature between the PV power plant and the desert landscape. Similarly, UHI is defined as the difference in temperature between the built environment and the desert. We reduced confounding effects of variability in local incoming energy, temperature, and precipitation by utilizing sites contained within a 1 km area.

At each site, we monitored air temperature continuously for over one year using aspirated temperature probes 2.5 m above the soil surface. Average annual temperature was 22.7 + 0.5 °C in the PV installation, while the nearby desert ecosystem was only 20.3 + 0.5 °C, indicating a PVHI effect. Temperature differences between areas varied significantly depending on time of day and month of the year (Fig. 2), but the PV installation was always greater than or equal in temperature to other sites. As is the case with the UHI effect in dryland regions, the PVHI effect delayed the cooling of ambient temperatures in the evening, yielding the most significant difference in overnight temperatures across all seasons. Annual average midnight temperatures were 19.3 + 0.6 °C in the PV installation, while the nearby desert ecosystem was only 15.8 + 0.6 °C. This PVHI effect was more significant in terms of actual degrees of warming (+3.5 °C) in warm months (Spring and Summer; Fig. 3, right).
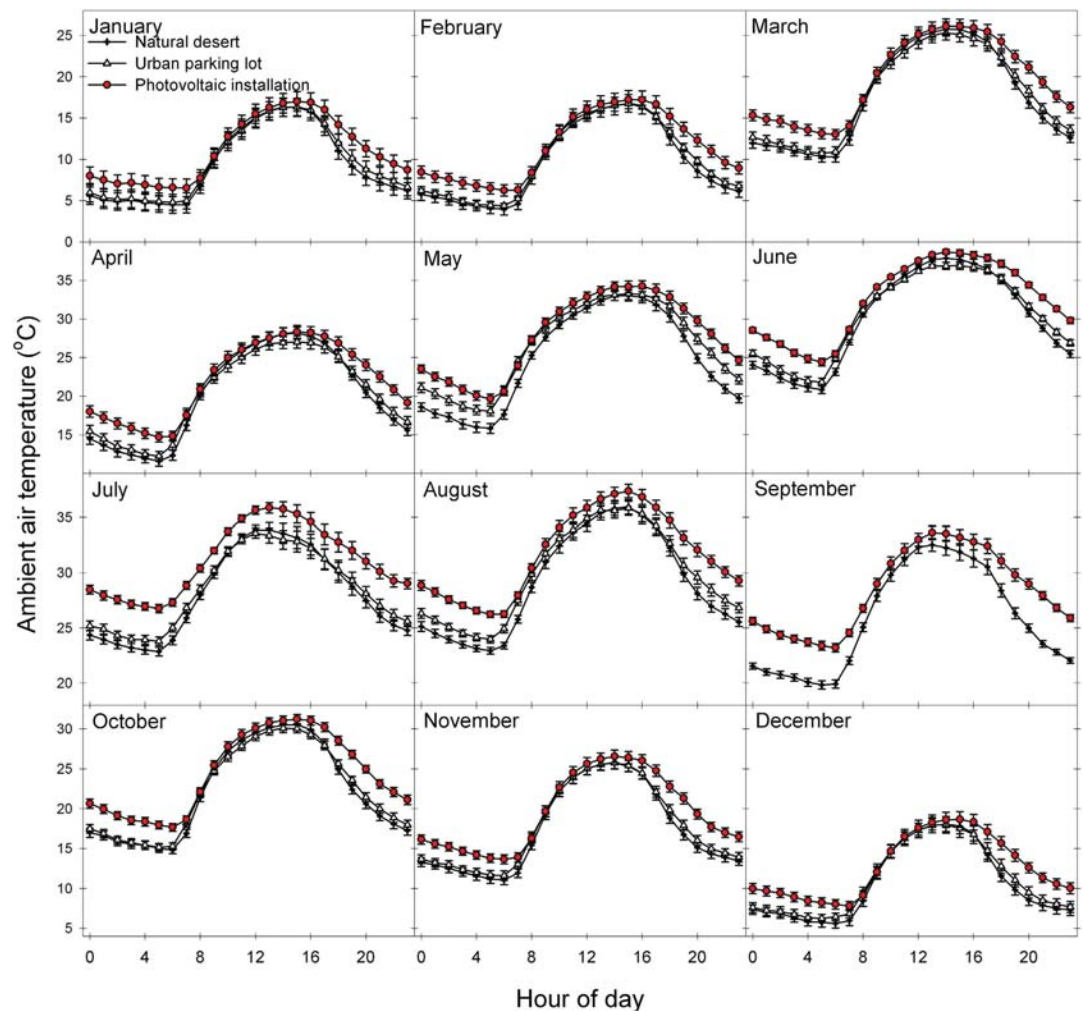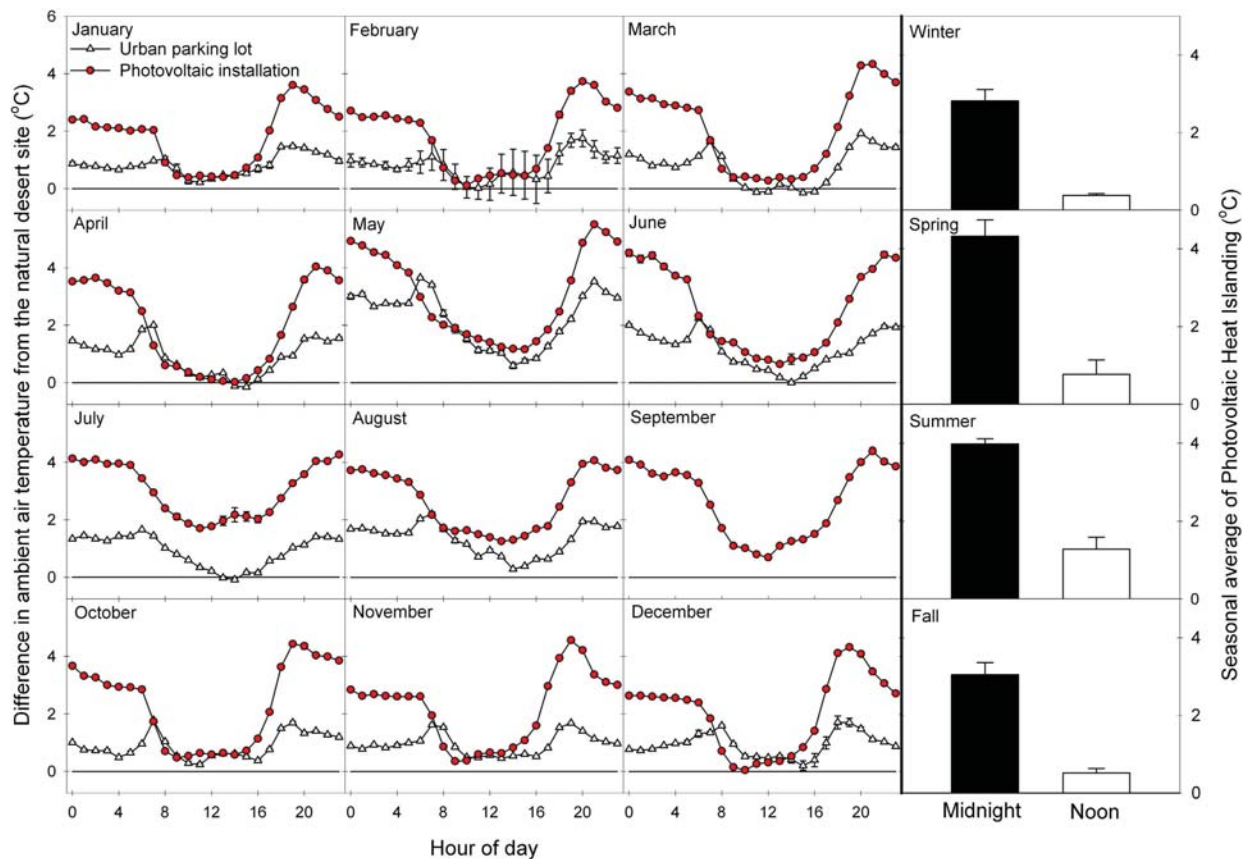
**Figure 2.** **Average monthly ambient temperatures throughout a 24-hour period provide evidence of a photovoltaic heat island (PVHI) effect.**

In both PVHI and UHI scenarios, the greater amount of exposed ground surfaces compared to natural systems absorbs a larger proportion of high-energy, shortwave solar radiation during the day. Combined with minimal rates of heat-dissipating transpiration from vegetation, a proportionally higher amount of stored energy is reradiated as longwave radiation during the night in the form of sensible heat (Fig. 1)[15]. Because PV installations introduce shading with a material that, itself, should not store much incoming radiation, one might hypothesize that the effect of a PVHI effect would be lesser than that of a UHI. Here, we found that the difference in evening ambient air temperature was consistently greater between the PV installation and the desert site than between the parking lot (UHI) and the desert site (Fig. 3). The PVHI effect caused ambient temperature to regularly approach or be in excess of 4 °C warmer than the natural desert in the evenings, essentially doubling the temperature increase due to UHI measured here. This more significant warming under the PVHI than the UHI may be due to heat trapping of re-radiated sensible heat flux under PV arrays at night. Daytime differences from the natural ecosystem were similar between the PV installation and urban parking lot areas, with the exception of the Spring and Summer months, when the PVHI effect was significantly greater than UHI in the day. During these warm seasons, average midnight temperatures were $25.5 + 0.5$ °C in the PV installation and $23.2 + 0.5$ °C in the parking lot, while the nearby desert ecosystem was only $21.4 + 0.5$ °C.

The results presented here demonstrate that the PVHI effect is real and can significantly increase temperatures over PV power plant installations relative to nearby wildlands. More detailed measurements of the underlying causes of the PVHI effect, potential mitigation strategies, and the relative influence of PVHI in the context of the intrinsic carbon offsets from the use of this renewable energy are needed. Thus, we raise several new questions and highlight critical unknowns requiring future research.

### What is the physical basis of land transformations that might cause a PVHI?

We hypothesize that the PVHI effect results from the effective transition in how energy moves in and out of a PV installation versus a natural ecosystem. However, measuring the individual components of an energy flux model remains a necessary task. These measurements are difficult and expensive but, nevertheless, are indispensable in identifying the relative influence of multiple potential drivers of the PVHI effect found here. Environmental

**Figure 3.** (Left) Average monthly levels of Photovoltaic Heat Islanding (ambient temperature difference between PV installation and desert) and Urban Heat Islanding (ambient temperature difference between the urban parking lot and the desert). (Right) Average night and day temperatures for four seasonal periods, illustrating a significant PVHI effect across all seasons, with the greatest influence on ambient temperatures at night.

conditions that determine patterns of ecosystem carbon, energy, and water dynamics are driven by the means through which incoming energy is reflected or absorbed. Because we lack fundamental knowledge of the changes in surface energy fluxes and microclimates of ecosystems undergoing this land use change, we have little ability to predict the implications in terms of carbon or water cycling[4,8].

### What are the physical implications of a PVHI, and how do they vary by region?

The size of an UHI is determined by properties of the city, including total population[26–28], spatial extent, and the geographic location of that city[29–31]. We should, similarly, consider the spatial scale and geographic position of a PV installation when considering the presence and importance of the PVHI effect. Remote sensing could be coupled with ground-based measurements to determine the lateral and vertical extent of the PVHI effect. We could then determine if the size of the PVHI effect scales with some measure of the power plant (for example, panel density or spatial footprint) and whether or not a PVHI effect reaches surrounding areas like wildlands and neighborhoods. Given that different regions around the globe each have distinct background levels of vegetative ground cover and thermodynamic patterns of latent and sensible heat exchange, it is possible that a transition from a natural wildland to a typical PV power plant will have different outcomes than demonstrated here. The paucity in data on the physical effects of this important and growing land use and land cover change warrants more studies from representative ecosystems.

### What are the human implications of a PVHI, and how might we mitigate these effects?

With the growing popularity of renewable energy production, the boundaries between residential areas and larger-scale PV installations are decreasing. In fact, closer proximity with residential areas is leading to increased calls for zoning and city planning codes for larger PV installations[32,33], and PVHI-based concerns over potential reductions in real estate value or health issues tied to Human Thermal Comfort (HTC)[34]. Mitigation of a PVHI effect through targeted revegetation could have synergistic effects in easing ecosystem degradation associated with development of a utility scale PV site and increasing the collective ecosystem services associated with an area[4]. But what are the best mitigation measures? What tradeoffs exist in terms of various means of revegetating degraded PV installations? Can other albedo modifications be used to moderate the severity of the PVHI?

**Figure 4. Experimental sites. Monitoring a (1) natural semiarid desert ecosystem, (2) solar (PV) photovoltaic installation, and (3) an "urban" parking lot – the typical source of urban heat islanding – within a 1 km² area enabled relative control for the incoming solar energy, allowing us to quantify variation in the localized temperature of these three environments over a year-long time period.** The Google Earth image shows the University of Arizona's Science and Technology Park's Solar Zone.

To fully contextualize these findings in terms of global warming, one needs to consider the relative significance of the (globally averaged) decrease in albedo due to PV power plants and their associated warming from the PVHI against the carbon dioxide emission reductions associated with PV power plants. The data presented here represents the first experimental and empirical examination of the presence of a heat island effect associated with PV power plants. An integrated approach to the physical and social dimensions of the PVHI is key in supporting decision-making regarding PV development.

## Methods

**Site Description.** We simultaneously monitored a suite of sites that represent the traditional built urban environment (a parking lot) and the transformation from a natural system (undeveloped desert) to a 1 MW PV power plant (Fig. 4; Map data: Google). To minimize confounding effects of variability in local incoming energy, temperature, and precipitation, we identified sites within a 1 km area. All sites were within the boundaries of the University of Arizona Science and Technology Park Solar Zone (32.092150°N, 110.808764°W; elevation: 888 m ASL). Within a 200 m diameter of the semiarid desert site's environmental monitoring station, the area is composed of a sparse mix of semiarid grasses (*Sporobolus wrightii, Eragrostis lehmanniana*, and *Muhlenbergia porteri*), cacti (*Opuntia* spp. and *Ferocactus* spp.), and occasional woody shrubs including creosote bush (*Larrea tridentata*), whitethorn acacia (*Acacia constricta*), and velvet mesquite (*Prosopis velutina*). The remaining area is bare soil. These species commonly co-occur on low elevation desert bajadas, creosote bush flats, and semiarid grasslands. The photovoltaic installation was put in place in early 2011, three full years prior when we initiated monitoring at the site. We maintained the measurement installations for one full year to capture seasonal variation due to sun angle and extremes associated with hot and cold periods. Panels rest on a single-axis tracker system that pivot east-to-west throughout the day. A parking lot with associated building served as our "urban" site and is of comparable spatial scale as our PV site.

**Monitoring Equipment & Variables Monitored.** Ambient air temperature (°C) was measured with a shaded, aspirated temperature probe 2.5 m above the soil surface (Vaisala HMP60, Vaisala, Helsinki, Finland in the desert and Microdaq U23, Onset, Bourne, MA in the parking lot). Temperature probes were cross-validated for precision (closeness of temperature readings across all probes) at the onset of the experiment. Measurements of temperature were recorded at 30-minute intervals throughout a 24-hour day. Data were recorded on a data-logger (CR1000, Campbell Scientific, Logan, Utah or Microstation, Onset, Bourne, MA). Data from this

instrument array is shown for a yearlong period from April 2014 through March 2015. Data from the parking lot was lost for September 2014 because of power supply issues with the datalogger.

**Statistical analysis.** Monthly averages of hourly (on-the-hour) data were used to compare across the natural semiarid desert, urban, and PV sites. A Photovoltaic Heat Island (PVHI) effect was calculated as differences in these hourly averages between the PV site and the natural desert site, and estimates of Urban Heat Island (UHI) effect was calculated as differences in hourly averages between the urban parking lot site and the natural desert site. We used midnight and noon values to examine maximum and minimum, respectively, differences in temperatures among the three measurement sites and to test for significance of heat islanding at these times. Comparisons among the sites were made using Tukey's honestly significant difference (HSD) test[35]. Standard errors to calculate HSD were made using pooled midnight and noon values across seasonal periods of winter (January-March), spring (April-June), summer (July-September), and fall (October-December). Seasonal analyses allowed us to identify variation throughout a yearlong period and relate patterns of PVHI or UHI effects with seasons of high or low average temperature to examine correlations between background environmental parameters and localized heat islanding.

## References

1. IPCC. IPCC Special Report on Renewable Energy Sources and Climate Change Mitigation. *Prepared by Working Group III of the Intergovernmental Panel on Climate Change* (Cambridge University Press, Cambridge, United Kingdom and New York, NY, USA, 2011).
2. REN21. Renewables 2014 Global Status Report (Paris: REN21 Secretariat; ISBN 978-3-9815934-2-6, 2014).
3. U.S. Energy Information Administration. June 2016 Monthly Energy Review. U.S. Department of Energy. Office of Energy Statistics. Washington, DC (2016).
4. Hernandez, R. R. *et al.* Environmental impacts of utility-scale solar energy. *Renewable & Sustainable Energy Reviews* **29,** 766–779, doi: 10.1016/j.rser.2013.08.041 (2014).
5. Bazilian, M. *et al.* Re-considering the economics of photovoltaic power. *Renewable Energy* **53,** 329–338, doi: http://dx.doi.org/10.1016/j.renene.2012.11.029 (2013).
6. Dale, V. H., Efroymson, R. A. & Kline, K. L. The land use-climate change-energy nexus. *Landsc. Ecol.* **26,** 755–773, doi: 10.1007/s10980-011-9606-2 (2011).
7. Copeland, H. E., Pocewicz, A. & Kiesecker, J. M. In *Energy Development and Wildlife Conservation in Western North America* (ed Naugle, David E.) 7–22 (Springer, 2011).
8. Armstrong, A., Waldron, S., Whitaker, J. & Ostle, N. J. Wind farm and solar park effects on plant-soil carbon cycling: uncertain impacts of changes in ground-level microclimate. *Global Change Biology* **20,** 1699–1706, doi: 10.1111/gcb.12437 (2014).
9. Hernandez, R. R., Hoffacker, M. K. & Field, C. B. Efficient use of land to meet sustainable energy needs. *Nature Climate Change* **5,** 353–358, doi: 10.1038/nclimate2556 (2015).
10. Hernandez, R. R., Hoffacker, M. K. & Field, C. B. Land-Use efficiency of big solar. *Environmental Science & Technology* **48,** 1315–1323, doi: 10.1021/es4043726 (2014).
11. Pociask, S. & Fuhr, J. P. Jr. Progress Denied: A study on the potential economic impact of permitting challenges facing proposed energy projects (U.S. Chamber of Commerce, 2011).
12. Michalek, J. L. *et al.* Satellite measurements of albedo and radiant temperature from semi-desert grassland along the Arizona/Sonora border. *Climatic Change* **48,** 417–425, doi: 10.1023/a:1010769416826 (2001).
13. Burg, B. R., Ruch, P., Paredes, S. & Michel, B. Placement and efficiency effects on radiative forcing of solar installations. *11th International Conference on Ceonctrator Photovoltaic Systems* **1679,** doi: 10.1063/1.4931546 (2015).
14. Solecki, W. D. *et al.* Mitigation of the heat island effect in urban New Jersey. *Environmental Hazards* **6,** 39–49, doi: 10.1016/j.hazards.2004.12.002 (2005).
15. Oke, T. R. The energetic basis of the urban heat island (Symons Memorial Lecture, 20 May 1980). *Quarterly Journal, Royal Meteorological Society* **108,** 1–24 (1982).
16. Smith, S. D., Patten, D. T. & Monson, R. K. Effects of artificially imposed shade on a Sonoran Desert ecosystem: microclimate and vegetation. *Journal of Arid Environments* **13,** 65–82 (1987).
17. Taha, H. The potential for air-temperature impact from large-scale deployment of solar photovoltaic arrays in urban areas. *Solar Energy* **91,** 358–367, doi: 10.1016/j.solener.2012.09.014 (2013).
18. Masson, V., Bonhomme, M., Salagnac, J.-L., Briottet, X. & Lemonsu, A. Solar panels reduce both global warming and Urban Heat Island. *Frontiers in Environmental Science* **2,** 14, doi: 10.3389/fenvs.2014.00014 (2014).
19. Roberts, B. J. Solar production potential across the United States. *Department of Energy, National Renewable Energy Laboratory.* http://www.climatecentral.org/news/eastern-us-solar-development-18714. *19 September* (2012).
20. Monteith, J. L. & Unsworth, M. H. *Principles of Environmental Physics Third Edition* (Elsevier, San Diego, CA, USA, 1990).
21. Campbell, G. S. & Norman, J. M. *An Introduction to Eenvironmental Biophysics Second Edition* (Springer, New York, USA, 1998).
22. Breshears, D. D. The grassland-forest continuum: trends in ecosystem properties for woody plant mosaics? *Frontiers in Ecology and the Environment* **4,** 96–104, doi: 10.1890/1540-9295(2006)004[0096:tgctie]2.0.co;2 (2006).
23. Oke, T. R. *Boundary Layer Climates. Second Edition* (Routledge New York, 1992).
24. Ahrens, C. D. *Meteorology Today. An Introduction to Weather, Climate, and the Environment Eighth Edition* (Thompson, Brooks/Cole USA 2006).
25. Fthenakis, V. & Yu, Y. Analysis of the potential for a heatisland effect in large solar farms. *Analysis of the potential for a heatisland effect in large solar farms; 2013 IEEE 39th Photovoltaic Specialists Conference* 3362–3366 (2013).
26. Santamouris, M. Analyzing the heat island magnitude and characteristics in one hundred Asian and Australian cities and regions. *Science of The Total Environment* **512–513,** 582–598, doi: http://dx.doi.org/10.1016/j.scitotenv.2015.01.060 (2015).
27. Oke, T. R. City size and the urban heat island. *Atmospheric Environment* **7,** 769–779, doi: 10.1016/0004-6981(73)90140-6 (1973).
28. Wang, W.-C., Zeng, Z. & Karl, T. R. Urban heat islands in China. *Geophysical Research Letters* **17,** 2377–2380, doi: 10.1029/GL017i013p02377 (1990).
29. Nasrallah, H. A., Brazel, A. J. & Balling, R. C. Jr Analysis of the Kuwait City urban heat island. *International Journal of Climatology* **10,** 401–405 (1990).
30. Montávez, J. P., Rodríguez, A. & Jiménez, J. I. A study of the Urban Heat Island of Granada. *International Journal of Climatology* **20,** 899–911, doi: 10.1002/1097-0088(20000630)20:8<899::aid-joc433>3.0.co;2-i (2000).
31. Buyantuyev, A. & Wu, J. Urban heat islands and landscape heterogeneity: Linking spatiotemporal variations in surface temperatures to land-cover and socioeconomic patterns. *Landsc. Ecol.* **25,** 17–33, doi: 10.1007/s10980-009-9402-4 (2010).
32. White, J. G. A Model Ordinance for Energy Projects; Oregon Department of Energy. http://www.oregon.gov/ENERGY/SITING/docs/ModelEnergyOrdinance.pdf (2005).

33. Lovelady, A. Planning and Zoning for Solar in North Carolina. *University of North Carolina at Chapel Hill, School of Government* (2014).
34. Coutts, A. M., Tapper, N. J., Beringer, J., Loughnan, M. & Demuzere, M. Watering our cities: The capacity for Water Sensitive Urban Design to support urban cooling and improve human thermal comfort in the Australian context. *Progress in Physical Geography* **37**, 2–28, doi: 10.1177/0309133312461032 (2013).
35. Zar, J. H. *Biostatistical analysis, Prentice-Hall, Englewood Cliffs, p 215* (1974).

## Acknowledgements

## Author Contributions

G.A.B.-G., R.L.M. and N.A.A. established research sites and installed monitoring equipment. G.A.B.-G. directed research and R.L.M. conducted most site maintenance. G.A.B.-G., N.A.A., A.D.C. and M.A.P.-Z. led efforts to secure funding for the research. All authors discussed the results and contributed to the manuscript.

## Additional Information

**Competing financial interests:** The authors declare no competing financial interests.

**How to cite this article**: Barron-Gafford, G. A. *et al.* The Photovoltaic Heat Island Effect: Larger solar power plants increase local temperatures. *Sci. Rep.* **6**, 35070; doi: 10.1038/srep35070 (2016).

# Analysis of the Potential for a Heat Island Effect in Large Solar Farms

Vasilis Fthenakis[1,2] and Yuanhao Yu[1]

[1] Center for Life Cycle Analysis, Department of Earth and Environmental Engineering, Columbia University, New York, NY

[2] PV Environmental Research Center, Brookhaven National Laboratory, Upton, NY

*Abstract* — **Large-scale solar power plants are being built at a rapid rate, and are setting up to use hundreds of thousands of acres of land surface. The thermal energy flows to the environment related to the operation of such facilities have not, so far, been addressed comprehensively. We are developing rigorous computational fluid dynamics (CFD) simulation capabilities for modeling the air velocity, turbulence, and energy flow fields induced by large solar PV farms to answer questions pertaining to potential impacts of solar farms on local microclimate. Using the CFD codes Ansys CFX and Fluent, we conducted detailed 3-D simulations of a 1 MW section of a solar farm in North America and compared the results with recorded wind and temperature field data from the whole solar farm. Both the field data and the simulations show that the annual average of air temperatures in the center of PV field can reach up to 1.9°C above the ambient temperature, and that this thermal energy completely dissipates to the environment at heights of 5 to 18 m. The data also show a prompt dissipation of thermal energy with distance from the solar farm, with the air temperatures approaching (within 0.3°C) the ambient at about 300 m away of the perimeter of the solar farm. Analysis of 18 months of detailed data showed that in most days, the solar array was completely cooled at night, and, thus, it is unlikely that a heat island effect could occur. Work is in progress to approximate the flow fields in the solar farm with 2-D simulations and detail the temperature and wind profiles of the whole utility scale PV plant and the surrounding region. The results from these simulations can be extrapolated to assess potential local impacts from a number of solar farms reflecting various scenarios of large PV penetration into regional and global grids.**

*Index Terms* – **PV, climate change, heat island, fluid dynamics**

## I. INTRODUCTION

Solar farms in the capacity range of 50MW to 500 MW are being proliferating in North America and other parts of the world and those occupy land in the range from 275 to 4000 acres. The environmental impacts from the installation and operation phases of large solar farms deserve comprehensive research and understanding. Turney and Fthenakis [1] investigated 32 categories of impacts from the life-stages of solar farms and were able to categorize such impacts as either beneficial or neutral, with the exception of the "local climate" effects for which they concluded that research and observation are needed. PV panels convert most of the incident solar radiation into heat and can alter the air-flow and temperature profiles near the panels. Such changes, may subsequently affect the thermal environment of near-by populations of humans and other species. Nemet [2] investigated the effect on

global climate due to albedo change from widespread installation of solar panels and found this to be small compared to benefits from the reduction in greenhouse gas emissions. However, Nemet did not consider local micro-climates and his analytical results have not been verified with any field data. Donovan [3] assumed that the albedo of ground-mounted PV panels is similar to that of underlying grassland and, using simple calculations, postulated that the heat island effect from installing PV on grassy land would be negligible. Yutaka [4] investigated the potential for large scale of roof-top PV installations in Tokyo to alter the heat island effect of the city and found this to be negligible if PV systems are installed on black roofs.

In our study we aim in comprehensively addressing the issue by modeling the air and energy flows around a solar farm and comparing those with measured wind and temperature data.

## II. FIELD DATA DESCRIPTION AND ANALYSIS

Detailed measurements of temperature, wind speed, wind direction, solar irradiance, relative humidity, and rain fall were recorded at a large solar farm in North America. Fig. 1 shows an aerial photograph of the solar farm and the locations where the field measurements are taken.
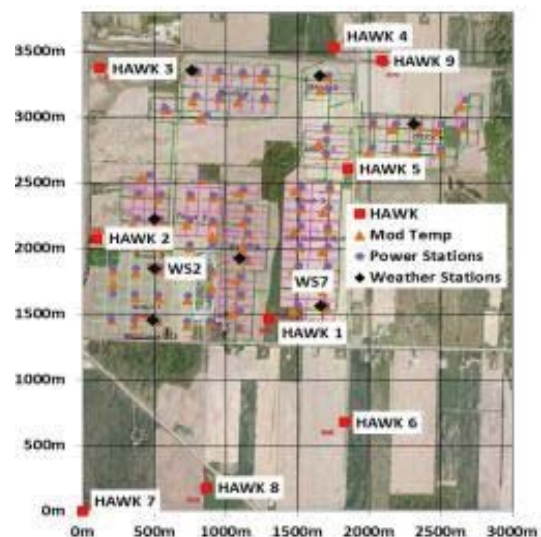


Fig. 1. A picture of the solar farm indicating the locations of the monitoring stations

The field data are obtained from 17 monitoring stations within and around the solar farm, including 8 weather stations (WS) and 9 Hawk stations (HK), all at 2.5 m heights off the ground. There also 80 module temperature (MT) sensors at the back-side of the modules close to each of the corresponding power stations. The WS and MT provide data at 1-min intervals, while the Hawk provides data every 30 minutes. The WS and MT data cover a period of one year from October 2010 to September 2011, while the Hawk data cover a period of 18 months from March 2010 through August 2011.

Hawk stations 3, 6, 7, 8 and 9 are outside the solar farm and were used as reference points indicating ambient conditions. The measurements from Hawk 3, 6, 8 and 9 agree very well confirming that their distances from the perimeter of the solar farm are sufficient for them to be unaffected by the thermal mass of the PV system; Hawk 7 shows higher temperatures likely due to a calibration inaccuracy. In our comparative data analysis we use Hawk 6 as a reference point and, since the prevailing winds are from the south, we selected the section around WS7 as the field for our CFD simulations. Figures 2 to 7 show the difference between the temperatures in Hawk 6 and those in the weather stations WS2 and WS7 within the field, and Hawks 1, 2, 4 and 5 around the solar field.
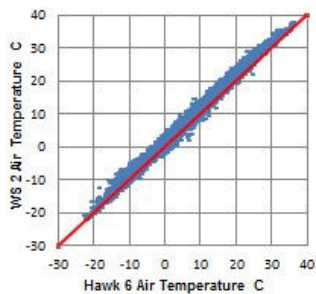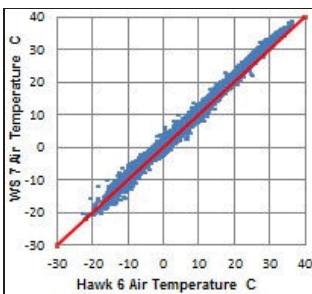

Fig. 2. Air temp WS2 vs. Hawk 6    Fig.3. Air temp WS7 vs. Hawk6
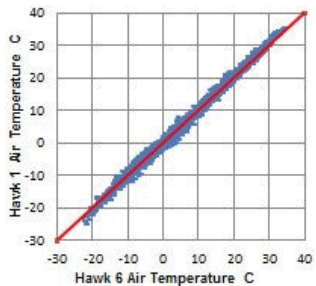

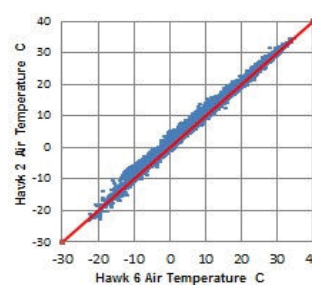Fig. 4. Air temp Hawk 1 vs. 6    Fig. 5. Air temp Hawk 2 vs. 6
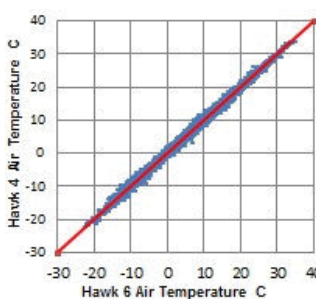

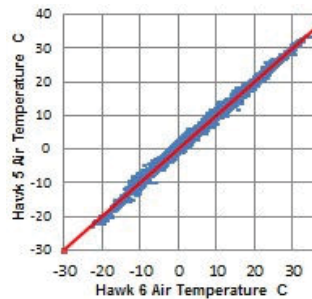Fig. 6. Air temp Hawk 1 vs. 6    Fig. 7. Air temp Hawk 2 vs. 6

These figures and Table 1 show that with the exception of Hawk 4, the closer the proximity to solar farm the higher the temperature difference from the ambient (indicated by Hawk 6). The relative high temperatures recorded at Hawk 4, and also the relative low temperatures at Hawks 1 and 5 are explained by the prevailing wind direction, which for the time period used in our analysis (8/14/2010-3/14/2011) was Southerly (158°-202°). Hawk 4 is downwind of the solar farm, whereas Hawks 1 and 5 are upwind; the downwind station "feels" more the effect of the heat generated at the solar farm than the ones upwind.

Fig. 8 shows the decline in air temperature as a function of distance to solar farm perimeter. Distances for WS2 and WS7 are negative since they are located inside the solar farm site. WS2 is further into the solar farm and this is reflected in its higher temperature difference than WS7.

TABLE I
DIFFERENCE OF AIR TEMPERATURE (@2.5 M HEIGHTS) BETWEEN THE LISTED WEATHER AND HAWK STATIONS AND THE AMBIENT

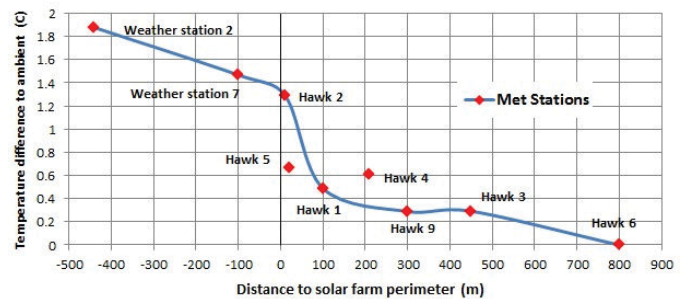| Met Station | WS2 | WS7 | HK1 | HK2 | HK3 | HK4 | HK5 | HK9 |
|---|---|---|---|---|---|---|---|---|
| Temp Difference from H6 (°C) | 1.878 | 1.468 | 0.488 | 1.292 | 0.292 | 0.609 | 0.664 | 0.289 |
| Distance to solar farm perimeter (m) | -440 | -100 | 100 | 10 | 450 | 210 | 20 | 300 |


Fig. 8. Air temperature difference as a function of distance from the perimeter of the solar farm. Negative distances indicate locations within the solar farm.

We also examined in detail the temperature differences between the modules and the surrounding air. These vary throughout the year but the module temperatures are consistently higher than those of the surrounding air during the day, whereas at night the modules cool to temperatures below ambient; an example is shown in Fig. 9. Thus, this PV solar farm did not induce a day-after-day increase in ambient temperature, and therefore, adverse micro-climate changes from a potential PV plant are not a concern.
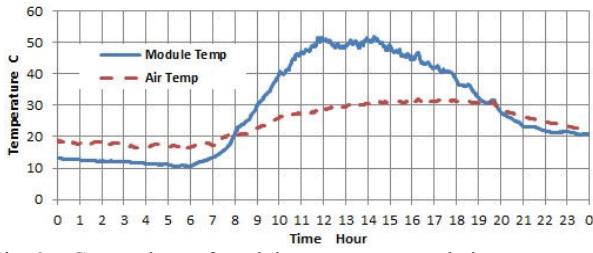
Fig. 9. Comparison of module temperature and air temperature 2.5 m off the ground on a sunny day (July 1, 2011)

## III. CFD MODEL DEVELOPMENT

In preliminary simulations we tested the Ansys CFX and FLUENT computational fluid dynamics codes (CFD) and decided to use FLUENT in detailed simulations. FLUENT offers several turbulence schemes including multiple variations of the k-ε models, as well as k-ω models, and Reynolds stress turbulence models. We used the standard, renormalized-group (RNG), and realizable k-ε turbulence closure scheme as it is the most commonly used model in street canyon flow and thermal stratification studies [5]. FLUENT incorporates the P-1 radiation model which affords detailed radiation transfer between the solar arrays, the ground and the ambient air; it also incorporates standard free convection and wind-forced convection models. Our choice of solver was the pressure-based algorithm SIMPLE which uses a relationship between velocity and pressure corrections to enforce mass conservation and obtain the pressure field. We conducted both three-dimensional (3-D) and 2-D simulations.

A 3-D model was built of four fields each covering an area of 93-meters by 73-meters (Fig. 10). Each field contains 23 linear arrays of 73-meter length and 1.8-meter width. Each array has 180 modules of 10.5% rated efficiency, placed facing south at a 25-degree angle from horizontal, with their bottom raised 0.5 m from the ground and their top reaching a height of 1.3 m. Each array was modeled as a single 73 m × 1.8 m × 1 cm rectangular. The arrays are spaced 4 meters apart and the roads between the fields are 8 m. Fig. 10 shows the simulated temperatures on the arrays at 14:00 pm on 7/1/2011, when the irradiance was 966 W/m$^2$. As shown, the highest average temperatures occur on the last array (array 46). Temperature on the front edge (array 1) is lower than in the center (array 23). Also, temperature on array 24 is lower than array 23, which is apparently caused by the cooling induced by the road space between two fields, and the magnitude of the temperature difference between arrays 24 and 46 is lower than that between arrays 1 and 23, as higher temperature differences from the ambient, result in more efficient cooling.

### TABLE II
MODULES TEMPERATURE

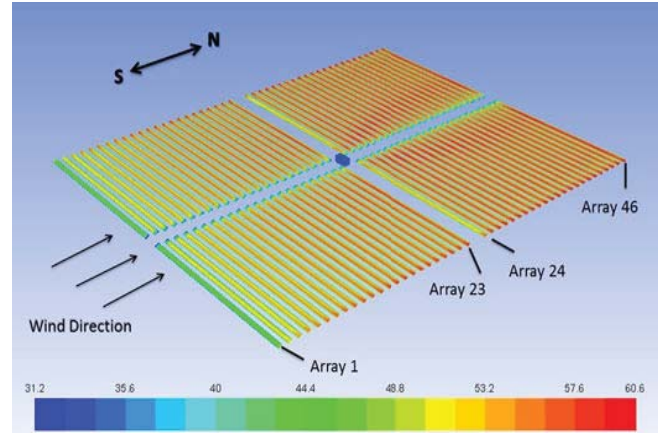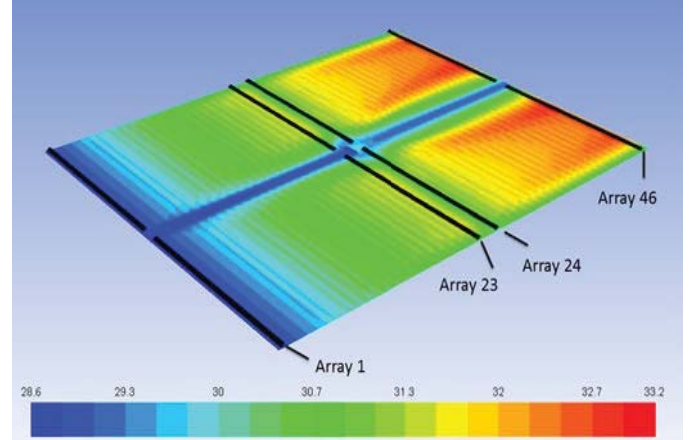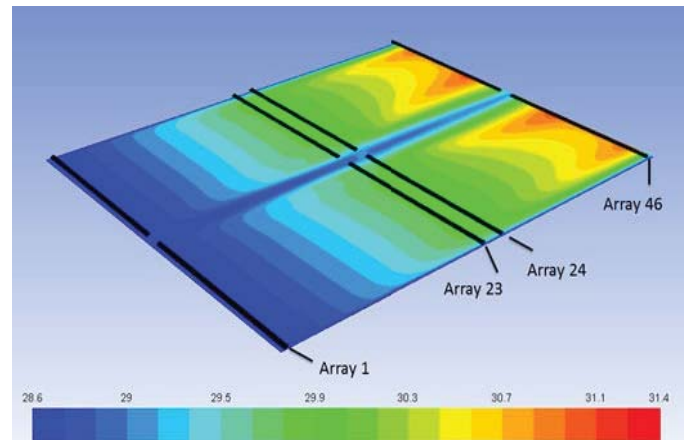| Arrays | 1 | 23 | 24 | 46 |
|---|---|---|---|---|
| Temperature °C | 46.1 | 56.4 | 53.1 | 57.8 |



Fig. 10. Module temperatures from 3-D simulations of air flows and thermal exchange during a sunny day

Our simulations also showed that the air temperatures above the arrays at a height of 2.5 m ranged from 28.6 to 31.1 ; the ambient temperature was 28.6 (Fig. 11).



(a)



(b)

Fig. 11 Air temperatures from 3-D simulations during a sunny day. a) Air temperatures at a height of 1.5 m; b) air temperatures at a height of 2.5 m.

| Temperature | Ambient (℃) | Low (℃) | High (℃) | Average (℃) |
|---|---|---|---|---|
| 2.5m height | 28.6 | 28.6 | 31.1 | 30.1 |
| 1.5m height | 28.6 | 28.6 | 33.2 | 30.8 |

These simulations show a profound cooling effect with increasing height from the ground. It is shown that the temperatures on the back surface of solar panels is up to 30°C warmer than the ambient temperature, but the air above the arrays is only up to 2.5°C higher than the ambient (i.e., 31.1℃). Also the road between the fields allows for cooling, which is more evident at the temperatures 1.5 m off the ground (Fig. 11a). The simulations show that heat build-up at the power station in the middle of the fields has a negligible effect on the temperature flow fields; it was estimated that a power station adds only about 0.4% to the heat generated by the corresponding modules.

The 3-D model showed that the temperature and air velocity fields within each field of the solar farm were symmetrical along the cross-wind axis; therefore a 2-D model of the downwind and the vertical dimensions was deemed to be sufficiently accurate. A 2-D model reduced the computational requirements and allowed for running simulations for several subsequent days using actual 30-min solar irradiance and wind input data. We tested the numerical results for three layers of different mesh sizes and determined that the following mesh sizes retain sufficient detail for an accurate representation of the field data: a) Top layer: 2m by 1m, b) Middle layer: 1.5m by 0.6m, c) Bottom layer: 1m by 0.4m. According to these mesh specifications, a simulation of 92 arrays (length of 388m, height 9m), required a total of 13600 cells. Figures 12-15 show comparisons of the modeled and measured module and air temperatures.
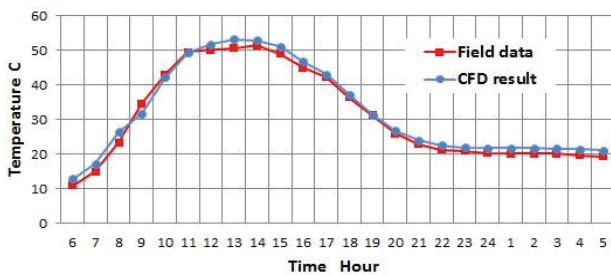


Fig. 12. Comparisons of field and modeled module temperatures; a sunny summer day (7/1/2011); 2-D simulations.
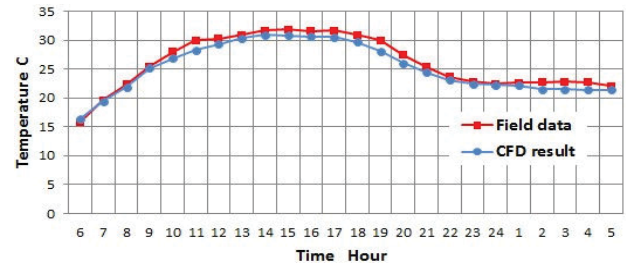


Fig. 13. Comparisons of field and modeled air temperatures at a height of 2.5 m; a sunny summer day (7/1/2011); 2-D simulations.
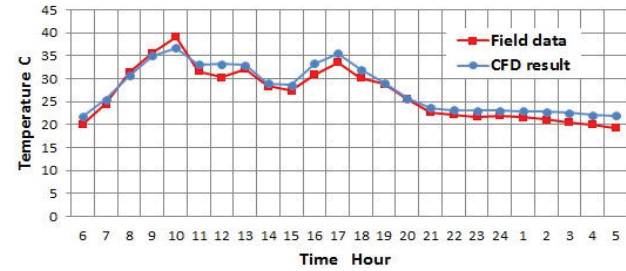


Fig. 14. Comparisons of field and modeled module temperatures; a cloudy summer day (7/11/2011); 2-D simulations.
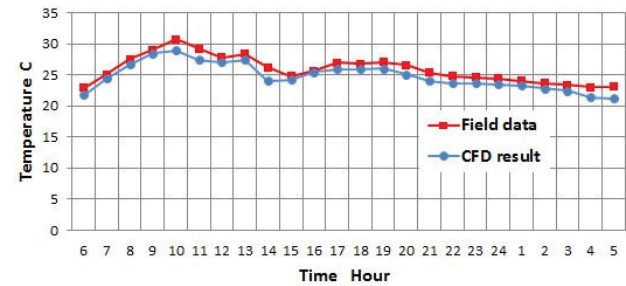


Fig. 15. Comparisons of field and modeled air temperatures at a height of 2.5 m; a cloudy summer day (7/11/2011); 2-D simulations.

Figures 16a and 16b show the air temperature as a function of height at different downwind distances in the morning and afternoon during a sunny summer day. At 9 am (irradiance 500 W/m2, wind speed 1.6 m/s, inlet ambient temperature 23.7℃), the heat from the solar array is dissipated at heights of 5-15m, whereas at 2 pm (irradiance 966 W/m$^2$, wind speed 2.8m/s, inlet ambient temperature 28.6℃, the temperature of the panels has reached the daily peak, and the thermal energy takes up to 18 m to dissipate.
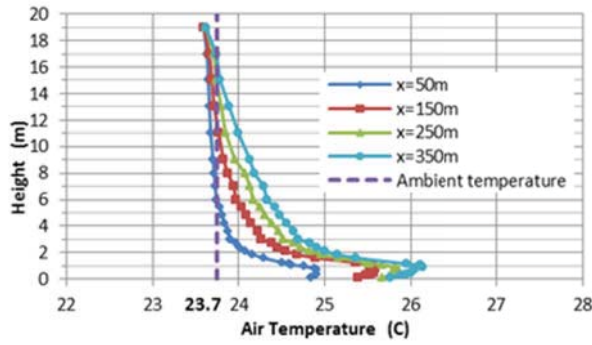
(a) 9:00 am
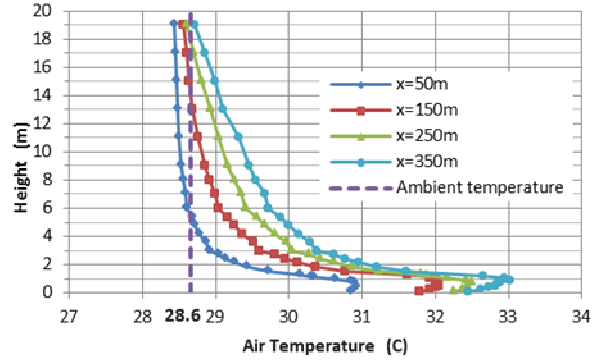


(b) 2:00 pm

Fig. 16 Air temperatures within the solar farm, as a function of height at different downwind distances. From 2-D simulations during a sunny summer day (7/1/2011) at 9 am and 2 pm.

## IV. CONCLUSION

The field data and our simulations show that the annual average of air temperatures at 2.5 m of the ground in the center of simulated solar farm section is 1.9 higher than the ambient and that it declines to the ambient temperature at 5 to 18 m heights. The field data also show a clear decline of air temperatures as a function of distance from the perimeter of the solar farm, with the temperatures approaching the ambient temperature (within 0.3 ), at about 300 m away. Analysis of 18 months of detailed data showed that in most days, the solar array was completely cooled at night, and, thus, it is unlikely that a heat island effect could occur.

Our simulations also show that the access roads between solar fields allow for substantial cooling, and therefore, increase of the size of the solar farm may not affect the temperature of the surroundings. Simulations of large (e.g., 1 million $m^2$) solar fields are needed to test this hypothesis.

### REFERENCES

[1] D. Turney and V. Fthenakis Environmental, "Impacts from the installation and operation of large-scale solar power slants," *Renewable and Sustainable Energy Reviews*, vol. 15, pp. 3261-3270, 2011.
[2] F.G. Nemet. "Net radiative forcing from widespread deployment of photovoltaics," *Environ. Sci. Technol.*, vol. 43, pp. 2173-2178, 2009.
[3] M. Donovan, "Memorandum: impact of PV systems on local temperature," *SunPower*, July 6, 2010. http://www.rurdev.usda.gov/SupportDocuments/EA_5_17_13_RUS_ PartA.pdf
[4] Y. Genchi, M. Ishisaki, Y. Ohashi, H. Takahashi, & A. Inaba, "Impacts of large-scale photovoltaic panel installation on the heat island effect in Tokyo, " *in Fifth Conference on the Urban Climate*, 2003.
[5] Theory Guide, *ANSYS Fluent HELP 13*.

RMetS
Royal Meteorological Society

# Impacts of land use land cover on temperature trends over the continental United States: assessment using the North American Regional Reanalysis

Souleymane Fall,[a,f] Dev Niyogi,[a,b]* Alexander Gluhovsky,[a,c] Roger A. Pielke Sr,[d]
Eugenia Kalnay[e] and Gilbert Rochon[f]

[a] *Department of Earth and Atmospheric Sciences, Indiana State Climate Office, Purdue University, West Lafayette, IN 47906, USA*
[b] *Department of Agronomy, Purdue University, West Lafayette, IN 47906, USA*
[c] *Department of Statistics, Purdue University, West Lafayette, IN 47906, USA*
[d] *CIRES and ATOC, University of Colorado, Boulder, CO, USA*
[e] *Department of Atmospheric and Oceanic Science, University of Maryland, College Park, Maryland, USA*
[f] *Purdue Terrestrial Observatory, Rosen Center for Advanced Computing, Purdue University, West Lafayette, IN 47906, USA*

**ABSTRACT:** We investigate the sensitivity of surface temperature trends to land use land cover change (LULC) over the conterminous United States (CONUS) using the observation minus reanalysis (OMR) approach. We estimated the OMR trends for the 1979–2003 period from the US Historical Climate Network (USHCN), and the NCEP-NCAR North American Regional Reanalysis (NARR). We used a new mean square differences (MSDs)-based assessment for the comparisons between temperature anomalies from observations and interpolated reanalysis data. Trends of monthly mean temperature anomalies show a strong agreement, especially between adjusted USHCN and NARR ($r = 0.9$ on average) and demonstrate that NARR captures the climate variability at different time scales. OMR trend results suggest that, unlike findings from studies based on the global reanalysis (NCEP/NCAR reanalysis), NARR often has a larger warming trend than adjusted observations (on average, 0.28 and 0.27 °C/decade respectively).

OMR trends were found to be sensitive to land cover types. We analysed decadal OMR trends as a function of land types using the Advanced Very High Resolution Radiometer (AVHRR) and new National Land Cover Database (NLCD) 1992–2001 Retrofit Land Cover Change. The magnitude of OMR trends obtained from the NLDC is larger than the one derived from the 'static' AVHRR. Moreover, land use conversion often results in more warming than cooling.

Overall, our results confirm the robustness of the OMR method for detecting non-climatic changes at the station level, evaluating the impacts of adjustments performed on raw observations, and most importantly, providing a quantitative estimate of additional warming trends associated with LULC changes at local and regional scales. As most of the warming trends that we identify can be explained on the basis of LULC changes, we suggest that in addition to considering the greenhouse gases–driven radiative forcings, multi-decadal and longer climate models simulations must further include LULC changes. Copyright © 2009 Royal Meteorological Society

KEY WORDS    land use land cover change; reanalysis; temperature trends; observed minus reanalysis approach; US historical climate network

*Received 2 January 2009; Revised 8 July 2009; Accepted 8 July 2009*

## 1. Introduction

Temperature trends result from natural and anthropogenic factors; the latter (especially $CO_2$ resulting from human activities) has been mainly seen as the result of increasing concentrations of greenhouse gases (IPCC 2001; Trenberth *et al.*, 2007). Recent investigations have also shown that climate forcing from land use/land cover (LULC) change also significantly impacts temperature trends (e.g. Bonan, 1997; Gallo *et al.*, 1999; Chase *et al.*, 2000; Feddema *et al.*, 2005; Christy *et al.*, 2006, Roy *et al.*, 2007; Wichansky *et al.*, 2008). Some studies suggest that new

metrics should be considered for characterizing climate changes (e.g. Pielke *et al.*, 2002a, 2004, 2007b; Joshi *et al.*, 2003; NRC, 2005; Williams *et al.*, 2005). Consequently, attention has been increasingly given to the impact of LULC change on climate. For example, it has been reported that land use changes due to agriculture lead to decreased surface temperatures (Mahmood *et al.*, 2006; Roy *et al.*, 2007; Lobell and Bonfils, 2008). LULC change can significantly influence climatological variables such as maximum, minimum and diurnal temperature range (Gallo *et al.*, 1996; Hale *et al.*, 2006, 2008). The effects of urbanization on climate trends have been analysed using classifications of meteorological stations as urban or rural based on population data (Karl *et al.*, 1988; Easterling *et al.*, 1997) or satellite measurements of night lights (Gallo *et al.*, 1999; Peterson *et al.*, 1999;

* Correspondence to: Dev Niyogi, Department of Earth and Atmospheric Sciences and Department of Agronomy, Purdue University, Indiana State Climate Office, West Lafayette, IN 47906, USA. E-mail: climate@purdue.edu

Hansen *et al.*, 2001). Various studies of urban heat island have determined land surface/temperature impacts of different magnitudes (Kukla *et al.*, 1986; IPCC, 2001; Peterson, 2003). Other non-climatic factors have been found to have significant impacts on temperature trends: e.g. corrections due to changes in the times of observation, type of equipment and station location (Karl *et al.*, 1986; Quayle *et al.*, 1991; Hansen *et al.*, 2001; Pielke *et al.*, 2002b; Vose *et al.*, 2003).

The increasing evidence that some non-radiative forcings such as LULC change may also be major factors contributing to climate change has prompted the National Research Council (NRC, 2005) to recommend the broadening of the climate change issue to include LULC processes as an important climate forcing.

Recent studies have used the 'observation minus reanalysis' (OMR) method to estimate the impact of land use changes by computing the difference between the trends of surface temperature observations and reanalysis datasets (Kalnay and Cai, 2003; Zhou *et al.*, 2004; Frauenfeld *et al.*, 2005; Lim *et al.*, 2005, 2008; Kalnay *et al.*, 2006, Pielke *et al.*, 2007b; Nuñez *et al.*, 2008). The OMR method is effective because some reanalyses do not assimilate surface temperature over land and therefore are not directly sensitive to near surface properties. Moreover, this method separates land surface effects from human-caused and natural climate variability caused by changes in atmospheric circulation, as these changes are included in both observations and reanalysis (Kalnay *et al.*, 2008).

Thus, the impact of land surface can be estimated by comparing trends observed by surface stations with surface temperatures derived from the reanalysis data. Likewise, the reanalysis can be used to detect non-climatic biases that are introduced by changes in observation practices and station locations (Kalnay *et al.*, 2006, Pielke *et al.*, 2007a, 2007b).

So far, the primary reanalysis datasets for the aforementioned OMR studies have been the NCEP/NCAR, NCEP/DOE and the European Center for Medium range Weather Forecasting (ECMWF) 40-year (ERA40) reanalyses. The OMR signals in the ERA-40 are similar but weaker than those in the NCEP reanalyses because the ERA-40 made some use of surface temperature observations over land to initialize soil moisture and temperature (Lim *et al.*, 2005). Building on the NRC (2005) recommendations and the IGBP integrated land ecosystem – atmosphere processes study (iLEAPS) framework, the objective of this study is to improve our understanding of LULC change impacts on temperature trends at local and regional scales using relatively new and high resolution datasets. The analysis is twofold: (1) we compare the trends of US historical climate network (USHCN) adjusted and unadjusted temperatures with the ones derived from the higher resolution North American Regional Reanalysis (NARR) as a method for detecting a signature of land surface properties on temperature trends. Like the NCEP global reanalysis, NARR does not use surface temperature observations (Mesinger *et al.*,

2006) and therefore is a good reanalysis to estimate the impacts of surface processes using OMR. (2) We investigate the sensitivity of surface temperature to LULC changes over the conterminous United States by analyzing OMR trends with respect to two datasets: the land cover classification derived from the advanced very high resolution radiometer (AVHRR) and the new national land cover database (NLCD) 1992/2001 Retrofit Land Cover Change.

Section 2 reviews the data and methods. Section 3 presents the results of (1) OMR trends over the United States and (2) the sensitivity of surface temperatures to land cover types. The summary and conclusions are presented in section 4.

## 2. Data and methods

The surface observation data used in this study consist of monthly mean temperatures for 1979–2003 from the USHCN (Easterling *et al.*, 1996) obtained from http://cdiac.ornl.gov/epubs/ndp/ushcn/monthly.html. We focus on raw as well as adjusted temperatures. However, even though most of the USHCN stations have very long periods of record, the raw data is not continuous and, in some instances, the amount of missing data makes it difficult to perform accurate trend analyses. For this reason, the use of the raw data was limited (15 stations for individual comparisons with the reanalysis), as compared to that of the adjusted data (586 stations used for the analysis at national level). We also used reanalysis data from NARR obtained at http://nomads.ncdc.noaa.gov. NARR has been developed as a major improvement upon the earlier NCEP/NCAR and NCEP/DOE in both resolution (32-km grid increments) and accuracy (Mesinger *et al.*, 2006). It has taken advantage of the use of a regional model (the Eta Model) and advances in modelling and data assimilation. With NARR, very substantial improvements in the accuracy of temperatures and winds compared to those of NNR have been achieved throughout the troposphere (Mesinger *et al.*, 2006). Also, as compared to the NCEP/NCAR and NCEP/DOE, NARR has a higher temporal resolution (3-h time intervals). Thus, not only are analysis and first-guess fields available at shorter time intervals but also a considerable fraction of the data are being assimilated at more frequent times (Mesinger *et al.*, 2006).

The set of stations used for a comparison with the reanalysis at individual site level span both rural and urban areas in the eastern United States. The choice was based on record length (all stations have less than 8% of missing data) and on information (station quality, geographical location, urban-rural type) provided by local climatologists and National Weather Service personnel.

As in Kalnay and Cai (2003), we applied the OMR method by linearly interpolating the NARR gridded temperatures to individual station sites and then removing the monthly mean annual cycle from both interpolated reanalysis and observations. The resulting time series

and their trends were compared at different time scales (monthly, seasonal and long term) by means of the linear trends of 10-year running windows, which smoothes out the short-term fluctuations and random variations and highlights long-term trends. As a result of this procedure, the trends were presented for the period December 1983–January 1998.

For the comparisons between temperature anomalies from unadjusted ($U$) or adjusted ($A$) observations and interpolated reanalysis data ($N$), we employed the mean squared differences (MSDs),

$$\mathrm{MSD}_1 = E\left[(U - N)^2\right] \text{ and}$$
$$\mathrm{MSD}_2 = E\left[(A - N)^2\right] \quad (1)$$

where E[] stands for the mathematical expectation, or the mean, or the ensemble average. The common practice is to use the correlations instead, which is less appropriate. First, correlation is only one among several factors contributing to MSD (e.g. Kobayashi and Salam, 2000); second, interpreting the correlation coefficient is complicated as various features of the data under study may strongly affect its magnitude (Wilcox, 2003).

In our analysis, a positive difference

$$d = \mathrm{MSD}_1 - \mathrm{MSD}_2 \quad (2)$$

would indicate that the adjustments are consistent with the reanalysis, and the larger the $d$, the better the adjustments perform in reducing the differences between NARR and the observed anomalies.

The difference $d$ is estimated from the data by

$$\hat{d} = \frac{1}{n}\sum_{i=1}^{n}(u_i - n_i)^2 - \frac{1}{n}\sum_{i=1}^{n}(a_i - n_i)^2, \quad (3)$$

where $n$ is the number of observations for a station, $u_i$, $a_i$ and $n_i$ are the unadjusted, adjusted and reanalysis values respectively. The accuracy of such estimation was characterized by 90% bootstrap confidence intervals for unknown true values of $d$ (for details see Appendix).

To investigate the spatial patterns of temperature trends, we generated a gridded USHCN dataset of the adjusted temperatures from 586 USHCN stations that are well distributed nationwide, and then regridded the resulting surface to the NARR resolution.[1] (An R script asks for a user-defined resolution (here, the NARR one), and interpolates observed values of the 586 stations to gridpoints using the simple Kriging method with the exponential variogram model.) Spatial patterns of OMR were derived from the new grids by using the Spline interpolation method (Spline with tension) with ArcGIS Spatial Analyst. Given the substantial amount of missing data, converting the raw USHCN observations into gridded information resulted in inaccurate values and, therefore, we did not include the raw data in this segment of the analysis. All trends were computed using

a simple linear regression and their degree of significance was assessed using the related $P$-values.

We examined the sensitivity of surface temperature to land cover types by using two land cover datasets:

- the land cover classification derived from AVHRR (Hansen *et al.*, 2000). The 1-km grid increment data originates from the Global Land Cover Facility (University of Maryland) and consists of 14 land cover types for North America (12 represented over the CONUS). The dataset has a length of record of 14 years (1981–1994), providing the ability to test the stability of classification algorithms (Hansen *et al.*, 2000), and the related OMR analysis was performed over the same period.

- the NLCD 1992/2001 Retrofit Land Cover Change (Homer *et al.*, 2007), obtained from the multi-resolution landcharacteristics (MRLC) website. This new US Geological Survey dataset was created using 76 standard mapping zones (65 over the CONUS) regrouped in 15 larger zonal areas (14 over the CONUS) and has a 30-m resolution. The dataset was generated using a decision tree classification of Landsat imagery from 1992 and 2001. The resulting product consisted of unchanged pixels between the two dates and changed pixels that are labelled with a 'from–to' land cover change value. In this study, out of 87 classes for the whole dataset, only 25 are considered: 5 unchanged LULC types (urban, barren, forest, grassland/shrubland and agriculture) and 20 classes that depict conversion types.

Using both datasets conveys much more information on land use/cover types and allows an analysis based on both static and dynamic datasets.

ArcGIS, which integrated the different data sources, was used to (1) create a subset of the AVHRR dataset for the CONUS; (2) compute OMR values from interpolated observations and reanalysis temperature trends (for the LULC change analysis, OMR values were computed over the same period as the period of acquisition of the dataset: 1992–2001); (3) convert the resulting OMR surface to gridpoints using the Spatial Analyst 'Sample' tool and (4) convert the gridded LULC datasets into polygon shapefiles representing land cover types. OMR gridpoints that belong to each LULC type were selected and exported as individual tables and summary statistics were derived for each type.

While the gridded analysis was done for all the USHCN sites, we chose 15 different CONUS stations for more detailed assessments that included reviewing station history files and related reports to document the local changes. As initially shown in Kalnay and Cai (2003) and verified in several follow-up studies, the analysis of a subset of stations provides robust results and conclusions regarding the processes and the impact of LULC on the temperature trends (Lim *et al.*, 2008).

## 3. Results

### 3.1. Observation, reanalysis and OMR trends

The comparison, on a station-by-station basis, of temperature anomalies from surface station observations and interpolated reanalysis data (e.g. Figure 1(a)), shows a good agreement in the inter-annual variability of surface observations and NARR (e.g. correlation coefficient of adjusted USHCN *vs* NARR for Orangeburg: 0.93). This agreement confirms findings from previous studies, which show that both NCEP/NCAR and NARR satisfactorily capture the observed intra-seasonal and inter-annual fluctuations (Kalnay and Cai, 2003; Kalnay *et al*., 2006; Pielke *et al*., 2007a). Furthermore, the combined use of observations and reanalysis can yield additional information that is related to station environment and observation practices. For example, Orangeburg, SC, which is located in a wooded residential area within the city limits with no significant obstruction within 200 feet, experienced a number of changes: moved 0.25 miles SW from its previous location (November 1984), new temperature equipment (August 1992), altered sensor elevation (February 1994) and time of observation (from 24 : 00 to 7 : 00 effective January 1996). The differences in the USHCN observations and reanalysis in Figure 1(a) can be attributed to these documented changes that took place at the station and were not recorded by NARR. As a result,

the 10-year running window trends (Figure 1(b)) show substantial differences between raw and analysed temperatures throughout most of the study period and highlights the stronger sensitivity of observed temperature trends to surface properties. Therefore, the comparison between surface observations and NARR is efficient in detecting LULC changes that took place at the vicinity of stations or changes related to observation practices.

The adjustments made at some stations considerably reduced the differences between NARR and observed anomalies. For example, the MSD method reveals that the impact of adjustments are particularly noticeable in Orangeburg (South Carolina), Portage (Wisconsin), Conception and Rolla University (Missouri), as attested by their larger value of $d$, which represents the difference between MSDs (Figure 2). The MSD results show that 14 out of 15 of the stations investigated in this study exhibit statistically significant differences. Of these, 11 stations show positive differences (Table I).

Table II shows the decadal temperature trends for the 15 stations, and their OMR (trend differences) for the 1979–2003 period. From one station to another, the trends vary considerably. However, fewer variations occur in the NARR trends (smaller standard deviation: 0.16 °C), as compared to the raw observed trends (0.22 °C) and, to a lesser extent, the adjusted trends (0.17 °C). Such patterns were also observed with the
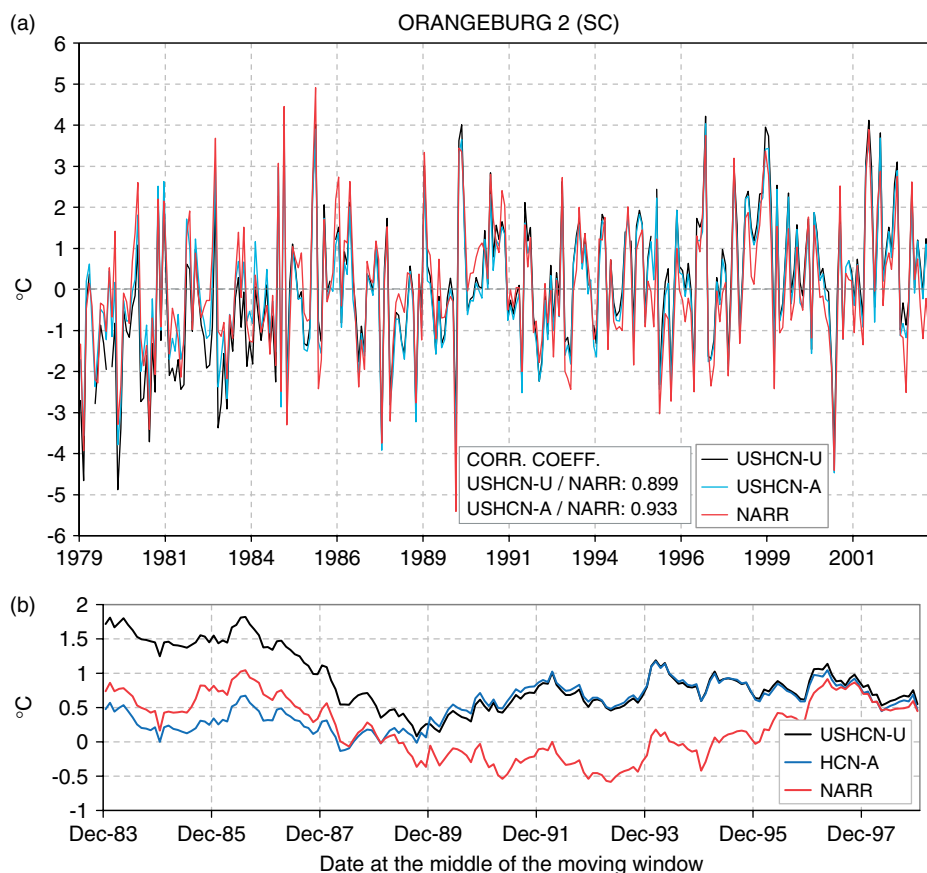


Figure 1. (a) Monthly mean temperature anomalies of observations at Orangeburg (SC). USHCN-U: unadjusted (raw) observations; USHCN-A: adjusted observations; and NARR: regional reanalysis; (b) Trends of 10-year running windows. This figure is available in colour online at wileyonlinelibrary.com/journal/joc
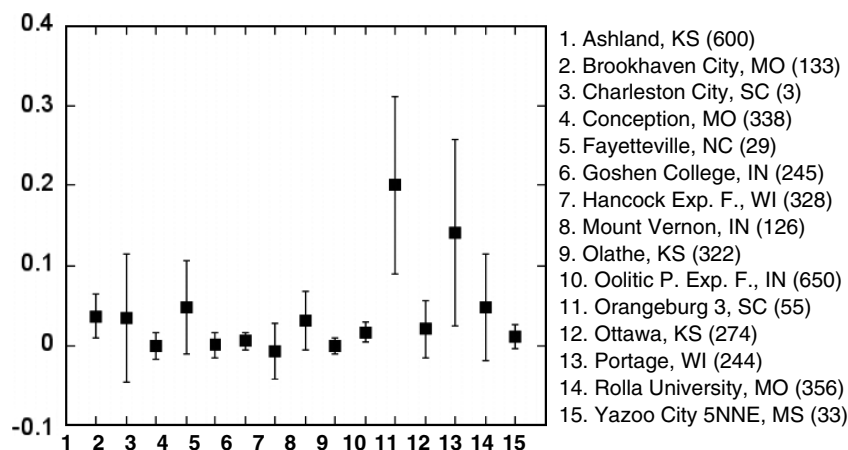
Figure 2. Difference $\hat{d}$ between $MSD_1$ and $MSD_2$ (filled squares) and their error bars (vertical lines) at 90% confidence level for selected stations (elevation in meters).

Table I. Difference $\hat{d}$ between $MSD_1$ and $MSD_2$ – mean squared differences between unadjusted station observations and NARR and adjusted station observations and NARR, respectively (units are the squares of the quantity being measured: °C/decade), and their 90% confidence intervals (CI). The land use 100-m radius around station is indicated.

| Stations | Land use | $\hat{d}$ | 90% CI |
|---|---|---|---|
| Ashland (KS) | Cropland/grassland/urban | 0.037 | (0.023, 0.051) |
| Brookhaven City (MS) | Unknown | 0.034 | (0.001, 0.082) |
| Charleston City (SC) | Cropland/grassland | 0 | (−0.008, 0.009) |
| Conception (MO) | Urban | 0.048 | (0.018, 0.076) |
| Fayetteville (NC) | Cropland/grassland | 0.001 | (−0.007, 0.009) |
| Goshen College (IN) | Urban | 0.006 | (0.001, 0.012) |
| Hancock Exp. F (WI) | Cropland/grassland | −0.007 | (−0.025, 0.010) |
| Mt Vernon (IN) | Urban | 0.031 | (0.012, 0.049) |
| Olathe (KS) | Cropland/grassland | 0 | (−0.005, 0.005) |
| Oolitic P. Exp. F (IN) | Cropland/grassland | 0.017 | (0.011, 0.023) |
| Orangeburg 3 (SC | Urban | 0.201 | (0.144, 0.255) |
| Ottawa (KS) | Urban | 0.021 | (0.004, 0.040) |
| Portage (WI) | Cropland/grassland | 0.141 | (0.083, 0.200) |
| Rolla University (MO) | Cropland/grassland | 0.048 | (0.016, 0.083) |
| Yazoo City 5NNE (MS) | Cropland/grassland | 0.011 | (0.004, 0.019) |

NCEP/NCAR reanalysis (Pielke *et al.*, 2007a), and show that, while station observations express local characteristics, the reanalysis effectively captures regional trends. Previous studies based on the NCEP/NCAR reanalysis have found that the reanalysis exhibits a smaller warming trend as compared to the surface observations (Kalnay and Cai, 2003; Lim *et al.*, 2005; Kalnay *et al.*, 2006) and as a result, the OMR trends (trend differences) are generally positive, especially for urban stations. With NARR, a station-by-station analysis reveals that this is not often the case; i.e. as seen in Table II, 9 stations out of the 15 exhibit negative OMRs when NARR is compared to unadjusted or adjusted observations, or both, regardless of the station type. For example, rural stations such as Goshen College (IN) and Hancock Experimental Farm (WI), as well as urban locations (Mount Vernon-IN and Portage-WI) show negative OMRs. This difference in the positive *versus* positive and negative trends seen in the NCEP/NCAR reanalysis and NARR-based OMR analysis

could be primarily due to the finer grid spacing represented in the NARR, which may be capturing some of the local- to regional-scale changes.

Trends of 10-year running windows obtained from the gridded USHCN (adjusted) and NARR over the CONUS (Figure 3) indicate that observations and reanalysis generally not only agree in terms of variability but also show that NARR exhibits a larger trend than the adjusted USHCN over most of the study period. Consequently, the OMR time series is dominated by a negative trend, as already observed in some surface observation stations. This further confirms that, unlike other reanalysis datasets (e.g. NCEP, ERA 40), NARR has larger trends than observations.

Figure 4 shows the geographical distribution of decadal temperature anomaly trends over the CONUS. As expected, the observations (Figure 4(a)) exhibit more local scale variations and the reanalysis (Figure 4(b)) shows more uniform patterns, especially in the eastern

Table II. Temperature anomalies and OMR decadal trends for selected stations over the eastern United States (missing data: %; trend units: °C/decade). U: unadjusted (raw) USHCN observations; A: adjusted USHCN observations; N: North American Regional Reanalysis (NARR). The asterix sign (*) denotes rural stations. Trends in bold are significant at the 5% level.

| STATIONS | Missing U (%) | Trend U | Trend A | Trend N | U − N | A − N |
|---|---|---|---|---|---|---|
| Ashland (KS)* | 3.33 | **0.54** | **0.35** | 0.26 | 0.28 | 0.08 |
| Brookhaven City (MS) | 7 | 0.25 | 0.18 | **0.26** | −0.01 | −0.08 |
| Charleston City (SC) | 5.33 | **0.48** | **0.46** | 0.05 | 0.43 | 0.41 |
| Conception (MO)* | 8 | 0.30 | 0.41 | 0.37 | −0.07 | 0.04 |
| Fayetteville (NC) | 4 | **0.41** | **0.36** | 0.19 | 0.22 | 0.17 |
| Goshen College (IN)* | 2 | 0.32 | 0.34 | **0.48** | −0.16 | −0.14 |
| Hancock Exp. F (WI)* | 2.33 | 0.02 | 0.06 | **0.49** | −0.47 | −0.43 |
| Mt Vernon (IN) | 7.33 | 0.30 | 0.30 | **0.53** | −0.23 | −0.23 |
| Olathe (KS) | 0.66 | **0.55** | **0.59** | 0.40 | 0.16 | 0.19 |
| Oolitic P. Exp. F (IN) | 1.66 | **0.42** | **0.43** | **0.71** | −0.29 | −0.29 |
| Orangeburg 3 (SC) | 3 | **0.95** | **0.58** | 0.29 | 0.66 | 0.29 |
| Ottawa (KS)* | 5 | **0.54** | **0.50** | 0.38 | 0.16 | 0.12 |
| Portage (WI) | 1 | 0.35 | **0.48** | **0.52** | −0.17 | −0.04 |
| Rolla University (MO) | 2.66 | 0.26 | **0.50** | 0.34 | −0.07 | 0.17 |
| Yazoo City 5NNE (MS) | 3.33 | 0.02 | 0.01 | 0.28 | −0.25 | −0.26 |
| Average | | 0.38 | 0.37 | 0.37 | 0.01 | 0.00 |
| Standard deviation | | 0.22 | 0.17 | 0.16 | | |



Figure 3. Trends of 10-year running windows for USHCN-A and NARR temperature anomalies averaged over the United States and the resulting OMR. This figure is available in colour online at wileyonlinelibrary.com/journal/joc

United States. The trends are significant at the 5% level in most of the eastern and southern United States (Figure 4(c)). Overall, USHCN and NARR agree in that they both show areas of warming trend around the Great Lakes, upper Midwest and the Northeast United States. The difference between the two samples is statistically significant (*t*-test, alpha = 0.05). On average, the adjusted observations and reanalysis show an increase of 0.27 °C/decade and 0.28 °C/decade respectively. As a result, the overall OMR is on average slightly negative, as confirmed by the average OMR value over the CONUS (Figure 5), but with positive and negative regions. It is mostly positive in the East Coast, and, east of the Rockies, it is negative in the northern portions of the country.

Kalnay *et al*. (2006) found qualitative agreement between the NCEP-NCAR OMR east of the Rockies, and the Hansen *et al*. (2001) 'urbanization' trend corrections, where 'rural' or 'urban' stations were defined on the basis of satellite nightlights. Figure 6 presents the NARR OMR with the Hansen *et al*. 'urban trend corrections', with the colours of the OMR reversed to facilitate the comparison. Once again, there is good qualitative agreement, even though Hansen *et al*'s urban corrections are calculated for a longer period (1950–1999). For example, over the Rockies (not included in Kalnay *et al*. (2006)), the OMR is more positive, sugesting a warming trend over mountainous regions due to surface effects, similar to the correction in Hansen *et al*. (2001). These results indicate that the differential trends based on the nightlight classification of stations, like the OMR, reflect changes in land use rather than simply urbanization, and that they can be either positive or negative.
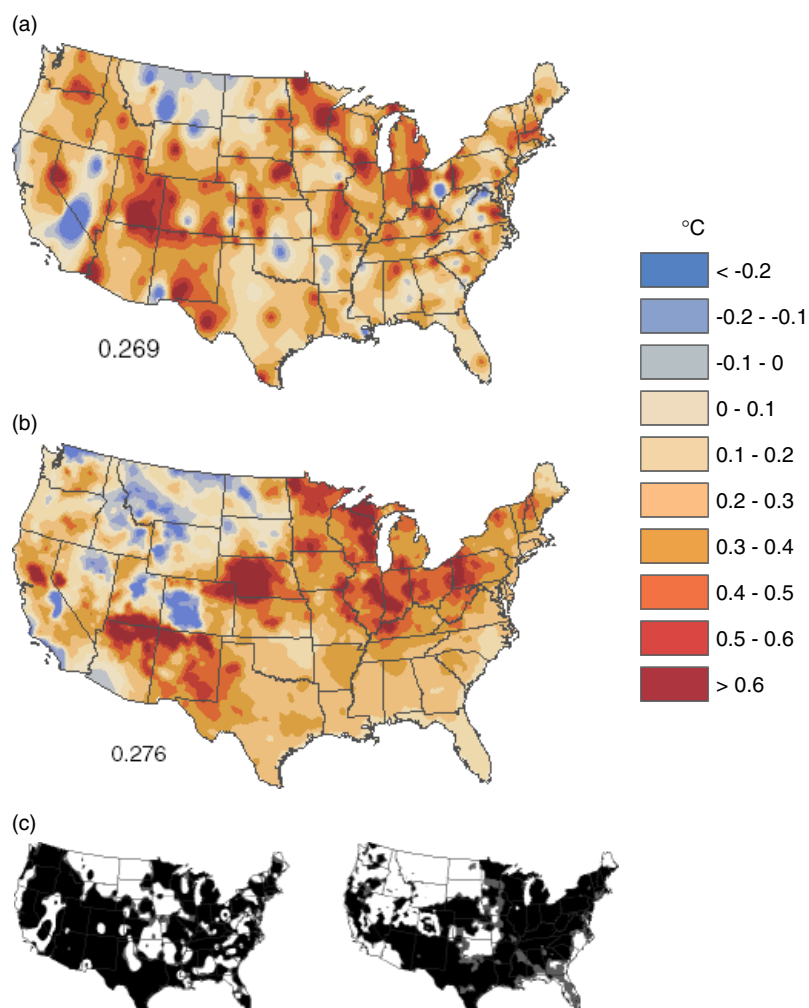
Figure 4. Mean temperature anomaly trends per decade based on monthly average data (1979–2003): (a) USHCN adjusted; (b) NARR; (c) Maps of *P*-values: 0.05 (black) and 0.1 (black & grey), left: USHCN adjusted and right: NARR. This figure is available in colour online at wileyonlinelibrary.com/journal/joc
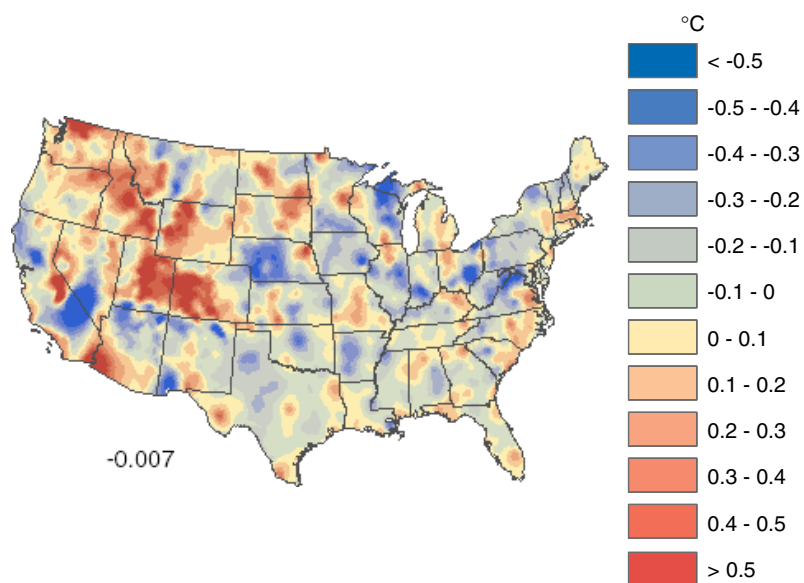


Figure 5. Adjusted observation minus reanalysis (OMR): anomaly trend differences for the 1979–2003 period. This figure is available in colour online at wileyonlinelibrary.com/journal/joc
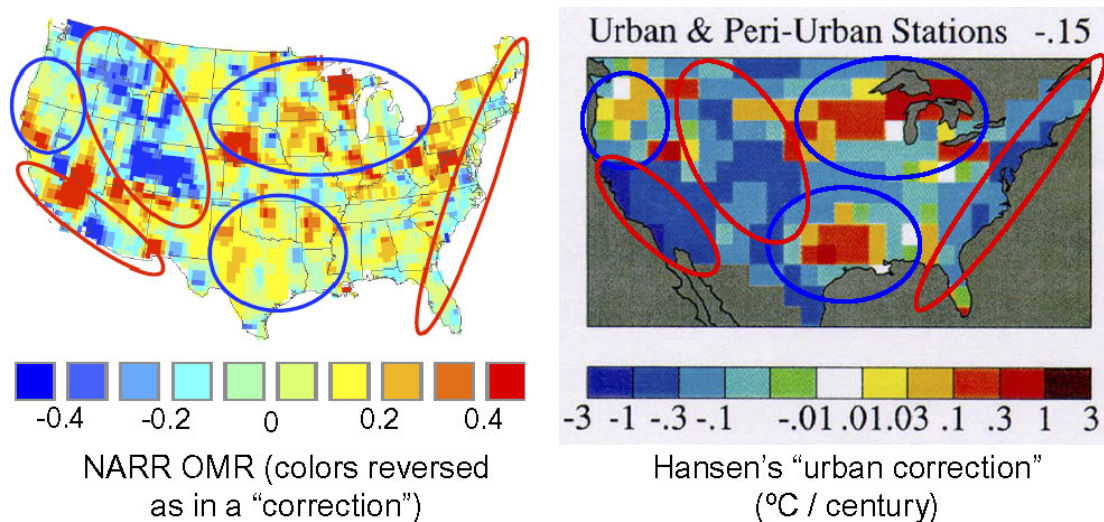
Figure 6. Comparison of the 'urbanization trends correction' derived by Hansen *et al.* (2001) using nightlights to classify stations as urban or rural, and the OMR trends with the sign changed to facilitate the comparison. This figure is available in colour online at wileyonlinelibrary.com/journal/joc
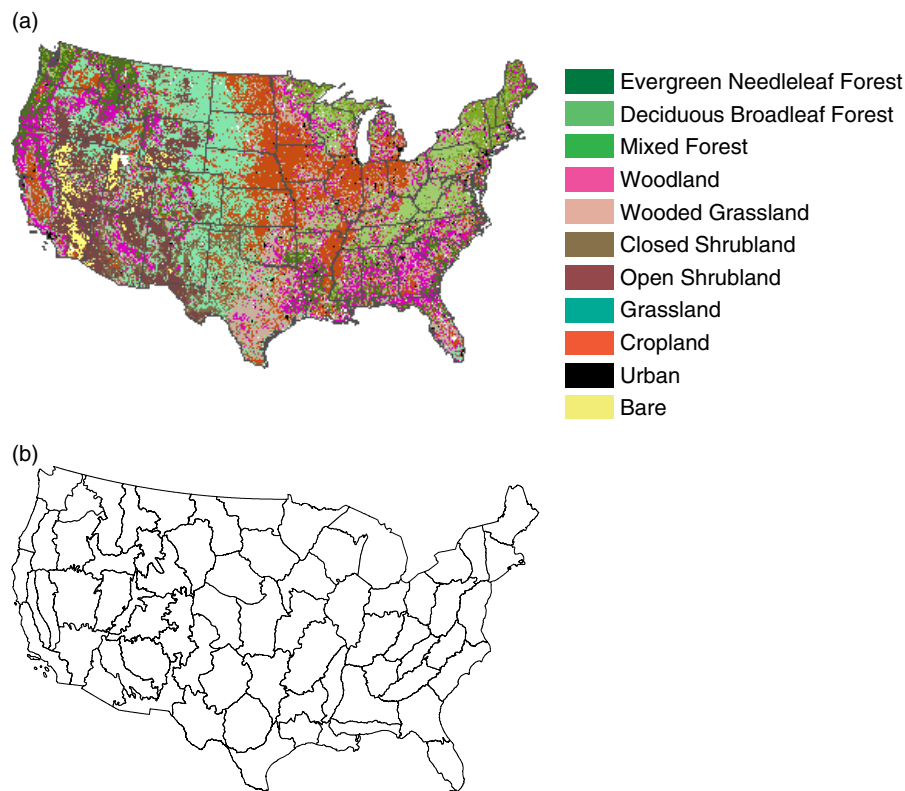


Figure 7. (a) 1-km increment land cover classification derived from AVHRR; (b) NLCD mapping zones for the CONUS. This figure is available in colour online at wileyonlinelibrary.com/journal/joc

## 3.2. Surface temperature trends with respect to LULC changes

To examine surface temperatures with respect to LULC, we associated the OMR trends with land cover types. Figure 7(a) shows the 1-km grid increment land cover classification derived from AVHRR. Only 11 land types were considered in this study. Urban areas, which represent only 0.31% of the surface, cannot be easily seen on the land cover map at this scale.

Anomaly trends per decade for the USHCN observations and reanalysis and the resulting OMRs as a function of land cover types are shown in Table III. Most land cover types show a weakly positive OMR trend per decade (0.034 °C to 0.004 °C) with the exception of wooded grassland, closed shrubland, mixed forest and deciduous broadleaf forest. Evergreen needleleaf forests, open shrublands, bare soils and urban areas exhibit the largest (positive) OMR values. These results are

Table III. Anomaly trends per decade for observations and reanalysis and the resulting OMRs as a function of AVHRR land cover types (units: °C).

| Land cover types | Area (%) | USHCN-A | NARR | OMR |
|---|---|---|---|---|
| Bare | 11.25 | 0.288 | 0.273 | 0.015 |
| Closed shrubland | 8.84 | 0.282 | 0.301 | −0.019 |
| Croplands | 6.97 | 0.274 | 0.271 | 0.003 |
| Deciduous broadleaf forest | 2.76 | 0.258 | 0.357 | −0.099 |
| Evergreen needleleaf forest | 10.97 | 0.265 | 0.231 | 0.034 |
| Grassland | 7.96 | 0.244 | 0.238 | 0.006 |
| Mixed forest | 5.32 | 0.289 | 0.323 | −0.034 |
| Open shrubland | 17.84 | 0.281 | 0.257 | 0.024 |
| Urban | 0.31 | 0.288 | 0.276 | 0.012 |
| Wooded grassland | 12.89 | 0.266 | 0.284 | −0.018 |
| Woodland | 14.90 | 0.272 | 0.268 | 0.004 |

All trends are significant at the 5% confidence level with the exception of the NARR trends for bare and grassland types.

consistent with the findings of Lim *et al.* (2005, 2008) who point to a weak evaporation feedback over arid areas (bare soils, open shrublands) and a probable linkage to soil moisture levels. OMR trends of opposite signs for forests, also in agreement with Lim *et al.* (2005), point to a number of studies that show that needleleaf forests have low evaporative fraction as compared to deciduous broadleaf forests, which exhibit higher transpiration rates with a greater leaf area index (Baldocchi *et al.*, 2000; Baldocchi, 2005; Bonan *et al.*, 2008), thus leading to a negative temperature trend.

We analysed decadal OMR trends based on LULC changes defined by the National Land Cover Database (NLCD) 1992/2001 Retrofit Land Cover Change in 65 mapping zones over the CONUS (Figure 7(b)). Decadal OMR trends for LULC types that did not change are presented in Figure 8. Barren, urban areas and grass/shrublands show the largest warming (0.077, 0.058 and 0.054 °C respectively). Forests exhibit a less pronounced warming (0.031 °C). On the basis of the AVHRR dataset, most of the forest warming can be attributed to evergreen needleleaf forests. In contrast, there is a cooling of −0.075 °C over agricultural lands. OMR trends derived from the NLDC dataset are larger in magnitude than the AVHRR trends, and the values for each LULC type are significantly different, as attested by their error bars (95% confidence interval).

As shown in Figure 9(a), almost all areas that have experienced urbanization are associated with positive OMR trends (indicative of warming), with values ranging form 0.103 °C (conversion from agriculture to urban) to 0.066 °C (from forest to urban). The only exception is the conversion from barren areas, which shows a slight cooling (−0.014 °C), and although this trend may be questionable because of a small sample size, it agrees with the results of Lim *et al.* (2005, 2008) who observed the largest OMR trends in barren areas, followed by urban areas. These results are consistent with findings from studies such as Kukla *et al.* (1986), Arnfield (2003), Zhou *et al.* (2004) and Hale *et al.* (2006, 2008) that document the warming often associated with urbanization.
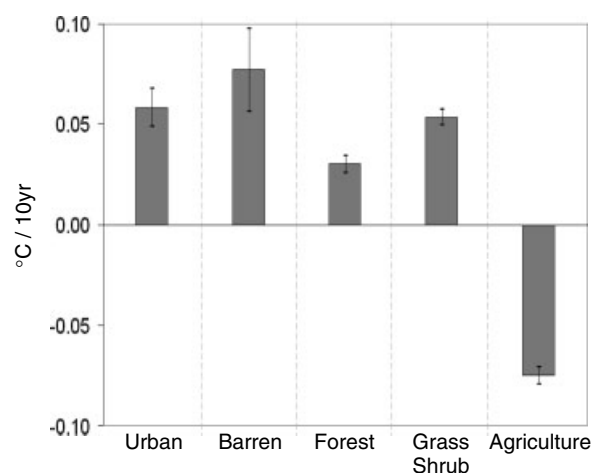


Figure 8. Decadal OMR trends of NLCD LULC types that did not change during 1992–2001. Error bars denote 95% confidence intervals.

Conversion to barren lands (Figure 9(b)) generally resulted in surface warming for all areas that were initially vegetated. The largest warming occurred in areas that changed from agriculture to barren (0.085 °C). Only moderate warming occurred in areas that shifted from forest (0.041 °C) and grass/shrub (0.039 °C). A slight cooling is recorded for locations that were initially in urban settings (−0.018 °C), but this estimate is uncertain, as attested by the large confidence intervals. Deforestation results in warming because of the shift of the surface energy partitioning into more sensible and less latent heat (Chagnon, 1992; Foley *et al.*, 2005). However, unlike studies that point to a significant increase in temperature for areas that experienced deforestation (e.g. Sud *et al.*, 1996; Lean and Rowntree, 1997; Werth and Avissar, 2004), our results suggest that only moderate warming occurred in deforested areas over the United States. Moreover, the relatively large standard deviation in this change class (0.41 °C) shows a great variability within areas that experienced deforestation.

Conversion to forest (Figure 9(c)) shows mixed results: croplands and bare soils that shifted to forests show
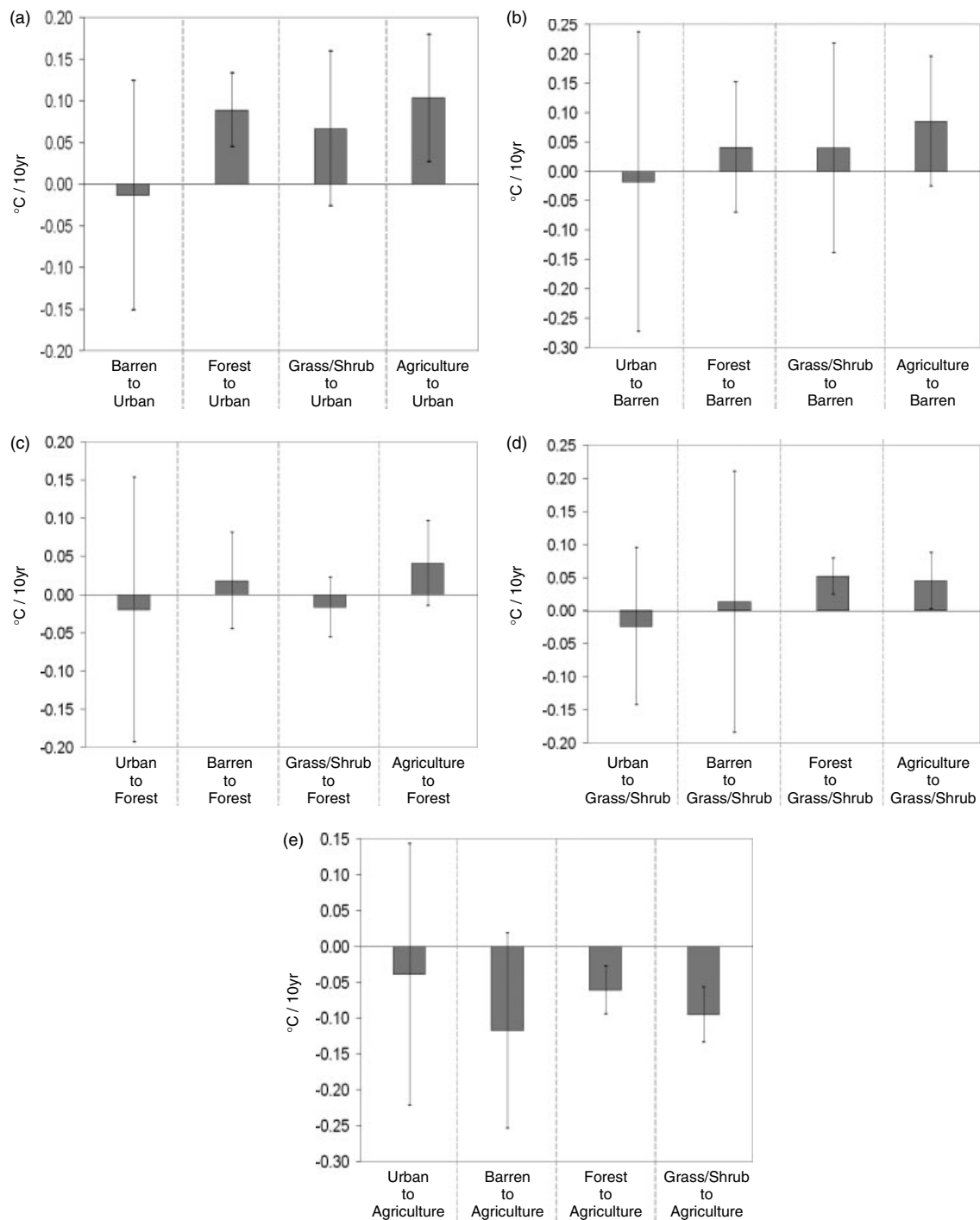
Figure 9. (a) Decadal OMR trends of NLCD LULC types that were converted to urban during 1992–2001, (b) except for barren lands, (c) except for forests,(d) except for grasslands/shrublands, (e) except for agriculture. Error bars denote 95% confidence intervals.

a moderate or small warming (0.041 and 0.018 °C respectively), while areas that were previously grassland/shrubland and urban have slightly negative OMRs (−0.016 and −0.019 °C respectively). The largest variability is found in areas that shifted from grassland/shrubland to forest (standard deviation: 0.36 °C). Results for areas that were previously urban have less reliability due to a small sample size. The warming effect of lower surface albedo that results from afforestation (Betts 2000; Feddema *et al.*, 2005; Gibbard *et al.*, 2005;

Betts *et al.*, 2007) was not seen in our results. Similarly, Hale *et al.* (2008) did not find a clear pattern in areas that experienced a clearcutting of forests.

Decadal OMR trends for areas that have been converted to grassland/shrubland are presented in Figure 9(d). With the exception of areas that were previously urban, where a slight cooling occurs (−0.023 °C), conversion to grassland/shrubland is associated with a modest warming. Trends of areas that were previously forested and agricultural (0.052 and 0.045 °C respectively) are

more reliable due to a larger sample size. Areas that were previously agricultural exhibit a largest standard deviation (0.37 °C), indicating that the amount of warming/cooling varied considerably within this class.

The shift to agriculture (Figure 9(e)) results in a cooling for all conversion types and presents the largest magnitudes of cooling. The conversion of barren areas and grasslands/shrublands are associated with the largest cooling (−0.12 and −0.096 °C respectively). A moderate or relatively small cooling occurs in previously forested and barren areas (−0.061 and −0.039 °C). These results are consistent with a number of studies that show that agricultural areas are often associated with negative trends in irrigated areas (e.g. Christy *et al*., 2006; Mahmood *et al*., 2006; Roy *et al*., 2007; Lobell and Bonfils, 2008) as well as in rainfed croplands (McPherson *et al*., 2004).

## 4. Summary and conclusions

The OMR approach is used to investigate surface temperature trends over the CONUS. This method is made possible by the ability of reanalysis to diagnose regional-scale atmospheric conditions based on observations above the surface being assimilated into a physically consistent atmospheric model. Therefore, as the surface observations are not used in the reanalysis, the difference between the surface observation and reanalysis temperature trends represents that part of the land cover and land use change effect on temperatures which does not extend higher into the atmosphere (and thus is not seen in the reanalysis).

In this study, OMR trends derived from monthly mean temperature anomaly trends computed from USHCN observations (raw and adjusted) and the high-resolution NARR were used to (1) analyse the long term, seasonal and monthly anomaly trends over the CONUS and (2) examine the sensitivity of surface temperatures to land use land cover by using OMR trends as a function of land cover types.

As in similar previous studies (Kalnay and Cai, 2003; Zhou *et al*., 2004; Frauenfeld *et al*., 2005; Lim *et al*., 2005; Kalnay *et al*., 2006), for individual stations as well as the CONUS, the results have shown a good agreement between the observed and analysed temperature anomaly trends (high temporal correlations larger than 90%) and confirm the ability of the reanalyses to satisfactorily capture the intra-seasonal and inter-annual variability.

The analysis of anomaly and OMR trends reveals some prominent results:

1. The MSD method is efficient at assessing the performance of station temperature adjustments with respect to the reanalysis data.
2. Despite the great variability from one station to another, NARR trends exhibit much smaller spatial variations and confirm that the reanalysis effectively captures regional rather than local trends.

3. In contrast with previous studies based on global reanalysis (Kalnay and Cai, 2003; Lim *et al*., 2005), the regional reanalysis often shows a slightly larger trend than the observations and, as a result, the OMR trend is on the average negative. However, the adjusted observations, which are mostly used in this study, are known for reducing the differences with the reanalysis. NCEP/NCAR global reanalysis and the newer NARR are two key datasets in climate studies and there is a large body of literature based on global reanalysis. The differences between results obtained from both datasets suggest the need of conducting comparative studies that may provide further understanding of processes relevant to climate studies.
4. Our results on a station-by-station basis did not suggest significant differences between rural and urban trends, rather they were dependent on regional land use, and agreed better with the classification based on nightlights used by Hansen *et al*. (2001). Kalnay and Cai (2003) found a strong urban–rural signal, but they used different datasets, a different study area (eastern United States) and different period (they also included the 1960–1990's trends). Future analysis with more stations would be therefore useful in understanding the urban–rural temperature differences.

Our analysis of OMR trends with respect to land types using the AVHRR dataset indicate that evergreen needleleaf forests, open shrublands, bare soils and urban areas exhibit the largest increasing trends. Grasslands, woodlands and crops are also modestly positive while wooded grassland, closed shrubland, mixed forest and deciduous broadleaf forest show cooling trends. Our results vary from Lim *et al*. (2005) in that we found much weaker positive OMR trends, e.g. 0.034 *versus* 0.3 °C for bare soils when using regional instead of global reanalysis.

The NLCD 1992/2001 Retrofit Land Cover Change offers a unique opportunity of examining the relationships between OMR trends and the type of land surface by taking into account the dynamic nature of LULC. We found that OMR trends derived from the NLCD dataset display approximately the same patterns as the ones obtained from the 'static' AVHRR dataset, but with a larger magnitude. For example, decadal OMR trends of bare and urban areas for AVHRR are 0.015 and 0.012 °C, whereas for non-changed NLCD they are 0.113 and 0.072 °C respectively. This discrepancy is probably explained by the fact that the AVHRR dataset reflects both non-changed and changed signals.

Moreover, the breakdown of the NLCD dataset into areas that did not change *versus* areas that were converted shows that land use conversion often resulted in more warming than cooling. With the notable exception of agricultural lands, most of the negative trends were derived from conversion types with a small sample size (e.g. the conversion of urban areas). The warming effect generally associated with LULC changes is confirmed in

a number of recent studies (e.g. Hale *et al.*, 2006, 2008; Kalnay *et al.*, 2006; Pielke *et al.*, 2007b).

Our results suggest that for both non-changed and converted land types, agriculture, urbanization and barren soils offered the clearest patterns in terms of sign and magnitude of the OMR trends. Conversion to agriculture resulted in a strong cooling. Conversely, all conversions of agricultural lands resulted in warming. Urbanization and conversion to bare soils were also mostly associated with warming. We conclude that these LULC types constitute strong drivers of temperature change.

Deforestation generally resulted in warming (with the exception of a shift from forest to agriculture) but no clear picture emerged for afforestation. Within each land use conversion type, a great variation of warming/cooling was observed, as attested by relatively large standard deviations. In addition, our analysis shows that there is not always a straightforward relationship between the different types of conversions: for example, (1) both conversion of urban to barren and the opposite resulted in slightly negative OMRs; (2) there was a weak warming of areas that shifted from bare soils to grassland/shrubland and for the opposite as well and (3) both conversion from forest to grassland/shrubland and the opposite were associated with a weak warming. In a number of cases, our estimates were hampered by the lack of significance due to a small number of samples. All these considerations lead us to conclude that the effects of LULC changes on temperatures trends are significant but more localized studies need to be conducted using high-resolution datasets.

Our results were limited due to the missing data often typical of the USHCN raw (unadjusted) observations over the study period. As a result, the trends obtained from this dataset cannot be as accurate as the ones derived from the adjusted observations and reanalysis, even though the anomaly trends at station level showed a good agreement between observed and analysed temperature anomalies. Such a constraint has resulted in spurious trends when we tried to convert the raw observations into gridded data.

However, our results further confirm the robustness of the OMR method for (1) capturing the climate variability at various time scales; (2) detecting non-climatic changes at the station level, including observation practices and land use changes, (3) evaluating the impacts of adjustments performed on raw observations and, most importantly, (4) providing a quantitative estimate of additional warming trends associated with LULC changes at local and regional scales. Despite some uncertainties, the effects of LULC dynamics on temperature trends are well captured by the OMR method, which shows a strong relationship with LULC changes. Furthermore, this study demonstrates that using datasets that reflect the dynamical nature of LULC (such as the new NLCD 1992−2001 Retrofit Land Cover Change) offers unique opportunities for assessing the impacts of LULC change on temperature trends at local and regional scales.

In conclusion, *in situ* observed surface temperatures are affected by local microclimate and non-climatic station changes, and also by the larger scale landscape within the region. By using multiple station observations, one can evaluate the part of the signal in the surface temperature data that is spatially correlated with the regional land cover/land cover characteristics. By comparing the surface temperature data with the reanalysis temperature data diagnosed at the same height, the degree to which the land use/land cover change effect on temperatures does not extend higher into the atmosphere can be assessed. The degree to which this effect occurs depends on landscape type (due to different boundary layer interactions with the free atmosphere above).

The need to separate the local from the regional land use change effect on the temperature record does merit further study, as the latter is a regional climate forcing effect, while the local microclimate and non-climatic station effects are a contamination of the temperature data in terms of constructing regional scale temperature trends.

Because most of the warming trends that we identify can be explained on the basis of LULC changes, we suggest that in addition to considering the well-mixed greenhouse gases and aerosol-driven radiative forcings, multi-decadal and longer climate models simulations must further include LULC changes. In terms of using long-term surface temperature records as a metric to monitor climate change, there also needs to be further work to separate the local microclimate and non-climate station effects from the regional LULC change effects on surface temperatures.

## Appendix: Confidence Intervals for Parameters Computed from Observed Data

The value of $\hat{d}$ is a point estimate of the true value of the parameter of interest $d$. To learn how much importance is reasonable to attach to $\hat{d}$, it is common to provide a

confidence interval (CI) that contains $d$ with a certain coverage probability (0.90 in our study). The unknown value of $d$ may be considered positive if its CI contains only positive numbers, as is the case for 11 out of the 14 stations in our analysis. Note also that it is incorrect to compare $MSD_1$ and $MSD_2$ by computing CIs for each and then considering $MSD_1$ and $MSD_2$ different if their CIs do not overlap (see, e.g. Schenker and Gentleman, 2001).

Classical statistical methods for computing CIs are based on assumptions about the data-generating mechanisms that are rarely met in climatology. One such assumption is that observations follow a Gaussian distribution. It has been realized, however, that even small deviations from the assumptions may result in misleading inference (e.g. Wilcox, 2003). Fortunately, modern computer-intensive resampling (bootstrap) techniques (e.g. Efron and Tibshirani, 1993; Davison and Hinkley, 1997; Lahiri, 2003) permit obtaining reliable inference without making questionable assumptions about the data. The CIs in Table I were computed using the basic bootstrap. This implies, however, that the observations are independent and identically distributed, while climatological variables are typically serially correlated. It is known that bootstrap may underestimate the width of CIs in this case (e.g. Zwiers, 1990). Thus, our results regarding statistical significance may need refinement, which could be accomplished by employing another bootstrap technique, subsampling (Politis *et al.*, 1999), whose practical implementation is now under active development (e.g. Gluhovsky *et al.*, 2005; Gluhovsky and Agee, 2007).

The same applies to our results on uncertainties in trends that may, in this respect, be considered as incremental. In time series analysis, the assumption is often made that the trend is linear, while the residuals from the trend follow a linear autoregressive model. Bloomfield (1992) fitted such a model and a linear trend to an 1861–1989 temperature time series and found a linear trend of 0.58 with 95% (classical) CI, (0.37, 0.76). More recently, Craigmile *et al.* (2004) and Kallache *et al.* (2005) employed wavelets to assess trends while modeling fluctuations with fractional ARIMA models that incorporate long-range dependence.

# References

Arnfield J. 2003. Two decades of urban climate research: a review of turbulence, exchanges of energy and water, and the urban heat island. *International Journal of Climatology* 23: 1–26.

Baldocchi D, Kelliher FM, Black TA, Jarvis PG. 2000. Climate and vegetation controls on boreal zone energy exchange. *Global Change* 6: 69–83.

Baldocchi D. 2005. The role of biodiversity on the evaporation of forests. In *Forest Diversity and Function: Temperate and Boreal Systems*, vol. 176, *Ecological Studies*, Scherer-Lorenzen M, Detlef Schulze E (eds). Springer-Verlag: Berlin, pp 131–148.

Betts R. 2000. Offset of the potential carbon sink from boreal reforestation by decreases in surface albedo *Eos Transactions: AGU* 81(48): Fall Meet. Suppl., Abstract B22C-07.

Betts RA, Falloon PD, Goldewijk KK, Ramankutty N. 2007. Biogeophysical effects of land use on climate: model simulations of radiative forcing and large-scale temperature change. *Agricultural and Forest Meteorology* 142: 216–233.

Bloomfield P. 1992. Trends in global temperature. *Climate Change* 21: 1–16.

Bonan GB. 1997. Effects of Land Use on the Climate of the United States. *Climatic Change* 37: 449–486.

Bonan GB. 2008. Forests and climate change: forcings, feedbacks and the climate benefits of forests. *Science* 320: 1444–1449.

Chagnon SA. 1992. Inadvertent weather modification in urban areas: lessons for global climate change. *Bulletin of American Meteorology Society* 73: 619–627.

Chase TN, Pielke RA, Kittel TGF, Nemani RR, Running SW. 2000. Simulated impacts of historical land cover chnages on global climate in northern winter. *Climate Dynamics* 16: 93–105.

Craigmile PF, Cuttorp P, Percival DB. 2004. Trend assessment in a long memory dependence model using the discrete wavelet transform. *Environmetrics* 15: 313–335.

Christy JR, Norris WB, Redmond K, Gallo KP. 2006. Methodology and results of calculating central California surface temperature trends: Evidence of human-induced climate change? *Journal of Climate* 19: 548–563.

Davison AC, Hinkley DV. 1997. *Bootstrap Methods and their Application*. Cambridge University Press: Cambridge.

Easterling DR, Karl TR, Mason EH, Hughes PY, Bowman DP, Daniels RC, Boden TA (eds). 1996. *United States Historical Climatology Network (U.S. HCN) Monthly Temperature and Precipitation Data*, ORNL/CDIAC-87, NDP-019/R3. Carbon Dioxide Information Analysis Center, Oak Ridge National Laboratory: Oak Ridge, Tennessee.

Easterling DR, Horton B, Jones PD, Peterson TC, Karl TR, Parker DE, Salinger MJ, Razuvayev V, Plummer N, Jamason P, Folland CK. 1997. Maximum and minimum temperature trends for the globe. *Science* 277: 364–367.

Efron B, Tibshirani R. 1993. *An Introduction to the Bootstrap*. Chapman and Hall: New York.

Feddema JJ, Oleson KW, Bonan GB, Mearns LO, Buja LE, Meehl GA, Washington WM. 2005. The importance of land-cover change in simulating future climates. *Science* 310: 1674–1678.

Foley JA, DeFries R, Asner GP, Barford C, Bonan GB, Carpenter SR, Chapin FS, Coe MT, Daily GC, Gibbs HK, Helkowski JH, Holloway T, Howard EA, Kucharik CJ, Monfreda C, Patz JA, Prentice IC, Ramankutty N, Snyder PK. 2005. Global consequences of land use. *Science* 309: 570–574.

Frauenfeld OW, Zhang T, Serreze MC. 2005. Climate change and variability using European Center for Medium-Range Weather Forecast analysis (ERA-40) temperatures on the Tibetan Plateau. *Journal of Geophysical Research* 110: D02101. DOI: 10.1029/2004JD005230.

Gallo KP, Easterling DR, Peterson TC. 1996. The influence of land use/land cover on climatological values of the diurnal temperature range. *Journal of Climate* 9: 2941–2944.

Gallo KP, Owen TW, Easterling DR, Jamason PF. 1999. Temperature trends of the U.S. historical climatology network based on satellite-designated land use/land cover. *Journal of Climate* 12: 1344–1348.

Gibbard SG, Caldeira K, Bala G, Philips TJ, Wickett M. 2005. Climate effects of global land cover change. *Geophysical Research Letters* 32: L23705.

Gluhovsky A, Agee E. 2007. On the analysis of atmospheric and climatic time series. *Journal of Applied Meteorology and Climatology* 46: 1125–1129.

Gluhovsky A, Zihlbauer M, Politis DN. 2005. Subsampling confidence intervals for parameters of atmospheric time series: block size choice and calibration. *Journal of Statistical Computation and Simulation* 75: 381–389.

Hale RC, Gallo KP, Owen TW, Loveland TR. 2006. Land use/land cover change effects on temperature trends at U.S. Climate Normals stations. *Geophysical Research Letters* 33: L11703. DOI: 10.1029/2006GL026358.

Hale RC, Gallo KP, Loveland TR. 2008. Influences of specific land use/land cover conversions on climatological normals of near-surface temperature. *Journal of Geophysical Research* 113: D14113. DOI: 10.1029/2007JD009548.

Hansen J, Ruedy R, Sato M, Imhoff M, Lawrence W, Easterling D, Peterson T, Karl T. 2001. A closer look at United States and global surface temperature change. *Journal of Geophysical Research* 106: 23947–23963.

Hansen M, DeFries R, Townshend JRG, Sohlberg R. 2000. Global land cover classification at 1km resolution using a decision tree classifier. *International Journal of Remote Sensing* 21: 1331–1365.

Homer C, Dewitz J, Fry J, Coan M, Hossain N, Larson C, Herold N, McKerrow A, VanDriel JN, Wickham J. 2007. Completion of the

2001 National Land Cover database for the conterminous United States. *Photogrammetric Engineering and Remote Sensing* **73**: 337–341.

Intergovernmental Panel on Climate Change (IPCC). 2001. In *Climate Change 2001: The Scientific Basis*, Houghton JT, Ding Y, Griggs DJ, Noguer M, Van Der Linden PJ, Dai X, Maskell K, Johnson CA (eds). Cambridge University Press: Cambridge, New York.

Joshi M, Shine K, Ponater M, Stuber N, Sausen R, Li ZX. 2003. A comparison of climate response to different radiative forcings in three general circulation models: towards an improved metric of climate change. *Climate Dynamics* **20**: 843–854.

Kallache M, Rust HW, Kropp J. 2005. Trend assessment: applications for hydrology and climate research. *Nonlinear Processes in Geophysics* **12**: 201–210.

Kalnay E, Cai M, Nunez M, Lim Y. 2008. Impacts of urbanization and land surface changes on climate trends. *International Association for Urban Climate* **27**: 5–9.

Kalnay E, Cai M, Li H, Tobin J. 2006. Estimation of the impact of land-surface forcings on temperature trends in eastern United States. *Journal of Geophysical Research* **111**: 1–13 (**Cite ID** D06106).

Kalnay E, Cai M. 2003. Impact of urbanization and land-use change on climate. *Nature* **423**: 528–531.

Karl TR, Williams CN Jr, Young PJ, Wedland WM. 1986. A model to estimate the time of observation bias associated with monthly mean maximum, minimum, and mean temperatures for the United States. *Journal of Climate* **25**: 145–160.

Karl TR, Diaz HF, Kukla G. 1988. Urbanization: its detection and effect in the United States climate record. *Journal of Climate* **1**: 1099–1123.

Kobayashi K, Salam MU. 2000. Comparing simulated and measured values using mean squared deviation and its components. *Agronomy Journal* **92**: 345–352.

Kukla G, Gavin J, Karl TR. 1986. Urban warming. *Journal of Climate and Applied Meteorology* **25**: 1265–1270.

Lahiri SN. 2003. *Resampling Methods for Dependent Data*. Springer-Verlag: New York.

Lim YK, Cai M, Kalnay E, Zhou L. 2005. Observational evidence of sensitivity of surface climate changes to land types and urbanization. *Geophysical Research Letters* **32**: L22712. DOI:10.1029/2005GL024267.

Lim Y, Cai M, Kalnay E, Zhou L. 2008. Impact of vegetation types on surface temperature change. *Journal of Applied Meteorology and Climatology* **47**: 411–424.

Lean J, Rowntree PR. 1997. Understanding the sensitivity of a GCM simulation of Amazonian deforestation to the specification of vegetation and soil characteristics. *Journal of Climate* **10**: 1216–1235.

Lobell DB, Bonfils C. 2008. The effect of irrigation on regional temperatures: a spatial and temporal analysis of trends in California, 1934–2002. *Journal of Climate* **21**: 2064–2071.

Mahmood R, Foster SA, Keeling T, Hubbard KG, Carlson C, Leeper R. 2006. Impacts of irrigation on 20th-century temperatures in the Northern Great Plains. *Global Planetary Change* **54**: 1–18.

McPherson RA, Stensrud DJ, Crawford KC. 2004. The impact of Oklahoma's wheat belt on the mesoscale environment. *Monthly Weather Review* **132**: 405–421.

Mesinger F, DiMego G, Kalnay E, Mitchell K, Shafran PC, Ebisuzaki W, Jovic D, Woollen J, Rogers E, Berbery EH, Ek MB, Fan Y, Grumbine R, Higgins W, Li H, Lin Y, Manikin G, Parrish D, Shi W. 2006. North American regional reanalysis: A long-term, consistent, high-resolution climate dataset for the North American domain, as a major improvement upon the earlier global reanalysis datasets in both resolution and accuracy. *Bulletin of American Meteorology Society* **87**: 343–360.

National Research Council (NRC). 2005. *Radiative Forcing of Climate Change: Expanding the Concept and Addressing Uncertainties*. Committee on Radiative Forcing Effects on Climate Change, Climate Research Committee, Board on Atmospheric Sciences and Climate, Division on Earth and Life Studies. The National Academies Press: Washington, DC.

Nuñez MN, Ciapessoni HH, Rolla A, Kalnay E, Cai M. 2008. Impact of land use and precipitation changes on surface temperature trends in Argentina. *Journal of Geophysical Research* **113**: D06111. DOI: 10.1029/2007JD008638.

Peterson TC. 2003. Assessment of urban versus rural in situ surface temperatures in the contiguous United States: no difference found. *Journal of Climate* **16**: 2941–2959.

Peterson TC, Gallo KP, Lawrimore J, Owen TW, Huang A, McKittrick DA. 1999. Global rural temperature trends. *Geophysical Research Letters* **26**: 329–332.

Pielke RA Sr, Marland G, Betts RA, Chase TN, Eastman JL, Niles JO, Niyogi D, Running S. 2002a. The influence of land-use change and landscape dynamics on the climate system – relevance to climate change policy beyond the radiative effect of greenhouse gases. *Philosophical Transactions of the Royal Society, Series A* **360**: 1705–1719.

Pielke RA Sr, Stohlgren T, Schell L, Parton W, Doesken N, Redmond K, Money J, McKee T, Kittel TGF. 2002b. Problems in evaluating regional and local trends in temperature: an example from eastern Colorado, USA. *International Journal of Climatology* **22**: 421–434.

Pielke RA Sr, Nielsen-Gammon J, Davey C, Angel J, Bliss O, Cai M, Doesken N, Fall S, Niyogi D, Gallo K, Hale R, Hubbard KG, Lin X, Li H, Raman S. 2007a. Documentation of uncertainties and biases associated with surface temperature measurement sites for climate change assessment. *Bulletin of American Meteorology Society* **88**: 913–928.

Pielke RA Sr, Davey C, Niyogi D, Fall S, Steinweg-Woods J, Hubbard K, Lin X, Cai M, Lim YK, Li H, Nielsen-Gammon J, Gallo K, Hale R, Mahmood R, McNider RT, Blanken P. 2007b. Unresolved issues with the assessment of multi-decadal global land surface temperature trends. *Journal of Geophysical Research* **112**: D24S08. DOI: 10.1029/2006JD008229.

Pielke RA Sr, Davey C, Morgan J. 2004. Assessing "global warming" with surface heat content. *Eos Transactions: AGU* **85**: 210–211.

Politis DN, Romano JP, Wolf M. 1999. *Subsampling*. Springer: New York.

Quayle RG, Easterling DR, Karl TR, Hughes RY. 1991. Effects of recent thermometer changes in the cooperative station network. *Bulletin of American Meteorology Society* **72**: 1718–1724.

Roy SS, Mahmood R, Niyogi D, Lei M, Foster SA, Hubbard KG, Douglas E, Pielke RA Sr. 2007. Impacts of the agricultural Green Revolution – induced land use changes on air temperatures in India. *Journal of Geophysical Research* **112**: D21108. DOI: 10.1029/2007JD008834.

Schenker N, Gentleman JF. 2001. On judging the significance of differences by examining the overlap between confidence intervals. *American Statistician* **55**: 182–186.

Sud YC, Yang R, Walker GK. 1996. Impact of *in situ* deforestation in Amazonia on the regional climate: a GCM simulation study. *Journal of Geophysical Research-Atmospheres* **101**: 7095–7110.

Trenberth KE, Jones PD, Ambenje P, Bojariu R, Easterling D, Tank AK, Parker D, Rahimzadeh F, Renwick JA, Rusticucci M, Soden B, Zhai P. 2007. Observations: surface and atmospheric climate change. In *Climate Change 2007: The Physical Science Basis*, Solomon S, Qin D, Manning M, Chen Z, Marquis M, Averyt KB, Tignor M, Miller HL (eds). Cambridge University Press: Cambridge, New York.

Vose RS, Williams CN, Peterson TC, Karl TR, Easterling DR. 2003. An evaluation of the time of observation bias adjustment in the U.S. Historical Climatology Network. *Geophysical Research Letters* **30**: 2046. DOI: 30 : 10.1029/2003GL018111.

Werth D, Avissar R. 2004. The regional evapotranspiration of the Amazon. *Journal of Hydrometeorology* **5**: 100–109.

Wichansky PS, Steyaert LT, Walko RL, Weaver CP. 2008. Evaluating the effects of historical land cover change on summertime weather and climate in New Jersey: part I: land cover and surface energy budget changes. *Journal of Geophysical Research* **113**: D10107. DOI: 10.1029/2007JD008514.

Wilcox RR. 2003. *Applying Contemporary Statistical Techniques*. Academic Press: San Diego.

Williams PD. 2005. Modelling climate change: the role of unresolved processes. *Philosophical Transactions of The Royal Society A* **363**: 2931–2946.

Zhou L, Dickinson RE, Tian Y, Fang J, Li Q, Kaufman RK, Tucker CJ, Myneni RB. 2004. Evidence for a significant urbanization effect on climate in China. *Proceedings of the National Academy of Sciences* **101**: 9540–9544.

Zwiers FW. 1990. The effect of serial correlations on statistical inferences made with resampling procedures. *Journal of Climate* **3**: 1452–1461.